

國立臺灣大學理學院海洋研究所



碩士論文

Graduate Institute of Oceanography

College of Science

National Taiwan University

Master Thesis

高屏峽谷之底棲生物食物網中的碳循環

Carbon Cycling in Benthic Food Web of the

Gaoping Submarine Canyon

董珏辰

Chueh-Chen Tung

指導教授：魏志潋 博士

Advisor: Chih-Lin Wei, Ph.D.

中華民國 111 年 8 月

August, 2022



國立臺灣大學碩士學位論文
口試委員會審定書
MASTER'S THESIS ACCEPTANCE CERTIFICATE
NATIONAL TAIWAN UNIVERSITY

高屏峽谷之底棲生物食物網中的碳循環

Carbon Cycling in Benthic Food Web of the Gaoping Submarine Canyon

本論文係 董珣辰 (姓名) R09241201 (學號) 在國立臺灣大學
海洋研究所 (系/所/學位學程) 完成之碩士學位論文，於民國 111 年
8 月 4 日承下列考試委員審查通過及口試及格，特此證明。

The undersigned, appointed by the Department / Institute of Oceanography
on 4 (date) 8 (month) 2022 (year) have examined a Master's thesis entitled above presented
by Chueh-Chen Tung (name) R09241201 (student ID) candidate and hereby certify
that it is worthy of acceptance.

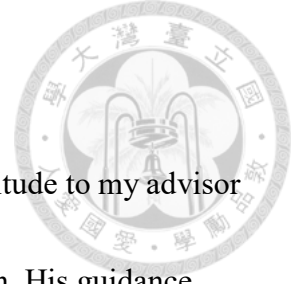
口試委員 Oral examination committee:

張志豪 林玉詩
(指導教授 Advisor)

謝志豪

系主任/所長 Director: 謝志豪

Acknowledgement



First and foremost, I would like to express my sincere gratitude to my advisor Prof. Wei for the support of my study, for his patience and motivation. His guidance helped me in all the time of research and writing of this thesis. I could not have imagined having a better advisor and mentor for my master's study. Thanks should also go to my committee, Dr. Yu-shih Lin and Dr. Chih-hao Hsieh, for their invaluable patience and feedback.

Additionally, I would like to thank my labmates in 412: Dr. Jian-Xiang Liao, Yen-Ting Chen, Jing Tang, and Hsin Chen, for the stimulating discussions and all the fun during the cruises on NOR1.

All the samples and data were collected by labmates. Detritus TOC measurements were conducted by Dr. Yu-shih Lin and Guan-Ming Chen; the bacteria samples were analyzed by Dr. Jian-Xiang Liao. The meiofauna samples were analyzed by Dr. Jian-Xiang Liao, Guan-Ming Chen, and Jing Tang. In addition, Yen-Li Liu, Guan-Ming Chen, Yen-Ting Chen, and Jing Tang contributed to the data on macrofauna.

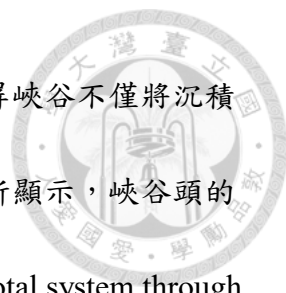
Last but not least, I would like to thank my family and friends for supporting me spiritually throughout my life.

摘要



雖然台灣西南海域高屏海底峽谷的地質和生物群落結構已被廣泛研究，然而我們對沉積物的碳循環和棲地對底棲生態系統功能性的影響仍不清楚。本研究透過量化底棲食物網的碳循環以了解與山溪型河川對接的海底峽谷生態系統功能。本研究使用 2014 年至 2020 年共 12 個航次的沉積物樣本來估算高屏峽谷頭（簡稱 GC1）和相鄰斜坡（簡稱 GS1）中的生物和非生物的碳存量，並檢驗其中是否存在季節性差異。接著，我結合不同食階的生地化數據來構建線性逆推模型（Linear Inverse Model; LIM）並比較兩地食物網中的碳流量。最後，我使用網路指數檢驗兩棲地食物網的生態系統功能。

本研究結果顯示生物以及沉積物的碳存量並無顯著季節性差異，然而不同棲地之間生物以及沉積物的碳存量則顯著不同。除了細菌的碳存量在峽谷頭較高之外，相鄰斜坡的生物以及非生物(沉積物)的碳存量都顯著高於峽谷頭。峽谷中相對較低的生物多樣性和生物碳存量顯示峽谷頭生態系受到劇烈物理擾動，其中峽谷的大型（Macrofauna）與中型（Meiofauna）底棲無脊椎生物的碳存量遠低於斜坡，然而沉積物群落耗氧量在兩棲地之間並沒有顯著差異，顯示了峽谷頭中細菌可能貢獻了絕大部分的耗氧量。相比之下，相鄰斜坡上生物對於碳循環的貢獻較高，為相對成熟的生態系統。LIM 結果顯示兩棲地之間的碳流量大小和分佈有巨大差異。峽谷頭和相鄰斜坡分別需要 $131.08 \text{ mg C/m}^2/\text{d}$ 和 $78.95 \text{ mg C/m}^2/\text{d}$ 的



有機碳通量來支持其生物系統。峽谷頭較高的碳埋藏率顯示高屏峽谷不僅將沉積物輸送到南海深處，也在碳封存中扮演重要角色。網路指數分析顯示，峽谷頭的總系統通量（Total system throughput; $T_{..}$ ）和總系統穿流量（Total system through flow; TST ）相當高，代表流經峽谷系統的碳流量較大。而峽谷的芬恩循環指數（Finn Cycling Index; FCI ）邊緣顯著低於相鄰斜坡，意味著高比例的碳未被利用而直接被埋藏，因此在系統中的分佈效率低下。

本研究是第一個量化高屏峽谷及相鄰斜坡底棲食物網碳流量的研究。透過 LIM 與網路指數分析，我們更理解海底峽谷的生態系統功能。未來山溪型河川的洪水強度跟頻度可能受氣候變遷的影響而增加，並且更頻繁地引發海底峽谷的地質災害。研究海洋環境中的物質和能量轉移將有助於我們了解生態系統功能以及其儲存碳的能力，而透過模擬高屏峽谷底棲生態系統的碳循環，我們或許能夠將本研究建構的模式運用在預測氣候變遷或人類活動對深海生態系統的影響。

關鍵字：高屏峽谷，食物網，線性逆推模型，碳流量，網路指數，深海生態系


Abstract



The Gaoping Submarine Canyon (GPSC) off Southwest Taiwan has been extensively studied for its geology and biological community structure. However, the carbon cycle across the sediment-water interface and the environmental control on benthic ecosystem functioning remained unclear. This study attempts to contribute knowledge gap in the benthic food web by quantifying the carbon cycling in this small mountain river (SMR)-fed submarine canyon ecosystem.

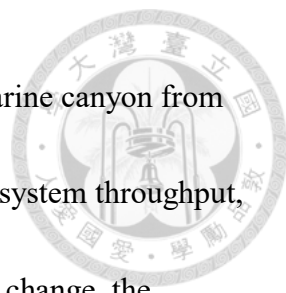
First, biotic and abiotic carbon stocks in the upper GPSC (GC1) and adjacent slope (GS1) were estimated and examined for the seasonal difference. Then, I combined biological and geochemical data from 2014 to 2020 with literature data to construct linear inverse models (LIM) and compared the carbon food webs between GC1 and GS1. Finally, I used selected network indices to examine the ecosystem function and food web characteristics between the canyon and slope habitats.

The analyses did not find seasonal differences in organic carbon stocks. However, except for the bacteria stocks, the biotic and abiotic carbon stocks in the GS1 were significantly higher than in GC1. The relatively lower biodiversity and faunal carbon stocks in the canyon show that the GC1 was a fragile ecosystem under severe physical perturbation. Nevertheless, despite the drastic difference in fauna stocks, the sediment



community oxygen consumption (SCOC) rates were similar between habitats, indicating the relatively higher microbial carbon remineralization in the GC1 than in GS1. By contrast, the higher fauna contribution to carbon processing in the GS1 suggests that the slope may be a relatively more mature ecosystem than the canyon. The LIM food web results showed that the magnitude and distribution of the carbon flows differed between GC1 and GS1. The GC1 required $131.08 \text{ mg C/ m}^2/\text{ d}$, and GS1 needed $78.95 \text{ mg C/ m}^2/\text{ d}$ of total organic carbon (TOC) flux to support the biological systems. The higher carbon burial rate in GC1 indicates that the GPSC not only transports sediment to the deep South China Sea but contributes considerably to carbon sequestration. Moreover, two network indices, the total system throughput ($T_{..}$) and total system through flow (TST), were markedly higher in GC1, indicating greater energy flowing through the system. The Finn Cycling Index (FCI) was marginally lower in the canyon, revealing that a large fraction of carbon is buried, and the remaining carbon were distributed inefficiently in the system.

This study presents the first food web model to examine carbon cycling in the GPSC and on the adjacent slope. Moreover, it is the first study that applied the LIM technique in Taiwan. The LIM model results provided a rare opportunity to study how the canyon affects food web structure compared to the slope habitat. Moreover, the LIM



model offered an insight into the ecosystem functioning of the submarine canyon from the aspect of energy flows and food web characteristics such as total system throughput, energy recycling, and food web maturity. Due to the ongoing climate change, the geohazards in the submarine canyons might become more frequent owing to new weather systems with a higher intensity of flooding in SMRs. Studying matter and energy transfer in the submarine canyon will help us determine the capacity of deep ecosystems to capture and store carbon. By better understanding carbon cycling in GPSC, we may be able to predict the impact of climate change or human influence on deep-sea ecosystems.

Keyword: Gaoping Submarine Canyon, Food web, Linear inverse model, Carbon flows, Network indices, Deep-sea ecosystems

Content

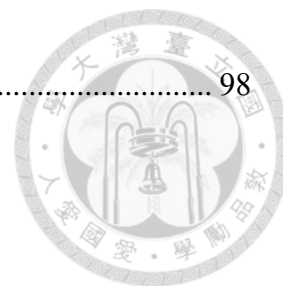


論文口試委員審定書	i
Acknowledgement	ii
摘要	iii
Abstract	v
Content	viii
List of figures	xiv
1 Introduction	1
1.1 Submarine canyon	1
1.2 Compare GPSC with GS in terms of physical conditions and community structure	5
1.3 Carbon flows and food webs in the deep-sea environment	9
1.4 Related food web studies in submarine canyons	13
1.5 Aim of this study	15
2 Materials and Methods	17
2.1 Studying sites	17
2.2 Definition of OC stocks	17
2.3 Sampling procedures of living component of OC	18
2.3.1 Prokaryote biomass	18
2.3.2 Meiofauna biomass	19

2.3.3	Macrofauna biomass.....	21
2.4	Sampling procedures of non-living component of OC.....	22
2.4.1	Detrital organic carbon	22
2.5	Sediment community oxygen consumption (SCOC)	23
2.6	Statistical analysis.....	25
2.7	Rain of POC.....	25
2.8	Burial rates of organic carbon.....	26
2.9	Linear inverse model formulation	26
2.9.1	Structure.....	27
2.9.2	Mass balances	27
2.9.3	Constraints	29
2.10	Model Solution: Likelihood method.....	32
2.11	Network indices of ecosystems	33
3	Results.....	37
3.1	Environment data.....	37
3.1.1	CTD	37
3.2	Stock of the non-living component of OC.....	37
3.2.1	Detrital organic carbon	37

3.3	Stocks of the living component of OC	38
3.3.1	Prokaryote biomass.....	38
3.3.2	Meiofauna biomass.....	39
3.3.3	Macrofauna biomass.....	40
3.4	Oxygen utilization	41
3.5	Model results	42
3.5.1	LIM result of GC1	44
3.5.2	LIM result of GS1.....	45
3.6	Turnover rates.....	46
3.7	Network indices results	47
4	Discussion	49
4.1	Carbon stock in different compartments.....	49
4.2	Implemented constraints and model limitations	51
4.3	Carbon demand from the benthic community	58
4.4	Network characteristics	59
4.5	Burial efficiency and carbon sequestration in the GPSC.....	63
5	Conclusion	67
6	Reference	69
	Table	85

Figure.....98



List of tables

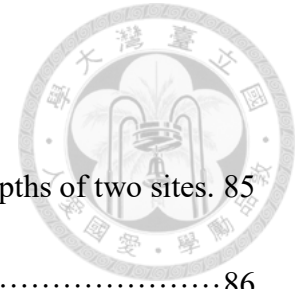


Table 1. Sampling cruises including dates, coordinates, and water depths of two sites.	85
Table 2. Definition of each flow in Fig. 2.	86
Table 3. The conceptual model of the food web structure formed the basis of our linear inverse model (LIM).	87
Table 4. Nomenclature of symbols used in calculation of network indices.	88
Table 5. Formula of the network indices.	89
Table 6. Standing stocks of the food web compartments for GC1 and GS1.	90
Table 7. Average bottom water temperature and the calculated "Tlim" of GC1 and GS1.	90
Table 8. PERMDISP and PERMANOVA on sediment carbon stock GC1 and GS1. ...	90
Table 9. T-test on bacteria carbon stock of GC1 and GS1.	91
Table 10. PERMDISP and PERMANOVA on meiofaunal carbon stock of GC1 and GS1.	91
Table 11. PERMDISP and PERMANOVA on macrofaunal carbon stock of GC1 and GS1.	92
Table 12. Average oxygen utilization rates of all cruises in GC1 and GS1.	92
Table 13. PERMDISP and PERMANOVA on TOU of GC1 and GS1.	93

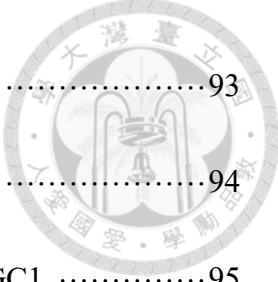


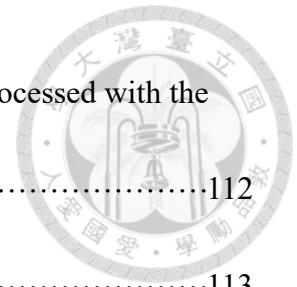
Table 14. PERMDISP and PERMANOVA on DOU of GC1 and GS1.	93
Table 15. PERMDISP and PERMANOVA on BMU of GC1 and GS1.	94
Table 16. Mean and standard deviation of the food web flows of the GC1.	95
Table 17. Mean and standard deviation of the food web flows of the GS1.	96
Table 18. Stock turnover calculated with the two different estimations of oxygen utilization rates.	97
Table 19. Comparison of network indices calculated for GC1 and GS1.	97

List of figures



Figure 1. The map of sampling stations of the upper Gaoping Submarine Canyon (GC1) and Gaoping Slope (GS1).	98
Figure 2. The conceptual model of the food web structure formed the basis of our linear inverse model (LIM).	99
Figure 3 Water temperature profile for each cruise of the two sites.	100
Figure 4. Light transmission profile for each cruise of the two sites.	101
Figure 5. Carbon stocks of sediment of GC1 and GS1.	102
Figure 6. Carbon stocks of bacteria of GC1 and GS1.	103
Figure 7. The abundance of meiofauna in each cruise of GC1 and GS1.	104
Figure 8. Carbon stocks of the meiofauna of GC1 and GS1.	106
Figure 9. The abundance of macrofauna in each cruise of GC1 and GS1.	107
Figure 10. Carbon stocks of macrofauna of GC1 and GS1.	108
Figure 11. Average total oxygen utilization (TOU) for each cruise of GC1 and GS1.	109
Figure 12. LIM results for each flow in the food web by the two different methods. ..	110
Figure 13. The conceptual model plotted with LIM results of GC1 processed with the MCMC algorithm.	111

Figure 14. The conceptual model plotted with LIM results of GS1 processed with the MCMC algorithm.	112
Figure 15. The selected network indices of GC1 and GS1.	113




1 Introduction



1.1 Submarine canyon

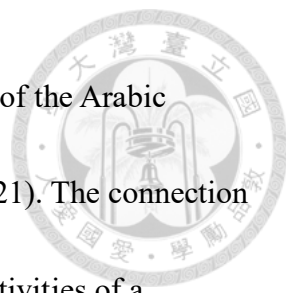
Submarine canyons are steep-walled, V-shaped valleys incised into continental margins (Shepard 1973; Shepard 1981), directly connecting continental shelves to deep ocean basins by transporting sediments and organic matters (OM) (Vetter & Dayton, 1999; Epping et al., 2002; Nittrouer & Wright, 1994). Shepard and Dill (1966) reviewed the distribution, characteristics, and origins of submarine canyons and mapped 96 major canyons worldwide. Later, Harris & Whiteway (2011) analyzed more detailed bathymetric data showing abundant and ubiquitous submarine canyons across continental margins globally.

Though the benthic community structure and productivity have been poorly studied in the submarine canyons, some findings suggest that the elevated benthic biomass and diversity in the canyon can be attributed to the high habitat heterogeneity (De Leo et al., 2014; McClain & Barry, 2010). For example, habitat heterogeneity among sampling localities may enhance meiofauna trophic complexity in the sedimentary environment (Ramalho et al., 2014). Moreover, commercially-important rockfishes may be benefited from the natural refuge provided by the Soquel Submarine Canyon in Monterey Bay (Yoklavich et al., 2000). The high-relief boulders and rock

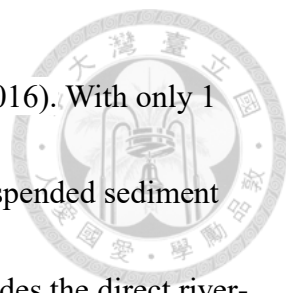


outcrops make these narrow, deep-water canyons less accessible to fishing activities (Yoklavich et al., 2000). Other remarkable ecological and physical characteristics of submarine canyons have also been reported. For instance, submarine canyons may reflect and focus internal waves and lead to strong bottom currents (Hall & Carter, 2011). The interactions between canyons and coastal ecosystems may lead to seasonal upwelling and contribute to high productivity (Sobarzo et al., 2001). Submarine canyons may also trap dense aggregation of diel vertical migrators and their predators (Greene et al., 1988; Maycas et al., 1999). These unique ecological and physical characteristics can be attributed to the interactions between complex topographic features and hydrodynamics in the submarine canyons.


A great variety of hypotheses has been proposed to explain the origin of submarine canyons. Still, the most critical factors in the development of canyons are the erosion triggered by turbidity currents (Shepard, 1981) and the mass failures during sea-level low stands (Walsh et al., 2007). The sediment transport efficiency of canyons is partly controlled by how far the canyon head extent into the shelf. When the distance between the canyon head and the shore is short, terrestrial sediment and organic carbon can be efficiently transported to the deep ocean (Covault et al., 2007; Galy et al., 2007), and the canyon stays active. There are many examples of these shore-connected canyons, which



frequently occur along the Californian coast, the Indian-Ocean coast of the Arabic Peninsula, and the Eastern Black Sea (Bernhardt & Schwanghart, 2021). The connection between a river and a canyon is not the only factor involved in the activities of a submarine canyon. Some canyons, such as the Monterey, La Jolla, and Hueneme Canyons, can capture longshore-transported sediments to feed their canyon head through the bottom currents (Covault & Graham, 2010). In a recent analysis, Bernhardt and Schwanghart (2021) examined 4,633 submarine canyons in the world's oceans. They found that most canyons can be classified as slope-incising (60%) and shelf-incising canyons (37%). There are only 183 shore-connected canyons. Using similar methods, Chiang & Yu (2022) also studied the submarine canyons around Taiwan. In contrast to the world's canyons, Taiwan's continental margin is dominated by shore-connected canyons ($n=7$, 54%) (Chiang & Yu, 2022). There are six shore-connected canyons located in the eastern Taiwan margin. These canyons receive sufficient input of terrestrial material, and their headward erosion rates are comparable to the Holocene's millennial-scale sea-level rise. The other shore-connected canyon in the southwestern margin is the Gaoping submarine canyon (GPSC). The GPSC is deeply incised into the Gaoping Shelf, and the canyon head is near the mouth of the Gaoping River (GPR). The GPR is a typical small mountain river (SMR) with steep elevation changes over a short



distance from its headwaters to its confluence or mouth (Liu et al., 2016). With only 1 km from the canyon head to the river mouth, a high proportion of suspended sediment discharged from the GPR (49 MT/ yr) is delivered to the GPSC. Besides the direct river-canyon connection, this region also experiences frequent earthquakes and typhoon events, such as the 2006 Pingtung Earthquake and 2009 Typhoon Morakot. These natural disasters can lead to recurring turbidity and episodic gravity-driven sediment flows in the GPSC, allowing for the continual erosion of the canyon floor and sediment transportation (Gavey et al., 2017; Ikehara et al., 2020; Chiang et al., 2020). Because of the extremely high sediment discharge from the GPR, the canyon head of GPSC remains active as a conduit for terrestrial sediment from Taiwan's high mountains to the deep South China Sea (SCS) (Liu et al., 2016). It has been suggested that the oceanographic settings in submarine canyons may increase the concentration of suspended particulate matter and sediment transport (Keller et al., 1973; Puig et al., 2008; Gaudin et al., 2009). The OM from the riverine inputs and coastal zone is essential energy to the undernourished deep-sea ecosystems (Rex et al., 2006; Wei et al., 2010). They may also be responsible for enhancing biodiversity and productivity (Rowe 1971; Vetter and Dayton, 1998; Schlacher et al., 2007). In the GPSC, the annual sediment discharge is approximately 30–80% of the Mississippi's annual export (Meade



and Moody, 2010), the world's third-largest river. It is remarkable given that the GPR basin only represents ~0.1% of the Mississippi drainage area (US Environmental Protection Agency, Taiwan Water Resources Agency). Liu et al. (2016) also reported that the particulate organic carbon (POC) transported through the GPR–GPSC system is $\sim 5.98 \times 10^6$ g C/ d in the dry season and $1.25\text{--}276 \times 10^6$ g C/ d in the flood season. Many researchers have investigated the source and spatiotemporal variations of riverine carbon fluxes under global climate changes and anthropogenic perturbations (Huang et al., 2012; Zhang et al., 2013; Li et al., 2017). However, little is known about the carbon cycling after the organic matter enters the canyon and accumulates on the seabed. Given the high association between sediment load and POC flux, it is vital to understand how submarine canyons mediate the fate of organic carbon entering the continental margin ecosystem. Hence, we focused on comparing carbon cycling between the head of GPSC and the adjacent Gaoping Slope (GS) off SW Taiwan.

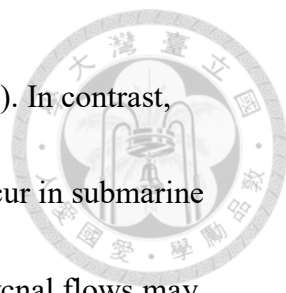
1.2 Compare GPSC with GS in terms of physical conditions and community structure

Gaoping River-Canyon system is the most extensive sediment dispersal system off SW Taiwan, including the Gaoping River drainage basin, the Gaoping Shelf, the Gaoping Slope, the Gaoping submarine canyon, and the Manila Trench in the northeast

margin of the SCS. The Gaoping slope (GS) continues from the narrow (< 20 km) continental shelf, extending southwest toward the northern SCS. The slope can be divided into upper and lower parts by 1000 to 1200-m water depth (Yu et al., 2009).

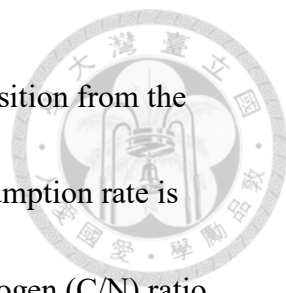
Embedded within the GS, the Gaoping submarine canyon (GPSC) extends 260 km from the Gaoping River (GPR) mouth, crossing through the continental shelf and slope and merging into the Manila trench (Liu et al., 2016). The canyon comprises three geographically distinct segments. The upper section meanders southwestward from 126 to 1750 m in water depth, featuring great relief. The middle reach runs southeastward along an elongate escarpment and then makes a sharp turn to the southwest, covering the water depths between 1750 and 2800 m. The lower canyon spans 2800 to 3600 m in water depths and finally connects to the northern opening of the trench (Yu et al., 2009).

The physical settings and topographic features are markedly different between the GPSC and GS. Hsu et al. (2013) suggested that the "filling-and-spilling" plays a key role in the sediment deposition across the GS. In contrast, other processes such as tectonic activities, mass wasting events, and canyon and channel feedings diversify the sediment transport dynamics from the inner to outer slopes. The bedding geometries in the slope basin revealed competition between local basin flank uplift and sediment deposition rates. As such, the upper GS tends to have higher accumulation rates and




relatively slower deposition rates than the lower GS (Hsu et al., 2013). In contrast, much more complex sediment deposition and transport processes occur in submarine canyons. For example, gravity currents such as turbidity and hyperpycnal flows may erode the surface sediment in the submarine canyons (Mulder et al., 2001). The erosion processes may be more pronounced in the canyons like GPSC subjected to frequent gravity currents and strong internal tides from the Luzon and southeastern Taiwan Strait (Chiou et al., 2011; Jan et al., 2008). Accompanying the semidiurnal tides (M₂), the head-ward propagation of the internal waves and bottom currents converges in beam patterns that move parallel to the canyon thalweg (Wang et al., 2008). Also, the existence of isopycnal surfaces in the head region of GPSC can be conducive to the generation and propagation of internal tides (Lee et al., 2009; Liu et al., 2002; Wang et al., 2008). Above the GPSC seafloor, a benthic nepheloid layer (BNL) thicker than 100 m with suspended sediment concentration (SSC) exceeding 30 mg/ l was documented and likely maintained by current-induced resuspension (Liu et al., 2002).

Besides the physical environment, food availability has been considered the most important driving force for the abundance, diversity, and composition of the deep-sea benthic ecosystem (McClain et al., 2012; Rex et al., 2006). Some proxies have been widely used to determine sedimentation sources. For example, the total organic carbon



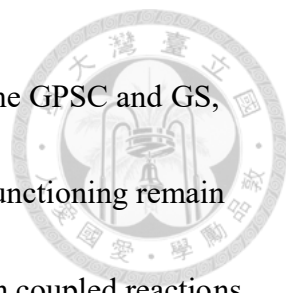
(TOC) content in marine sediments is a common proxy for OM deposition from the water column to the seafloor. Meanwhile, because the nitrogen consumption rate is higher than carbon (Danovaro, 2009; Meyers, 1994), the TOC to nitrogen (C/N) ratio can estimate the aging and sources of OM. Generally, the benthic population densities decline with depth because of the attenuated sinking particulate organic matter (POM) flux (McClain and Rex, 2015; Wei et al., 2010), while higher population densities are expected in the submarine canyon head and near the shelf break due to the higher concentration of OM. Liao et al. (2017) compared the TOC contents and C/N ratios between the surface sediment from GPSC and GC. However, they found that the TOC was negatively related to the bottom current velocity, resulting in a lower TOC, faunal abundance, and diversity near the canyon head due to stronger bed flows. In comparison, the TOC increased toward the GS and resulted in higher benthos population density, indicating significant influences of food supplies on benthic community structure.

The benthic macrofaunal and meiofaunal community structures in the GPSC and GS were studied by Liao et al. (2017, 2020). Unlike the typical high-productivity submarine canyons, the upper GPSC was severely impacted by physical disturbance triggered by internal tides and gravity flows. The biological responses, such as reduction



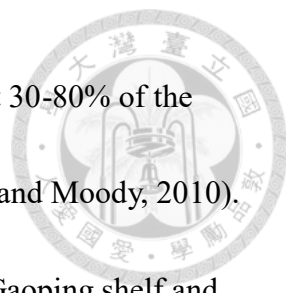
and loss in species richness or total abundance, alteration of taxonomic composition, and the dominance of deep-dwelling burrowing infauna, showed that the benthic communities underwent intense physical disturbances in the GPSC (Liao et al., 2017). Moreover, distinct nematode assemblages were identified between the GPSC and GS (Liao et al., 2020). They also found that the nematodes species, functional and trophic diversity, and community maturity were severely depressed in the GPSC. These physical extremes, such as strong near-bottom currents and associated sediment sorting, likely outweigh the focusing effect of OM delivery in active submarine canyons like GPSC. Liao et al. (2020) also attributed the distinct nematode assemblages in the GPSC to the species filtering by the environmental stresses in the canyon. As a result, the nematode assemblages in the GPSC were dominated by r-strategist and non-selective deposit feeders with clavate tails. In contrast, the species with longer lifespans, diverse feeding strategies, and tail shapes were found in the GS. Though environmental filtering was the primary mechanism structuring the benthic community between the GPSC and GS, the nestedness patterns (Baselga, 2010; 2012) were also evident, indicating that species immigration and local extinction might also occupy crucial roles in shaping the species composition in the canyon.

1.3 Carbon flows and food webs in the deep-sea environment




Despite the unique geology and community structure between the GPSC and GS, their effects on the sediment biogeochemical cycles and ecosystem functioning remain unknown. The biogeochemical cycles in aquatic sediments depend on coupled reactions and transport processes, including diffusion, advection, and biologically induced transport (Meile et al., 2001). For example, macrobenthos burrowing (i.e., bioturbation and bioirrigation activities) enhances solute transport between the sediment and water interface. In the sediment with high macrofauna densities (e.g., Hammond and Fuller 1979; Archer and Devol 1992), the fluxes across the sediment-water interface are mainly attributed to bioirrigation instead of diffusion. On the other hand, ecosystem functioning is defined as the flow of matter and energy transfer within or between different trophic levels or ecosystems (Danovaro et al., 2008; Loreau, 2008). For instance, burrowing infauna and epifauna may affect microbial carbon remineralization, sediment oxygen penetration, carbon storage, and nutrient regenerations through reworking sediment and bioirrigation (Lohrer et al., 2004). In addition, the feeding, growth, predation, and mortality of the benthos directly affect the productivity, nutrient cycling, organic matter decomposition, and carbon sequestration on the seafloor (Snelgrove et al., 2014).

The estimate of annual sediment exporting from the Gaoping Rivers into the GPSC



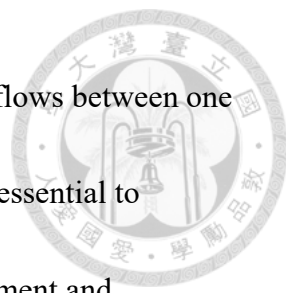
ranges from 45.6 to 110 MT (Hsu et al., 2014). This quantity is about 30-80% of the sediment transported by the Mississippi River (~145 MT/ yr, Meade and Moody, 2010). However, the sediment accumulation rates were 2-12 MT/ yr in the Gaoping shelf and slope area (Hsu et al., 2014; Huh et al., 2009), which is approximately 4 to 55 times less than the transporting mass flux. Thus, most of the sediment, primarily the organic carbon (OC), is likely exported down through the GPSC and buried in the deep SCS (Hsu et al., 2014; Kao et al., 2014; Liu et al., 2016, 2013). However, this view completely ignores the role of benthos, which likely oxidizes the OC through their feeding, respiration, burrowing, and predation activities. It may lead to an erroneous estimate of OC cycling on the seafloor (Snelgrove et al., 2018).

Previous studies suggested that the active canyon may transport a higher quantity and quality of sedimentary OC than the slopping environment at a similar depth (Garcia et al., 2007; Pusceddu et al., 2010; Vetter and Dayton, 1999). The high quantity and quality OM in submarine canyons are known to enhance the carbon oxidation rates (Epping et al., 2002; Rabouille et al., 2009), benthic standing stocks of nematodes (Ingels et al., 2009), and holothurians deposit-feeding (Amaro et al., 2009; De Leo et al., 2010; Vetter and Dayton, 1999). These processes indicate intensified carbon cycling in the benthic food web. Though we know that the unfavorable physical disturbance in



the GPSC may severely impact the benthic communities, how the carbon cycling within the canyon food web may be affected remains unclear. In addition, most of the marine benthic studies focused on individual components of the food web (e.g., Ramirez-Llodra et al., 2010; Bianchelli et al., 2010) and suggested that the entire benthic systems may be benefited from the increased OM flux into the canyons. However, these comparisons were only based on single biomass-to-biomass or process-by-process comparisons. A comprehensive understanding of the benthic ecosystem structure is needed to evaluate the carbon cycle within the food web.

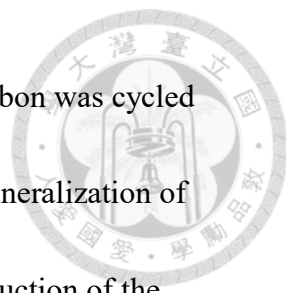
The deep-sea benthic ecosystems depend on the slow sinking of detritus derived from primary production in the euphotic zone. Before detritus settle on the seabed, suspension feeders first consume the detritus from the overlying bottom water (Gage and Tyler, 1996). Bacteria (Lochte and Turley, 1988) and deposit feeders (Blair et al., 1996) of all sizes, who respond rapidly to the food supplies with metabolic activities, such as growth and reproduction, consume the remaining detritus deposited on the seafloor (Tyler et al., 1982; Smith et al., 2008). Then, the detritivores are predated by larger animals such as megafauna and fish. The waste products of all consumers again become food for deposit-feeders and bacteria or are released back to the water column as dissolved inorganic carbon (DIC) or nutrients. In brief, the food web comprises the



abiotic (detritus, DIC, etc.), biotic compartments, and the linkage of flows between one another. Identifying and quantifying energy flows in the food web is essential to understanding their functional interactions. However, direct measurement and experimentation are notoriously tricky, even for relatively well-studied shallow-water benthic ecosystems (e.g., van Oevelen et al., 2006), not to mention the undersampled deep sea. Nevertheless, a linear inverse model (LIM) has been developed and applied to marine food web studies to deal with data limitations (Vézina and Platt, 1988). Also, network analysis developed from the information theory has been used to solve information in a complex network (e.g., a food web) and then condense this information into interpretable indices (Fath and Patten, 1999; Ulanowicz, 2004).

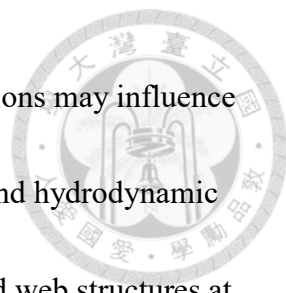
1.4 Related food web studies in submarine canyons

To my knowledge, only two studies have attempted to construct a comprehensive benthic carbon food web in submarine canyons. The first study was conducted in the northern Gulf of Mexico (Rowe et al., 2008). The carbon food webs were contrasted between the head of the Mississippi Canyon and the adjacent mid-slopes. A single species of amphipod dominated the Mississippi Canyon head, resulting in extremely high macrofauna abundance ($> 20,000$ individual/ m) and biomass (> 400 mg C/ m²) (Wei et al., 2012). Therefore, based on the secondary production estimates and total



sediment community oxygen consumption (SCOC), considerable carbon was cycled mainly through the macrofauna stock. At the same time, the OC remineralization of bacteria and meiofauna was reduced in the canyon. Because the production of the amphipods was considered a food source for larger invertebrates and fishes, the biomass of megafauna and fishes were relatively higher in the Mississippi Canyon than on the middle continental slopes. Notably, the POC input was two times higher than the required amount to support the calculated biological demand (i.e., the sum of total respiration, production, and export), suggesting almost 40% of POC rain was exported through the Mississippi Canyon (Rowe et al., 2008). In contrast, the carbon demand at the continental slope was greater than the estimated POC input, indicating that the organic resources required by the community were supplemented from the basin margin (Rowe et al., 2008).

In the other study, carbon food web models were contrasted within the three sections of the Nazaré Canyon (eastern Atlantic Ocean) off Portugal's coast (van Oevelen et al., 2011), including the upper (300–750 m water depth), middle (2700–3500 m) and a lower sections (4000–5000 m) of the canyon. Compared to Rowe et al. (2008), the food webs were constructed with linear inverse modeling, which combined the biomass, data of carbon processes, and the general physiological constraints from

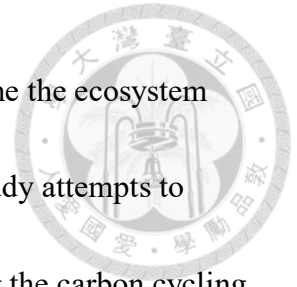


literature to examine how the characteristics of different canyon sections may influence the food webs. The environmental conditions, especially OM input and hydrodynamic activity, vary significantly along the canyon, resulting in distinct food web structures at different canyon sections. For example, the prokaryote uptake of dissolved organic carbon (DOC) and its respiration to DIC dominated the carbon flows in the upper canyon food web. The meiofauna also has a higher density and contributes more to the carbon flows than the macrofauna, suggesting that the meiofauna may tolerate the high current speeds and sediment resuspension in the upper canyon better than the macrofauna. In the mid-canyon, holothurians benefited from the high OM inputs and accreted sediments, resulting in a megafaunal hotspot. In the low canyon, all carbon flows diminished, but the prokaryote uptake of DIC dominated the food web, resembling the food web of the lower slope and abyssal plain sediments.

1.5 Aim of this study

This study estimated biotic and abiotic carbon stocks in the upper GPSC and adjacent slope off SW Taiwan. Firstly, I examined whether the seasonal difference existed in these stock estimates. Then, I combined biogeochemical data from literature and *in situ* data collected in the GPSC and GS. Thirdly, I constructed LIM models from the literature and *in situ* data to compare carbon flows in simplified food webs between

the GPSC and GS. Finally, I used selected network indices to examine the ecosystem function and characteristics of the GPSC and GS food webs. This study attempts to contribute to knowledge gaps in the benthic food web by quantifying the carbon cycling in an SMR-fed submarine canyon ecosystem.



2 Materials and Methods




2.1 Studying sites

From 2014 to 2020, the upper GPSC and GS were repeatedly visited by the National Taiwan University's R/V Ocean Researcher 1 and New Ocean Researcher 1, with results published in Liao et al. (2017, 2020) (Fig. 1). The two shallowest stations of Liao and coworkers were chosen in this study and were abbreviated as GC1 and GS1, respectively. At each visit, CTD/ rosette cast and UNSEL box corer (Hessler and Jumars, 1974) or OSIL megacorer were deployed. The hydrocasts of temperature and salinity were measured with a CTD recorder (Sea-Bird SBE 911). For the box core operation, five transparent polycarbonate tubes (i.d. = 67 mm) were inserted into the sediments to take subsamples. For the megacorer operations, a maximum of 12 polycarbonate tubes (i.d. = 105 mm) were recovered as the replicate samples. The cruise details, sampling sites, and sampling gears are listed in Table 1.

2.2 Definition of OC stocks

In the deep-sea sediments, the total inventory of OC can be divided into the living and the non-living components. The living component of OC is mainly made up of the biomass of prokaryotes (mostly bacteria), protozoan (mostly foraminifera), meiofauna




(> 40 μm in length), and macrofauna (> 1 mm in length) (Burnett, 1979; Mare, 1942; Rowe 1983). The non-living component of OC comprises labile, semi-labile, and refractory OC. The labile OC (e.g., neutral sugars and amino acids) supports rapid microbial production with turnover time scales of minutes to days (Hansell and Carlso, 2001). The semi-labile OC (i.e., polysaccharides) cycles with intermediate time scales of weeks to years (Benner et al., 1992; Ogura 1972). The refractory OC (e.g., humic and fulvic acids) is structural carbohydrates and "black" carbon, with very low degradation rates (Danovaro, 2009). The source of OC is mainly supplied by the rain of POC from the euphotic zone, and the lateral advection of POC from terrestrial or marine organics. On the other hand, the loss of OC balances the input through biological utilization of labile OC, predation on living components of OC, carbon remineralization, the long-term burial of refractory OC, and down-slope export (e.g., by turbidity currents).

2.3 Sampling procedures of living component of OC

2.3.1 Prokaryote biomass

A cutoff 10 ml sterile syringe (i.d. 15 mm) was used to take the subsample from the top 1 cm of sediment within a core tube. The syringe plunger was held fixed at the sediment surface as the operation of a piston core, and then the barrel was pushed into



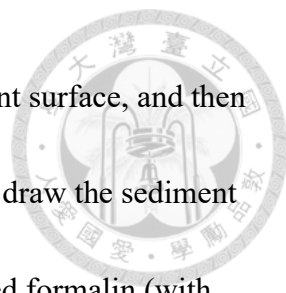
the sediment to take 2 ml of the subsample. Then, the subsample was added to a 15 ml polyethylene centrifuge tube which contained 2 ml of pre-filtered PBS solution. Later, 0.3 ml of 16% formaldehyde was also added to the centrifuge tube until the sample reached a concentration of 2% formalin, and then it was stored in a 4°C fridge. In the lab, the sediment samples were further diluted by 500- or 1000-fold in PBS solution depending on the number of potentially interfering particles, treated with Triton-X detergent to loosen attached or aggregated cells, centrifuged through Nycodenz®, and then placed on a 0.2 µm pore size filter. The filtered sample was stained with SYBR Green and DAPI stains and mounted on a slide for enumeration (Deming and Carpenter, 2008; Kallmeyer et al., 2008). The prokaryote abundance was counted using epifluorescence microscopy. The cellular dimensions in each slide were estimated from an image taken by a CCD digital camera. By assuming a conversion factor of 10 fg C per cell (Deming & Carpenter 2008), the stock of bacterium OC was calculated as,

$$\# \text{ bac} \cdot 10 \text{ fg C} / (\text{volume}(\text{cm}^3) \cdot \text{depth} (\text{cm})) \quad (\text{eq. 1})$$

and finally converted to the unit of mg C/ m².

2.3.2 Meiofauna biomass

A cutoff 10 ml sterile syringe (i.d. 15 mm) was used to take the subsample from the top 5 cm of sediment, as suggested by Montagna et al. (2017). When taking the



meiofauna samples, the syringe plunger was held fixed at the sediment surface, and then the barrel was pushed into the sediments to create vacuum suction to draw the sediment samples into a 250 ml specimen jar. An equal volume of 10% buffered formalin (with borax, sodium tetraborate $\text{Na}_2\text{B}_4\text{O}_7$, and 1 g/l Rose Bengal) is added to the sediment sample to make a concentration of 5% formalin. Later in the lab, the sediment samples were wet sieved through a 1000 μm sieve with a 40- μm sieve underneath, and then transferred to 70% ethanol. The meiobenthos specimens were extracted from the sediments using Ludox HS40 solution (gravity = 1.18 g/ cm^3) after centrifuging at 8,000 rpm for 10 min with 3-times repeat (Danovaro, 2009; Montagna et al., 2017). Then the meiofauna was enumerated into major taxonomic groups under a high-power stereomicroscope (Olympus® SZX16; 0.7-11.5 X zoom). The body volume of meiofauna specimens was calculated with the formula:

$$V = L \cdot W^2 \cdot C \text{ (eq. 2),}$$

where V was the volume, L was the length, W was the width, and C is the taxon-specific conversion factors (Warwick and Gee, 1984). The biovolume was converted into wet weight by assuming a specific gravity of 1.13 (Warwick and Gee, 1984) and converted into OC using the conversion factor of 12% (Baguley et al., 2004). Finally, the meiofauna OC stock was divided by the sampling area and then converted to the

unit of mg C/ m².

2.3.3 Macrofauna biomass



Once the sediment cores were recovered, the supernatant water above the sediment surface was siphoned carefully through a 300- μ m sieve. Then, the top 10 cm of the sediments, where the macrofauna may dwell, were extruded by an extruder and washed with 5 μ m filtered seawater through the same 300- μ m sieve as suggested by Montagna et al. (2017). Later, the remaining sediment was kept in a 250 ml specimen jar with an equal volume of 10% buffered formalin (with borax, sodium tetraborate Na₂B₄O₇, and 1 g/1 Rose Bengal) to fix the samples for at least 24 hours. Macrobenthos samples were sorted and enumerated into major taxonomic groups using a stereo sorting microscope (Olympus® SZ61; 0.67-4.5X zoom) and then permanently-preserved in 70% ethanol. The body volume of macrofauna specimens was estimated by the same length-width relationship as eq.2.

For the common taxa such as polychaetes and nematodes, the conversion factor was from the previous study (i.e., Warwick and Gee, 1984). For the taxa whose conversion factors were unavailable, the biovolume was calculated from length and width using the nearest geometric shapes (e.g., cone shape: scaphopods; cylinder shape: aplacophorans, sipunculans, and nemerteans; ellipsoid shape: ophiuroids and asteroids.)

The biovolume was also converted into wet weight by assuming a specific gravity of 1.13 (Warwick and Gee, 1984) and then multiplied by 4.3 % to obtain the organic carbon content (Rowe, 1983). Finally, the OC stock of macrofauna was divided by the sampling area and then converted to the unit of mg C/ m².

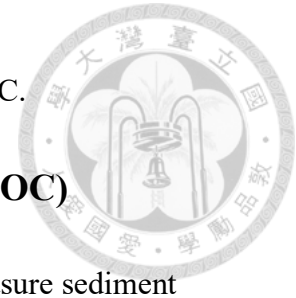
2.4 Sampling procedures of non-living component of OC

2.4.1 Detrital organic carbon

Surface sediment was taken and stored in 50-ml centrifuge tube in -20°C freezer. In the lab, the sediment samples were freeze-dried for 3 to 5 days to measure wet weight (before freeze-drying), dry weight (after freeze-drying), water content, and porosity. An aliquot of freeze-drying sediment (~0.4 g) was acidified with HCl to remove calcium carbonate, combusted at 1000°C with pure oxygen, and analyzed with a Flash EA 1112 elemental analyzer for total organic carbon (TOC).

Before calculating the stock of detritus OC, the core area (m²) was first converted to volume (m³) by multiplying the depth (i.e., 10 cm) at which the macrofauna may dwell. The volume was then converted into mass by assuming the sediment bulk density of 2.65 (g/ cm³) (Eleftheriou, 2013). Finally, the OC stock was sediment mass multiplying TOC content (%) and divided by the sampling area to the unit of mg C/ m². Because only a small aliquot of sediment was used in TOC measurement, the sample

likely missed the larger fauna and was considered only containing OC.

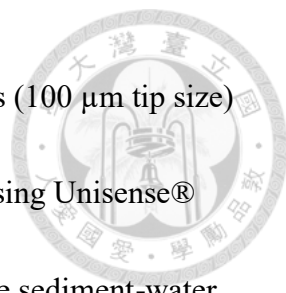


2.5 Sediment community oxygen consumption (SCOC)

Three core tubes recovered from a megacorer were used to measure sediment community oxygen consumption (SCOC). The incubation was taken place in a dark, temperature-controlled water bath. If the supernatant water was insufficient to fill the core tube, the sediment core was carefully filled with bottom water collected from the CTD rosette. The core tube was then closed hermetically with a custom-built HDPE lid, and air bubbles were carefully removed. A magnetically driven impeller (60–80 rpm) attached to the core lid gently circulated the water during the incubation. Then, the sediments were acclimated for approximately 6 hours until the flocculent materials settled and the overlying water was clear. The dissolved oxygen concentration was measured every 8 hours with a miniature oxygen optode (i.d. 2 mm) through a sampling port on the core lid (PreSens® Microx 4). According to Glud (2008), the dissolved oxygen concentration was measured until it decreased by 15% of the initial concentration to prevent hypoxic stress. The fluxes of oxygen into or out of the sediments were calculated as:

$$\text{Flux} = \frac{[\text{Change in concentration}] \cdot V}{\text{Core area} \cdot \text{Time}} \text{ (eq. 3),}$$

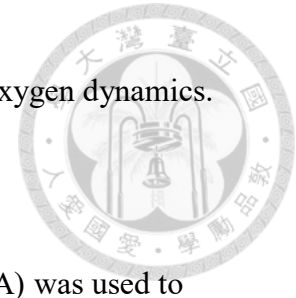
where V was the volume of overlying water.



After shipboard incubation, one to three oxygen microelectrodes (100 μm tip size) were inserted simultaneously into sediments at 100 μm increments using Unisense® Field Microprofiling System. The diffusive oxygen fluxes through the sediment-water interface were calculated according to Fick's first law of diffusion (Berg et al., 1998; Glud, 2008). The oxygen concentration profile, sediment porosity, initial concentrations in the overlying water, and oxygen diffusion coefficient corrected by temperature were inputs to calculate diffusive oxygen fluxes using Unisense® Profile software. The oxygen penetration depth (OPD) was determined by the depth of dissolved oxygen concentration $< 5 \mu\text{mol/l}$. The diffusive carbon remineralization was calculated by the flux of oxygen in moles multiplying a respiratory quotient of 0.85 (Rowe et al., 2008).

In general, the sediment oxygen profile concentration measures the diffusive oxygen utilization (DOU) mainly contributed by aerobic respiration of microorganisms through slow diffusion of oxygen molecules. In contrast, the sediment incubation experiment measures the total oxygen utilization (TOU, also known as sediment community oxygen consumption or SCOC). The TOU not only accounts for DOU but also for benthos' respiration and the benthos-mediated oxygen utilization (BMU) through their bioirrigation and bioturbation activities (Glud, 2008; Lichtschlag et al., 2015; Wenzhöfer and Glud, 2004). Therefore, the difference between the TOU and

DOU is the BMU, characterizing benthos' contribution to sediment oxygen dynamics.



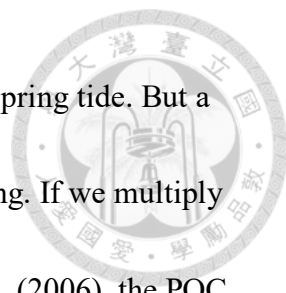
2.6 Statistical analysis

Mixed effect permutational analysis of variance (PERMANOVA) was used to examine the effects of habitat (canyon v.s. slope) and season (spring, summer, and fall) on the biotic, abiotic carbon stocks and oxygen utilization. The assumption of homogeneous variance was examined by permutational analysis of dispersion (PERMDISP, Anderson et al., 2008). Except for the calculated BMU, the number of permutations for each test was set to 9999. The number of permutations was set to 999 for BMU due to the small sample size. All statistical tests used α -value = 0.05. Statistical analyses used software R (R Development Core Team 2020), and PERMANOVA and PERMDISP were conducted with the "vegan" package.

2.7 Rain of POC

To balance the sediment carbon budget, accurate estimates of the sinking POC flux are essential. Traditionally, sediment trap has been widely used in oceanographic studies to capture vertically sinking materials (Giering et al., 2014; Steinberg et al., 2008). However, the local conditions, such as hydrodynamic variables and the sinking particle characteristics, can lead to erroneous POC flux estimates (Baker et al., 2020).

In the GPSC, Liu & Lin (2004) and Liu et al. (2006) reported that the estimated



mass flux collected by sediment traps exceeded $700 \text{ g/ m}^2/\text{ d}$ during spring tide. But a lower value (c.a. $200 \text{ g/ m}^2/\text{ d}$) was observed before spring tide passing. If we multiply this value with the TOC content (c.a. 0.4-0.6 %) reported by Liu et al. (2006), the POC flux would be 800 to $4200 \text{ mg C/ m}^2/\text{ d}$. Considering the ignored process before and after POC settled down on the seafloor and the huge variations between the POC fluxes and organic carbon accumulation rates estimated by different techniques, the organic carbon demand determined by the food web model can provide an alternative estimate of POC flux to the seafloor.

2.8 Burial rates of organic carbon

The sedimentation rates of the Gaoping continental shelf and canyon system were studied by Huh et al. (2009) and Hsu et al. (2014). Therefore, our model used the reported sedimentation rates and burial efficiency as *in situ* data. For GS1, the average mass accumulation rate in the upper slope region ranging from 200 to 600 m water depth was $0.43 \text{ g/ cm}^2/\text{ yr}$. In contrast, a higher mass accumulation rate ($> 1.0 \text{ g/ cm}^2/\text{ yr}$) was estimated in the GPSC at a water depth of 300 m (GC1). With this information, we converted the accumulation rate into the unit of $\text{mg C/ m}^2/\text{ d}$ and then multiplied by TOC content (%) measured in two areas, respectively.

2.9 Linear inverse model formulation



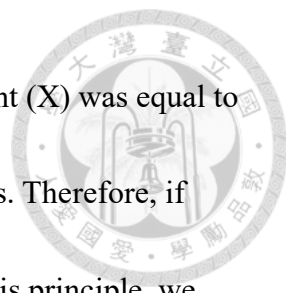
2.9.1 Structure

The linear inverse model starts with choosing relevant abiotic and biotic compartments and specifying the links between them (Fig. 2; Table 2). We assumed that the influx of TOC was a complex assemblage of organic matters derived from the water column with a portion of energy flowing out of the sedimentary system through the process of burial and/or export (orange flows). Then, the general idea was that the predators of each size class preyed on organisms of the same and smaller size classes. For instance, the black flows assumed that bacteria fed only on detrital OC; meiofauna fed on bacteria and detrital OC; macrofauna fed on meiofauna, bacteria, and detrital OC. The grey flows indicated that carbon was lost as feces and was consumed by benthopelagic/pelagic predators (Fig. 2). In this LIM model, the compartments with orange color were part of the food web model. In contrast, the compartments with blue color were only considered carbon influx or efflux but were not directly modeled.

2.9.2 Mass balances

A broadly accepted physical constraint is that mass is conserved for each chemical element, and this mass balance principle is the backbone of the food web model. First, the mass balance could be written in the general form:

$$\frac{dx}{dt} = \sum f_{in} - \sum f_{out} \quad (\text{eq. 4}),$$




indicating that the temporal mass change ($\frac{dX}{dt}$) of a compartment (X) was equal to the difference between the incoming (f_{in}) and outgoing (f_{out}) flows. Therefore, if $\sum f_{in}$ was larger than $\sum f_{out}$, X would increase in time. Based on this principle, we could derive the mass balance equations of all the compartments with the assumption that all the compartments were invariant in time:

$$\frac{dCompartment}{dt} = \sum f_{in} - \sum f_{out} = 0 \quad (\text{eq. 5})$$

Furthermore, this mass balance principle could also be applied to organisms' physiological behaviors. For example, when organisms ingest food, only part of the food is assimilated, and the rest is expelled as feces. The assimilated food is used to maintain its basal metabolism, growth, and reproduction. For heterotrophic organisms, the energy needed for growth and maintenance was paid by respiration. Thus, we could write this process as:

$$\frac{dC}{dt} = \text{Growth} = \text{ingestion} - \text{defecation} - \text{respiration} - \text{mortality} \quad (\text{eq. 6}),$$


Where C is the biomass of the organism, and $\frac{dC}{dt}$ is its growth rate. This mass-balance equation states that the biomass changes due to the difference between feeding and loss terms. Note that the balance of all food web compartments was tightly linked. For instance, if species A feeds on species B, not only does an increased flux flow into A, but a loss of the same magnitude of flux flows out of B. As a result, the direction of



the flows matters, and we could take the mass-balanced equation as sums and subtractions of these unknown quantities of flows. We classified this linear mass balance equation as the "equality equation". It could be expressed with matrix notation in the general form: $\mathbf{A} \cdot \mathbf{x} = \mathbf{b}$, in which \mathbf{A} was a coefficient matrix, \mathbf{x} was a vector consisting of unknown flows, and \mathbf{b} was a vector consisting of changed rates of the component, and the flows are non-negative quantities, $\mathbf{x} \geq \mathbf{0}$.

2.9.3 Constraints

On the other hand, the physiology and behavior of organisms impose a limitation on their feeding and growth rates with upper and lower bounds. For example, when organisms search for food, the encounter rate and the external handling time determine the maximal foraging capacity (Holling, 1966). Also, physiological and digestive constraints regulate the process of assimilation of ingested food. Therefore, animals can only process a finite amount of food per unit per time. These maximum rates imposed an upper bound on ingestion flows, providing important constraints on the magnitudes of the grazing flows in the model. Similarly, respiration flows are restricted by allometric rules (e.g., Mahaut et al., 1995). The minimal basal respiration rate required to sustain metabolism was imposed as lower bounds. Other physiological constraints restricted the relationships between flows. For example, growth efficiency was defined



as the ratio of secondary production to assimilated food, which is suggested to be 60-80% (Calow, 1977; Schroeder, 1981). These constraints can also be transformed into a matrix equation with inequality: $\mathbf{G} \cdot \mathbf{x} \geq \mathbf{h}$, in which \mathbf{G} was a coefficient matrix, \mathbf{x} was still an unknown-flows vector, \mathbf{h} was a vector comprising constraints. Most of these constraints could be extracted from literature.

Here, we applied the four most used constraints in LIM studies (van Oevelen et al., 2006; Stratmann et al., 2018) to our model, including respiration (R), assimilation efficiency (AE), production (P), and net growth efficiency (NGE).

For meiofauna and macrofauna, R was defined as the sum of maintenance respiration (biomass-specific respiration, MR) and growth respiration (associated with growth processes, e.g., synthesis of new structures in growth, GR). The maintenance respiration was taken proportional to 1% at 20°C of the biomass per day (Fenchel, 1982; Nielsen et al., 1995), and then corrected with a temperature correction factor: T_{lim} , which could be calculated as,

$$T_{lim} = Q_{10} \cdot \exp\left(\frac{T - 20}{10}\right) \quad (\text{eq. 7}),$$

where $Q_{10} = 2$, T was the bottom water temperature for each site. Q_{10} is a measure of temperature dependence based on the process or reaction. For most biological systems, this value is ~2 to 3. Therefore, the relationships of respiration could

be expressed as:

$$MR = 0.01 \cdot Tlim \cdot Stock \text{ (eq. 8),}$$

$$GR = R - MR \text{ (eq. 9).}$$

AE was calculated as,

$$AE = (I - F)/I \text{ (eq. 10),}$$

where I was the ingested food and F was the feces (Crisp,1971). The minimum-maximum range was set from 0.456 to 0.699 for meiofauna (Conover 1966) and from 0.6 to 0.7 for macrofauna (Loo & Rosenberg 1996).

The secondary production (P) was calculated as,

$$P = I - F - GR \text{ (eq. 11),}$$

$$P/B = \frac{I - F - GR}{Stock} \text{ (eq. 12).}$$

The P/B ratio for meiofauna was set between 0.0009 and 0.0493 (Fenchel, 1982; Fleeger and Palmer, 1982), while for macrofauna is set between 0.0008 and 0.0048 (Stratmann et al., unpublished). On the other hand, bacterial growth efficiency (BGE) was defined as the amount of new bacterial biomass produced per unit of assimilated OC, and it could be used to relate to the production and respiration of bacteria (del Giorgio & Cole,1998). The range of BGE was set from 0.02 to 0.61.

Finally, NGE was calculated as (Clausen and Riisgård, 1996),



$$NGE = \frac{I-F-GR}{I-F} = \frac{P}{P+GR} \quad (\text{eq. 13}),$$



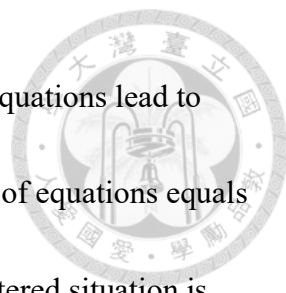
The minimum-maximum range was set from 0.3 to 0.5 for meiofauna (Herman & Heip, 1985; Banse & Mosher, 1980; Herman et al., 1983; 1985), and from 0.6 to 0.72 for macrofauna (Navarro et al., 1994, Nielsen et al., 1995).

The data types mentioned above are derived from the general principles applied to most ecosystems; however, the *in situ* data is still necessary to deal with a food web model in a specific location. Because of the valuable information from site-specific measurements, this type of data is generally implemented as equality equations: $\mathbf{E} \cdot \mathbf{x} = \mathbf{f}$, where \mathbf{E} was a coefficient matrix, \mathbf{f} represents the vector that contains *in situ* data.

In our model, besides the estimated biomass were the stocks of organism compartments, the SCOC data served as directly measured flows. As Mahaut et al. (1995) suggested, the value of bacterial carbon remineralization (the flow of bacteria to DIC in our model) represented about 30% of the TOU. All the constraints implemented in our models are summarized in Table 3.

2.10 Model Solution: Likelihood method

To achieve the final model, we combined three types of data, including mass balance equations, physiological constraints, and *in situ* data. The solution of this model was a set of flow values (\mathbf{x}). Depending on the number of equations and the numbers of



the unknowns, different methods of solution were used. Ideally, the equations lead to only one set of solutions that perfectly fits the data when the number of equations equals the numbers of the unknowns. However, the most commonly encountered situation is that the number of equations is far less than the number of unknowns. As a result, there is no unique solution set, whereas an infinite number of valid solution sets exist, creating a multidimensional solution space. Earlier modeling studies usually selected one solution from this solution space. The principle of parsimony, the flow set with the minimal sum of squared value, has often been applied as the selection criterion (Vézina and Platt, 1988). However, the parsimonious food web model usually takes extreme values to meet the criterion (Difendorfer et al., 2001; Kones et al., 2006). Alternatively, a likelihood approach based on Markov Chain Monte Carlo (MCMC) algorithm has been developed, which calculates the mean values and standard deviations of the flows from the possible solution sets (Kones et al., 2006). The standard deviation was artificially set to a $\pm 2\%$ error margin to iterate until the convergence of solution sets. We used *LIM* package (Soetaert and Herman, 2009; van Oevelen et al., 2010) in R (R Development Core Team 2020) to set up and solve the conceptual food-web model (Fig. 2) using MCMC and likelihood approach.

2.11 Network indices of ecosystems

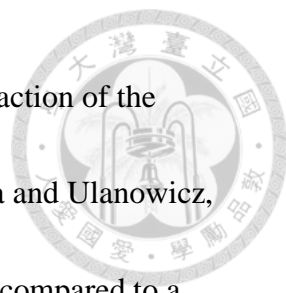
After *LIM* solved the food web model, we conducted the network analysis to better understand the structural properties and energy transformations in the ecosystem.

Several network indices were calculated from the outputs of LIM to examine the food-web functioning with uncertainty estimation (Kones et al., 2009). Network indices were robust estimators of food web function despite the uncertainty (i.e., uncontrollability and unpredictability) in the exact value of food web flows.

Considering our simplified model, we only used three types of network indices which were widely calculated in deep-sea LIM food web studies, including (1) general indices: Total system throughput ($T_{..}$), Total system throughflow (TST), and Total system cycled throughflow (TST_C); (2) pathway analysis: Finn's cycling index (FCI); (3) network uncertainty: Average mutual information (AMI).

$T_{..}$ is a measure of the growth and size of the system, obtained by summing all flow magnitudes, while the total system throughflow (TST) is the sum of compartmental throughflows. These two indices infer the general properties of the food web system. That is, the more material or energy flowed through the system, the larger the value of TST and $T_{..}$ would be.

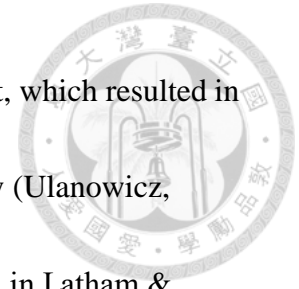
The cycled portion of the total system through flow (TST_C) was the sum of cycled flow in all through flows (Finn, 1976). The proportion of TST_C in the TST was



referred to as the Finn cycling index (*FCI*), which summarized the fraction of the material/energy that was generated by the recycling process (Allesina and Ulanowicz, 2004). *FCI* also denoted how much further a unit of inflow traveled compared to a straight-through flow during a cycling process (Finn, 1976). For example, if the straight pathway was 10 and $FCI = 0.5$, meaning that an average unit of inflow travels 15 (i.e. $10 \cdot (1 + 0.5) = 15$) because it cycled through the system. *FCI* helps understand the stability, stress, and structural difference in different models. The more cycling, the more efficiently input matter/energy is distributed in the system. For a valid comparison between systems, the food webs needed the same structure and level of organization. (Finn, 1976)

Finally, the index average mutual information (*AMI*) based on information theory measures the average amount of constraint placed on a single unit of flow anywhere in the network (Ulanowicz, 1997). To put it simply, *AMI* is a measure of uncertainty regarding the energy/material exchange in the network. For example, if the chances of energy/material flow from any particular compartment to any potential compartment are equal, the uncertainty of flows in the network maximizes. If all energy/material from a particular component flow to only one recipient, the uncertainty of the source will no longer exist. Ulanowicz (1980, 1986, 1997) hypothesized that an ecosystem form

greater mutual constraints as autocatalytic loops during development, which resulted in a higher *AMI* value in a trophic specialization or climax community (Ulanowicz, 2004). More details on the derivation and calculation could be found in Latham & Scully (2002), Ulanowicz (2004), and Kones et al. (2009). A summary of nomenclature (Table 4) and calculation algorithms are included in Table 5. All the network indices will be directly calculated in R using R-package NetIndices (Kones et al., 2009).



3 Results



3.1 Environment data

3.1.1 CTD

The temperature profile was presented in Fig. 3. The average bottom water temperature was 13.54°C in GC1 and 13.90°C in GS1. As a result, the calculated *T_{lim}* equaled 1.05 and 1.09 for GC1 and GS1, respectively (Table 6). These *T_{lim}* values were important correction factors controlling the biomass-specific maintenance respiration in the LIM model. While the bottom water density, salinity, and temperature were comparable between GC1 and GS1, the profiles of light transmission showed a notable distinction (Fig.4). For instance, little to no light transmission was observed near the GC1 seafloor throughout the sampling cruises, indicating the presence of a persistent benthic nepheloid layer (BNL) over a long period. This result coincided with the observation in Liu et al. (2010), who suggested a 100 m thick BNL with high suspended sediment concentration (SSC) in GPSC based on mooring observations.

3.2 Stock of the non-living component of OC

3.2.1 Detrital organic carbon

For the abiotic detritus OC stock, the average TOC content in the upper 10 cm of the sediment was 0.39 % and 0.53% in GC1 and GS1, respectively. This value fits in the

range of TOC content (c.a. 0.3-0.75 %) reported previously in the southwestern margin of Taiwan (Kao et al., 2006; Hsu et al., 2014).



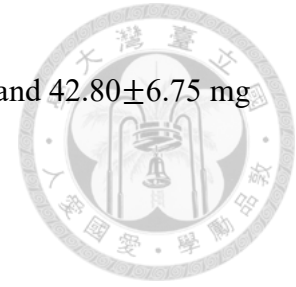
Considering the seasonal variation in sediment fluxes (e.g., the monsoon effect on hydrodynamics, Lee et al., 2009), the seasonality (if present) of sediment organic carbon (OC) stock was first examined. Results from PERMDISP showed that the assumption of homogenous variation was not violated between habitat groups or season groups (Table 7, Habitat, $p=0.1051$; Season, $p=0.2263$). The seasonal variation in the mean OC was also not evident (Table 7, PERMANOVA, $p=0.8816$), but the sediment OC stock in the GS1 was significantly higher than in the GC1 (Table 7, PERMANOVA, $p=0.0003$). The sediment OC content in each cruise was shown in Fig. 5. Since the seasonal signal was not evident, the average OC was taken for the input of the LIM model, i.e., $350270 \pm 104003350, 270 \pm 104,003.4$ mg C/ m² for GC1 and $524,425.7 \pm 34,800.15$ mg C/ m² for GS1.

3.3 Stocks of the living component of OC

3.3.1 Prokaryote biomass

Prokaryotes were only sampled during the cruise OR1_1190. Figure 6 shows each of the ten replicates from GC1 and GS1. In addition, the prokaryote biomass in GC1 was significantly higher than in GS1 (Table 8, t-test, $p<0.001$). For the model input, the

average bacteria biomass was set to 65.31 ± 12.74 mg C/ m² in GC1 and 42.80 ± 6.75 mg C/ m² in GS1, respectively.



3.3.2 Meiofauna biomass

Among the meiofauna taxa, nematodes were always the most abundant group, accounting for more than 90% of abundance (Giere, 2009; Danovaro, 2012). The meiofauna abundance with and without nematodes was presented in Fig. 7. The total meiofaunal abundance in GS1 was about two times higher than in GC1. Besides, the meiofaunal composition differed between the two sites. Without nematodes, copepods were the most abundant group in GC1. In contrast, after removing nematodes, multiple groups dominated the GS1, including copepods, polychaetes, kinorhynchs, and turbellarians.

Fig. 8 shows the consolidated biomass from all taxa groups. The PERMDISP indicates that the variation between habitat and season groups might not be homogeneous (Table 9, Habitat, $p=0.0001$; Season, $p=0.0001$). The PEMANOVA shows that the biomass in GS1 was significantly higher than GC1 (Table 9, PEMANOVA, $p=0.0002$). Regardless of the habitat or seasonal effect, it should be noted that there were only three samples for each site and only one sampling cruise for each season. Given the limited sample size, the average meiofaunal biomass was used in the LIM

model, which is 1.49 ± 1.53 mg C/ m² in GC1 and 33.39 ± 26.48 mg C/ m² in GS1.

3.3.3 Macrofauna biomass

Macrofauna sampling was conducted for eight cruises across the two habitats. In general, polychaetes account for half of the total abundance and around one-third to half of the total species richness in macrofauna communities (Gage and Tyler, 1991). In our sampling, polychaetes dominated the macrofauna assemblages in all cruises (Fig. 9), but the community on the slope was relatively more diverse than in the canyon.

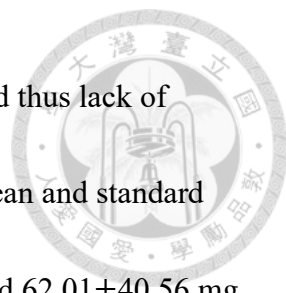
Macrofaunal biomass in two sites was calculated and presented in Fig. 10. Note the difference in the scale of the y-axis. The biomass was about an order of magnitude lower, and abundance was about five times lower in the GC1 than in GS1. The PERMDISP showed a significant difference in variance between habitat groups but not between season groups (Table 10, PERMDISP, Habitat, $p=0.0001$; Season, $p=0.298$). In addition, there was a significant biomass difference between habitats but not between seasons (Table 10, PERMANOVA, Habitat, $p<0.0001$; Season, $p=0.1906$). Consequently, the average biomass was taken with the values of 3.65 ± 7.70 mg C/ m² for GC1 and 80.20 ± 66.10 mg C/ m² for GS1.

The standing stocks of all compartments for the model were presented in Table 5, while only the mean values were used for the LIM model input. Except for the bacteria,

the OC contents in standing stocks were higher in GS1 than in GC1. The stock of non-living components constituted the largest part of OC in both sites, which was four orders of magnitude higher than that of living components. The meiofauna and macrofauna biomass and richness were remarkably depressed in the canyon due to the physical disturbances (Liao et al., 2017; 2020). In contrast, the larger group of macrofauna had greater biomass than meiofauna on both the slope and canyon.

3.4 Oxygen utilization

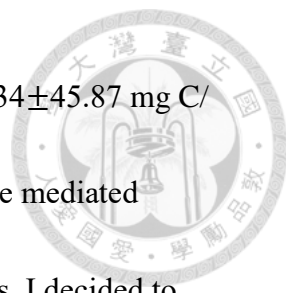
The TOUs from the incubation experiments were converted to the carbon unit (Fig.11). The means and standard deviations were 72.59 ± 16.60 mg C/ m²/ d for GC1 and 53.38 ± 4.06 mg C/ m²/ d for GS1 (Table 11). Moreover, the measured DOUs representing aerobic respiration of bacteria showed little difference between the two sites, with values of 19.81 ± 22.73 mg C/ m²/ d in the canyon head and 11.68 ± 8.15 mg C/ m²/ d on the slope (Table 11). Note that the standard deviations were greater than or closer to the mean value in both sites, suggesting wide variations between each cruise. Surprisingly, TOUs were not different between GC1 and GS1 (Table 12, PERMANOVA, Habitat, $p=0.2867$). Despite the higher bacterial biomass, the DOU in GC1 was not statistically different from GS1 (Table 13). The other partition of oxygen utilization was BMU, calculated as the difference between TOU and DOU. It was



presumed that BMU was lower in GC1 because of lower biomass and thus lack of benthos-mediated oxygen utilization. Nevertheless, the calculated mean and standard deviation values of BMU were 62.34 ± 45.87 mg C/ m²/ d in GC1, and 62.01 ± 40.56 mg C/ m²/ d in GS1 (Table 11), showing no statistical difference between the two habitats (Table 14). Note that BMUs were calculated only when both the TOUs and DOUs were measured in the same cruise. This mean value was first derived from the difference between TOU and DOU and then taken for the average. These oxygen utilization rates were combined into LIM model input as the constraints of respiration. TOUs were assigned to be the total respiration (i.e., the sum of all the respiration flow), and DOUs were set as the flow of bacterial respiration (the grey flow of Bacteria→DIC in Fig. 2). Finally, BMUs were specified as the combined flow of Meiofauna→DIC and Macrofauna→DIC in Fig. 2.

3.5 Model results

The first attempt to solve the model, which combined the OC stocks and default setting, was unsuccessful, indicating that some of the data included in LIM conflicted with each other. The main problem arose from the contradiction between low biomass and relatively high oxygen utilization. For example, the sum of maintenance meiofauna and macrofauna respiration in GC1 would be $1.05 * 0.01 * (1.49 + 3.65) = 0.05397$



mg C/ m²/ d, which was far less than the constraint of BMU (c.a. 62.34±45.87 mg C/ m²/ d). The BMU comprised not only benthos' respiration but also the mediated utilization through their bioturbation by definition (Glud, 2008). Thus, I decided to remove BMU as the constraint of meiofaunal and macrofaunal respiration. The respirations of benthos (Meiofauna→DIC and Macrofauna→DIC in Fig. 2) were left to be determined by the models. The *in situ* measurements of oxygen consumptions were still important site-specific field data, so I decided to retain the constraints on bacterial respiration (Bacteria→DIC) but modify it to 30% of TOUs (Mahaut et al., 1995) instead of directly using the measured DOUs.

The other unknown awaited to be solved was the rain of POC. To solve this disagreement, the mass accumulation rates reported in Huh et al. (2009) were converted to carbon units by multiplying the TOC contents, which were 106.92±30.994 mg C/ m²/ d in GC1 and 61.99±4.81 mg C/ m²/ d in GS1. The mean values plus and minus one standard deviation were set as constraints for the minimum and maximum carbon burial, respectively (flow Sediment→Burial, Fig. 2). After setting the constraints of burial, the minimal burial efficiency (i.e. 24%; Hsu et al., 2014) was retained to back-calculate the POC input (POC→Sediment in Fig. 2). Henceforward, the LIM not only solves the unknown flows between the compartments but gives a more comprehensive view of

carbon demands in the two modeling systems.

3.5.1 LIM result of GC1



Fig. 12 showed the results solved by LIM modeling with different algorithms. The black dots in Fig. 12 marked the values solved by the most parsimonious method, whereas the pink dots labeled the mean values from MCMC algorithms with 10,000 iterations. Except for the interaction flow between meiofauna and macrofauna (MEI→MAC), all solutions solved by the most parsimonious method underestimated the flow quantity. Note that the x-scale was expressed in exponential form with base 10.

MCMC-solved flows in the GC1 model could be generally separated into three parts according to the order of magnitude of the mean values (Fig. 13 and Table 16). First, the mean value for POC flux was 131.08 mg C/ m²/ d. The burial export occupied about 88% of the POC input (115.77 mg C/ m²/ d). Both fluxes were directly related to the detritus stock. The second-largest flow values were those related to bacteria and the interactions between bacteria and the environment, including SED→BAC (24.65 mg C/ m²/ d), BAC→SED (9.33 mg C/ m²/ d), and BAC→DIC_W (15.13 mg C/ m²/ d). Although the remaining flows were all less than 1 mg C/ m²/ d, we could still differentiate the flows related to meiofauna and macrofauna stocks by the mean values, which the meiofauna-related flows were an order of magnitude higher than the

macrofauna-related flows.

3.5.2 LIM result of GS1

Similar trends were found in Fig. 14 and Table 17. Most of the solutions by the most parsimonious method were lower than that solved by the MCMC algorithm, except for MEI→MAC and the burial flux (SED→EXP_S). The estimated burial fluxes were similar between the two different methods. The estimated POC flux was 78.95 mg C/ m²/ d in the GS1 b MCMC method, with about 80% of POC flux flowing out of the system (SED→EXP_S, 63.23 mg C/ m²/ d). On the other hand, the interaction flows between bacteria and environment in GS1 were not as strong as those in GC1. Instead, the metazoan contribution increased due to higher mean flows between the compartments of meiofauna and macrofauna. Likewise, in GS1, the meiofauna-related flows were an order of magnitude higher than those related to macrofauna.

Because the two food webs share the same structure, the LIM results can be compared directly. For instance, the values of the internal flows (black flows in Fig. 14) representing biological interactions in GS1 were higher than GC1, corresponding to the higher biomass of meiofauna and macrofauna on the slope. Although the bacteria stock accounted for a larger proportion of the biomass in the canyon compared to the slope, the energy flows between bacteria and sediment stock were not distinctly different

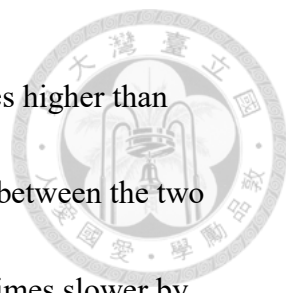


between the two habitats. On the other hand, the flow values of biotic outputs (i.e., energy loss through predation and respiration) were reasonably consistent with the standing stocks. Finally, the ratio of the burial flux to input flux, representing the fraction of unused OC which flowed out of the system to reach the balanced steady-state, was about 8% higher in the canyon head than on the upper slope.

3.6 Turnover rates

The turnover rate was calculated by dividing the carbon stock with measured oxygen consumption (i.e., TOU) or model estimated flows, respectively (Table 15). For example, the turnover rate of total carbon was calculated as the sum of detrital and biotic carbon divided by observed TOU or by the sum of flows $BAC \rightarrow DIC$, $MEI \rightarrow DIC$, and $MAC \rightarrow DIC$, which corresponds to the definition of TOU.


The measurement and modeling results showed that organic carbon turnover was much slower in GS1. The carbon turnover based on TOU was about 1.5 times slower in GS1 than in GC1, and the carbon turnover based on model results was about five times slower than the turnover based on TOU measurement for both sites. Bacteria turnover rates in two habitats calculated by different methods were almost consistent, with 3.3 to 4.3 days in GC1 and 3.7 days in GS1. However, the turnover time for meiofauna and macrofauna estimated by the two methods were distinctly different. In GC1, the



turnover time estimated by observed (calculated) BMU was 550 times higher than which calculated by the model. Though the turnover time difference between the two estimated methods in GS1 was not as vast as in GC1, it was still 40 times slower by model estimation. The turnover time was much shorter in GC1 with the calculation of BMU (GC1: 0.08 day; GS1:1.83 day). In contrast, the turnover times estimated by models were much longer in GC1 (GC1: 44.64 day; GS1:42.06 day).

3.7 Network indices results

In addition to comparing the flow values directly, network indices were calculated to examine the food web functioning. Selected indices were calculated for the complete set of LIM solutions (10,000 solutions for each site) and compared between canyon and slope. The distributions of calculated network indices values in the two habitats were plotted in Fig. 15, showing that the median value of the $T_{..}$ and TST were higher in the food web of GC1 ($T_{..}$: 295.13 mg C/ m²/ d; TST : 164.62 mg C/ m²/ d) than in that of GS1 ($T_{..}$: 203.92 mg C/ m²/ d; TST : 125.24 mg C/ m²/ d). TST_C , FCI and AMI were relatively lower in the canyon. Median values of FCI were 0.07 and 0.134 for the canyon and the slope, respectively. Median AMI values were not distinctly different between the two sites, with median values of 1.157 and 1.191 for GC1 and GS1, respectively.



Another way to determine if the indices differed between the two sites was to calculate the fraction of indices (from 10,000 solutions) from the GC1 was greater than GS1. For instance, when this fraction was 0.9, it implies that 90% of indices of GC1 were greater than those of GS1. When this fraction was 0.1, it implies that 90% of indices of GC1 were smaller than those of GS1. As defined in van Oevelen et al. (2011), the difference was considered highly significant when the fraction was greater than 90% or smaller than 10% (i.e., fraction <0.10 or >0.90). The difference was considered highly significant when the distinction was more than 95% (i.e., fraction <0.05 or >0.95). The comparison result was presented in Table 16. Only $T_{..}$ and TST were significantly higher in the canyon head, while FCI of GC1 was marginally significantly lower (fraction=0.1043).

4 Discussion



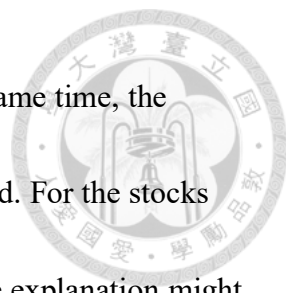
4.1 Carbon stock in different compartments

The estimated detritus carbon stocks are of the same order of magnitude as the previous submarine canyon studies by Rowe et al. (2008) and van Ovelen et al. (2011), being 760,000 mg C/ m² in the Mississippi canyon head (Rowe et al., 2008) and about 858,789 mg C/ m² at the Nazaré canyon head (van Ovelen et al., 2011). However, the quantity of detritus OC in the Gaoping Submarine Canyon head (350,270 ± 104003 mg C/ m²) is only half of the Mississippi or Nazaré canyons. In comparison with TOC content in the Mississippi Canyon (c.a. 1.9%), the average TOC content of GPSC are much lower (0.39%). The lower TOC content is directly linked to the lower quantity of detritus OC in the GPSC.

The bacteria samples were only collected in one cruise and thus could not be examined for seasonal variation. Generally, bacteria biomass and production can be affected by temperature, physical disturbance, substrate type, and sediment composition (Yamamoto and Lopez, 1985; Alongi, 1988); however, which factors may have stronger control is site-specific (van Duyl and Kop, 1994). For instance, seasonal variation in bacterial population and biomass was reported in the shallow slope site in the Baltic Sea (Meyer-Reil, 1983) and several locations ranging from 40 to 1570 m depth in the Cretan

Sea (Danovaro et al., 2000). The bacterial abundance and biomass are mainly influenced by the flux of labile organic compounds (Danovaro et al., 2000). Thus the bacterial stock may change in response to the food supply on the seafloor. Due to the lack of repeated sampling, it is impossible to determine whether seasonal variation in bacteria stock is present in the GPSC.

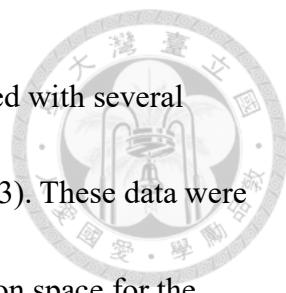
Given the impact of typhoons and the monsoon climate, rainfall is highly seasonal in the GPR basin (Liu et al., 2016). Distinct dry (winter) and wet (summer) seasons are attributed to the monsoon climate over the annual precipitation cycles. In addition, typhoons mainly occur in summer and early fall, which bring excessive rainfall. On top of the extreme precipitations, the steep topography, highly erodible drainage basin, and intense human activities lead to extremely high suspended-sediment load and fluvial discharges from the GPR during the wet season (Huh et al., 2009; Liu et al., 2013; Liu et al., 2016). On the other hand, frequent earthquakes also give rise to the development of turbidity currents (Hsu et al., 2008; Talling et al., 2013; Carter et al., 2014). For example, the 2006 Pingtung earthquake is reported to trigger submarine landslides and gravity flows in the lower GPSC and the nearby Fangliao Submarine Canyon (Hsu et al., 2008; Su et al., 2012). Therefore, assuming the seasonal difference in each carbon stock estimate may be reasonable. Nevertheless, among all the OC stock estimates, only



meiofauna showed a significant difference between seasons. At the same time, the limitation of the small sample size of meiofauna should be recognized. For the stocks without seasonal differences (e.g., detritus, macrofauna), the possible explanation might be related to the timing of sampling. The sampling cruises were mostly conducted in the dry spring (March to April) and fall (October to November). The OC stocks could have already recovered from presumably more perturbed wet seasons and thus without a notable seasonal difference. Since there is no apparent seasonal pattern in the OC stock estimates (Table 5), only the mean value from each component was used in the LIM model.

On the other hand, the current food web models lack larger size groups, such as megafauna and fish. Although the abundance and biomass of larger organisms are significantly lower and decrease rapidly with depth in the deep sea (Rex et al., 2006), the megafauna and fish can reach great densities in some study areas (e.g., Sibuet, 1977; Hecker, 1994; Fodrie et al., 2009). The high density of benthic megafauna invertebrates can affect the redistribution and quality of OM in the marine sediments (Smallwood & Wolff, 1999). Since no empirical stock data is available, the role of megafauna and fish in OM cycling (e.g., predation) is solved by food web models.

4.2 Implemented constraints and model limitations



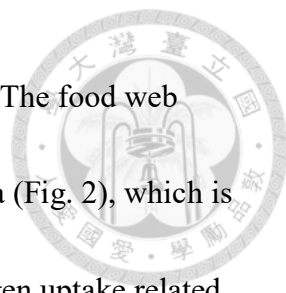
Except for the OC stocks, the modeled food webs were combined with several physiological and geochemical constraints from the literature (Table 3). These data were implemented as lower and upper bounds, creating the possible solution space for the algorithm to iterate and find a solution set of all flows. However, the input of these constraints creates two levels of uncertainty.

Firstly, the physiological constraints in our models all come from the reference, including *in situ* and laboratory experiments from other food webs in different areas, which were considered low quality (van Oevelen et al., 2010). Also, there is no constraint on benthic species that have been quantified in our study sites due to practical and technical difficulties in invertebrate physiological experiments. Despite the lack of site-specific physiological constraints, we used the reference constraints as other LIM studies did. For example, Stratmann et al. (2018) studied the abyssal plain food web of the Peru Basin; however, some physiological constraints of benthos in the food webs were derived from the shallow-water or intertidal species (e.g., Drazen et al., 2007; Koopmans et al., 2010). In other food web studies, the physiological constraint of the dominant species was used as the representative for that size group (De Smet et al., 2016). Another study separated the dominant species from the size group as an independent compartment (e.g., De Smet et al., 2016). Although these low-quality

constraints bring some uncertainty to our model results, the flow solution was still more convincing than without any constraint. For instance, the model solved the external flow to meiofauna and macrofauna predators (MEI→EXP_B and MAC→EXP_B in Fig. 2) with the only assumption of mass balance for the stock.

The geochemical constraints imposed on our models are site-specific, which can be considered high quality (van Oevelen et al., 2010). Although the sedimentation rates and sediment burial efficiency were not directly measured in GC1 and GS1, these values were extracted from the previous GPSC studies (i.e., Huh et al. 2009 and Hsu et al. 2014).

Although the measured DOU was not used as model input, the maximum modeled DOU flow was set to 30% of the measured TOU. In fact, the measured DOUs were 27% of the measured TOU in the GC1 and 22% of the measured TOU in the GS1, suggesting that the maximal constraints were reasonable. Surprisingly, the estimated DOU flows seem to increase the confidence level in the model. In GC1, the measured DOU was 19.81 mg C/ m²/ d, which was slightly higher than that resulting from LIM (15.13 mg C/ m²/ d); In GS1, the modeled DOU was 11.66 mg C/ m²/ d, which corresponded well to the direct measurement (11.53 mg C/ m²/ d). In addition, the magnitude of modeled TOU flows was the same as observed TOU, enhancing the credibility of LIM results.



The main difficulty lies in modeling the exact amount of BMU. The food web structure only considers the respiration of meiofauna and macrofauna (Fig. 2), which is overly simplified. The BMU includes faunal respiration and the oxygen uptake related to biological activities (Glud et al., 2003). Macrobenthos may modify diagenetic reactions, sediment-water exchange, and sediment composition (e.g., Aller, 1982, 1994) through their activities, such as feeding, burrowing, tube construction, bioirrigation (Jørgensen et al., 2005), and bioresuspension (Graf and Rosenberg, 1997). For example, Forster & Graf (1995) reported that two macrofauna species, *Callianassa subterranea* (Decapoda) and *Lanice conchilega* (Polychaeta), enhance TOU by 85% through their pumping behaviors in the shallow North Sea. The animal-induced changes in oxygen distribution are notoriously difficult to quantify and separate from their maintenance respiration. Therefore, the most straightforward and robust procedure to evaluate the fauna activities in mixed communities is to subtract DOU from TOU (Glud, 2008). Unfortunately, our biomass-based modeled BMU can only consider the respiration of fauna; thus, it turned out to be far less than the calculated results.

On the other hand, the total biomass of meiobenthos and macrobenthos was significantly higher on the slope, which explained the higher modeled BMU in the GS1. However, the observed (calculated) BMU was not distinctly different between the two

sites (GC1: 62.34 mg C/ m²/ d; GS1:62.01 mg C/ m²/ d), suggesting that the biomass may not predict bioturbation and thus calculated BMU. Glud et al. (2003) also found it challenging to relate faunal biomass to benthos-mediated oxygen uptake of a community undergoing seasonal changes. Therefore, macrobenthos biomass may not be a good proxy to estimate fauna-related oxygen uptake in natural benthic communities.

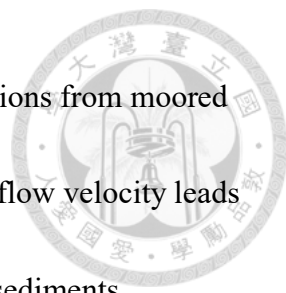
Liao et al. (2017) have examined the vertical distributions of macrofauna in the sediments. Their results indicated that the vertical positions of macrobenthos were significantly deeper in the sediment (down to 0.5-7.8 cm) of upper GPSC than the slope (down to 1-3.6 cm). Several polychaete families capable of burrowing deep into the sediment, including paraonids, cossurids, capitellids, and sternaspids, thrived in the canyon habitats (Liao et al., 2017). In contrast, the discretely motile, surface deposit, and suspension feeders (e.g., cirratulids, ampharetids, and spionids) dominated the slope sediment but diminished in the canyon. Therefore, the surprisingly high BMU value in GC1 may be caused by the active bioturbation behaviors of these subsurface deposit feeders.

TOU is the most reliable proxy of total benthic carbon degradation in marine sediments because it integrates aerobic activity, nitrification, and re-oxidation of reduced inorganic compounds (Stratmann et al., 2019). Therefore, the benthic activity

which responds to a variation in POC input should be reflected by a variation in TOU.


However, the vertical POC flux determined by sediment traps usually does not match the carbon demand of the benthic community (Smith, 1987). Smith and Kaufmann (1999) and Smith et al. (2016) reported a long-term discrepancy between food supply and demand in the Eastern North Pacific, with the POC fluxes contributing only around half of the TOU. Moreover, the imbalance between carbon supply and demand varied by region on the abyssal plain in the deep Arabian Sea (Witte & Pfannkuche, 1999). The sediment trap fluxes matched 50% of the benthic carbon demand in their southernmost station but only 20% in the westernmost station. These mismatches were mainly explained as the uncertainties concerning relatively short-term TOU incubations via long-term sediment trap deployment (Witte & Pfannkuche, 1999). The sediment traps also fail to capture episodic flux events due to their low temporal resolution (Huffard et al., 2020).

Besides, the benthic oxygen consumption rates can be affected by a combination of factors, including primary production, quality of OM, and bottom-water oxygen concentrations (Jahnke, 1996; Wenzhöfer and Glud, 2002). It has been reported that the dissolved oxygen concentration in bottom water increased toward the canyon head in GPSC (Liao et al., 2017). Also, Wang et al. (2008) reported that the flow velocity near



the head of GPSC regularly exceeded 1 m/s with the *in situ* observations from moored and shipboard acoustic Doppler current profilers (ADCP). This high flow velocity leads to strong bottom-water currents and strong resuspension of surficial sediments (Moodley et al., 1998), which may result in the increased oxygen consumption rates measured at GC1. In short, the peculiarly high value of observed BMU in GC1 might be associated with underestimated bioturbation, physical disturbances, and chemical oxidation.

Another issue is the different flow values calculated by parsimonious and MCMC algorithms (Fig. 12). Despite the various constraints imposed in our model, it was still insufficient to quantify a unique solution set. These constraints, however, imply that a “solution space” exists (van Oevelen et al., 2010). Within the solution space, an infinite number of solutions set consistent with the data are present (Soetaert and van Oevelen, 2009). The conventional single-solution modeling approach typically provided a mathematically “the best” solution set. However, the solution flows were mostly close to the boundaries of the solution space (Fig. 12). On the other hand, the likelihood method based on the MCMC algorithm provided multiple solution sets, which could form a distribution of a probability density function (PDF) in the solution space. With this multi-solution approach, the solution sets are sampled from the solution space (Van

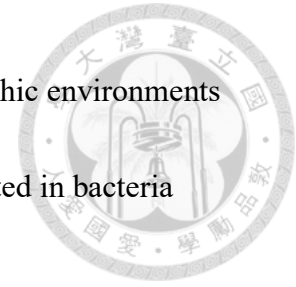


den Meersche et al., 2009), and the mean of this sampled set could represent the central flow values which are less sensitive to the boundaries of the solution space (Van Oevelen et al., 2010). For each flow in our model, the mean and standard deviations of the 10,000 solutions were calculated. These standard deviations represent how the uncertainty in the data set propagates to the flow values (Van Oevelen et al., 2010).

4.3 Carbon demand from the benthic community

The initial attempt to insert the referenced POC flux in the models failed. This conflict is often seen in LIM studies (e.g., van Oevelen et al., 2011; De Smet et al., 2016). For example, De Smet et al. (2016) studied the *L. conchilega* reef with LIM. Most of their models could not be solved when they directly set the *in situ* primary production rates as the input, because this rate did not consider the OM brought from the external water flow. Therefore, they added a flow as additional OM input, and then left the value of which to be determined by the model itself. Similarly, in our food web structure, we only considered the particulate form of OC input and may ignore the direct consumption of dissolved organic matter (DOM) by the bacteria. DOM is expected to be taken up more easily than POM for bacteria because they need to produce enzymes to hydrolyze polymeric sinking particles before the material pass through cell membranes and is metabolized (Verdugo et al., 2004). Moreover, Pape et al. (2013)

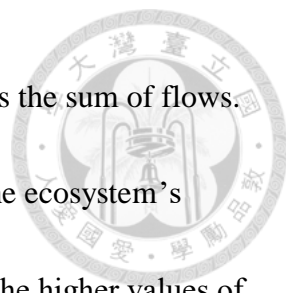
conducted experiments to evaluate the fate of DOM in different benthic environments (North Atlantic and Western Mediterranean slope sites), which resulted in bacteria dominating DOM carbon uptake.



To resolve the discrepancy in OC input between literature values and the requirement to sustain the modeled ecosystem, the research objective has shifted to quantifying the amount of the minimum carbon demand in the system under the simplified food web structure. The additional DOM input is a possible cause but we do not have strong evidence to support it. On the other hand, the converted POC flux reported by Liu et al. (2006) was 6 to 10 times higher than the reference estimation (Huh et al., 2009) and our modeled value. This mismatch might be resulted from sediment resuspension or lateral transports of POC flux which cannot be proven in our study. For instance, the mismatch between modeled and measured POC flux has been found in the Nazaré Canyon (de Stigter et al. 2007), which may be resulted from the sediment resuspension triggered by the strong bottom currents.

4.4 Network characteristics

Network indices are often calculated to describe the function of the food web (Kone et al., 2009). Here, five indices were used to examine the food web structures in GC1 and GS1.



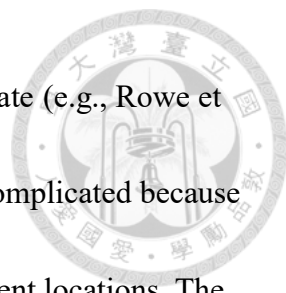
TST and $T_{..}$ quantify the energy which belongs to the system as the sum of flows. As a result, the magnitude of these two indices is directly linked to the ecosystem's growth. The greater carbon processing in the canyon head results in the higher values of TST and $T_{..}$, which represent the total amount of energy flowing through the system (Ulanowicz, 1986; 2004). However, the growth cannot provide detail about how the material is distributed within the system. In other words, two systems with totally different food web structures can have the same TST (Bodini, 2012). Therefore, two other indices were compute to estimate the maturity of the two ecosystems. According to Odum (1969), a mature ecosystem should involve a higher information content, high biomass, and a high capacity to seize and hold the nutrients for cycling within the system. Our data show that the FCI is marginally greater in GS1 than in GC1, indicating that the slope system might have a higher degree of energy recycling and was a relatively mature ecosystem that develops more completed nutrient conservation routes (Odum, 1969) in contrast to the canyon system. Moreover, the higher biodiversity (Fig. 7 and Fig. 9) and biotic carbon stock (Table 5) in the GS1 than in GC1 also show that the ecosystem on the slope is more mature than the frequently disturbed canyon, mainly dominated by the bacteria-related process. The low carbon stock of the larger-size faunal group in GC1 indicates that the head of Gaping

Submarine Canyon is a fragile ecosystem under severe physical perturbation, as reported by Liao et al. (2017) and Liao et al. (2020). The *FCI* in different sections of Nazare canyon and previously reported benthic ecosystems are found in the range of 5% to 20% (van Oevelen et al., 2011; Kones et al., 2009; Anh et al., 2015), while our *FCIs* are well within this range (GC1: 7 %; GS1: 13%).

The index of average mutual information, *AMI*, indicates the developmental status of an ecological network (Ulanowicz, 1980). The number of constraints determines the magnitude of *AMI* value. That is, the more the constraints are in effect, the less the uncertainty is in the system; therefore, the higher value the *AMI* will be.

In a food web model, if the energy distribution passes through only a few efficient routes, the maintenance cost for the whole system would decrease (Bodini, 2012). On the other hand, a highly redundant network that is less organized would have a lower *AMI* value. It follows that *AMI* value is expected to be lower at the early immature stage of the ecosystem (Mukherjee et al., 2019). In this study, the marginally higher *AMI* in the GS1 than in GC1 suggests that the upper slope was in lower physical disturbance conditions than the canyon head.


The turnover rate (or residence time) of OM can be considered as a function of stock size and energy transfer in/out of the stock. In deep-sea studies, scientists quantify



the sediment stock and the POC fluxes and thus derive the turnover rate (e.g., Rowe et al., 2008). However, the quantification of OM turnover is far more complicated because of the varying OM composition and taxonomic assemblages at different locations. The turnover rate also describes the mechanism for consuming OM through aerobic or anaerobic utilization by the whole benthic community (Rowe et al., 1990). Therefore, carbon stocks divided by the oxygen demand (i.e., TOU, DOU, and BMU) in terms of carbon equivalents can be adopted as an alternative method of OC turnover rate derivation.

The turnover time of total OC estimated by the model results (Table 15) was in the time scale of decades in the canyon head, while it appeared to be over a century on the slope. The turnover time in GC1 (63 year) is similar to the turnover rate reported at the head of Mississippi Canyon (57 years; Rowe et al., 2008). Similarly, the turnover rate of GS1 (101 years) is similar to the turnover on the slope station near the Demerara Abyssal Plain (132 years; Rowe et al., 1990). The longer residence time in GS1 corresponds to the interpretation of *FCI*, revealing the carbon is recycled in the slope habitat.

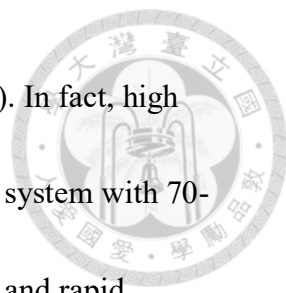
On the other hand, the turnover time derived from the direct measurements of TOU, DOU, or BMU was much shorter than that derived from modeled estimations. For



example, Rowe et al. (1991) reported the OC residence time on a mean of 11 years on the continental shelf, which is 150 meters deep. The longer OC turnover rates estimated by models might be because the models underestimate the bioturbation or physical disturbance in the natural environment. Note that though Rowe et al. (1990, 1991, and 2008) calculated the OC turnover time as OC stocks divided by the OC fluxes; Rowe et al (1990, 1991) used the sediment trap-measured POC fluxes, while Rowe et al. (2008) used the measured SCOC as the OC fluxes.


4.5 Burial efficiency and carbon sequestration in the GPSC

In our model, the burial efficiency was calculated as the ratio of burial flow (Sediment→Burial in Fig. 2) to POC flux (POC→Sediment in Fig. 2). The fractions of burial in the two study sites were peculiarly high, which might be resulted from multiple factors. First, the burial flow was constrained by the sedimentation rate measured by Huh et al. (2009) and Hsu et al. (2014). Then, the quantity of this flow is again used as the constraint of the POC flux based on the burial efficiency estimated by Hsu et al. (2014). That is, reported burial efficiency (24%; Hsu et al.,2014) was set as the lower bound of POC flux, and the upper bound was set as 100%. Herein lies the high uncertainty of the burial efficiency. Secondly, though the study site in Hsu et al. (2014) is on the Gaoping continental shelf close to the GPSC and adjacent slope, this literature



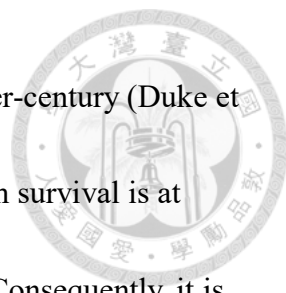
value may not represent the local conditions (van Ovelen et al., 2010). In fact, high burial efficiency of terrestrial POC has been proposed for small river system with 70-85% (Galy et al., 2007; Hilton et al., 2011) due to hyperpycnal flows and rapid deposition on the narrow continental margin off the SMRs. Moreover, Kao et al. (2014) analyzed the isotopic and elemental composition of samples from marine sediment traps above the seafloor in the GPSC, providing a conservative estimate of terrestrial OC preservation efficiency larger than 70%. In contrast, Hsu et al. (2014) calculated the burial efficiency as the ratio of accumulation flux of sediment to annual sediment load. While the range of burial efficiency varied with different estimation techniques, it was better to set the lower bound for this parameter rather than the unsure higher bound. Nevertheless, the flow quantities in the whole food web were calculated with the MCMC algorithm considering all biogeochemical constraints in the system. Hence, the unusually high burial efficiency is not groundless and can be considered a logical outcome under the current model structure and input setting.

Submarine canyon head has been considered significant for carbon sink and the process of carbon sequestration. It has been suggested that the burial efficiency in the Nazaré Canyon head be about 30%-80% (Masson et al., 2010) according to different estimation techniques. Furthermore, Krause-Jensen & Duarte (2016) suggests



macroalgal detritus can be sequestered through the burial and transport in the submarine canyon. It has also been reported that the submarine canyon in the northwestern Mediterranean features efficient carbon sequestration through the dense water cascading along with phytoplankton blooms (Canals et al., 2006). As part of the carbon “source to sink” system, the GPSC not only transports a large amount of matter from the continental shelf to the deep ocean basin but also performs the important function of carbon sequestration.

Another often discussed blue carbon ecosystem in Taiwan is the relatively well-studied mangrove area distributed along the western coast. Given the mangrove wetlands located between rivers downstream and the coastline, the mangrove trees also play a crucial role in carbon sequestration. Owing to their high productivity (Bouillon et al., 2008), the mangroves can store up to 88% of their OC in the deeper sediment (Donato et al., 2011). However, multiple reasons could affect the carbon burial rates in different mangrove ecosystems, such as temperature, seasonal differences (Alongi et al., 2004; Van Santen et al., 2007), and hydrological disturbance (Marchio et al., 2016). Li et al. (2018) have reported that the carbon burial rates in Taiwan are much lower than the global average rate, which might be resulted from the faster decomposition process. On the other hand, deforestation and rapid sea-level rise are major threats to mangroves



(Polidoro et al., 2010), causing a 35-86% decline over the past quarter-century (Duke et al., 2007). When mangrove areas become fragmented, their long-term survival is at great risk, and their ecosystem services may functionally disappear. Consequently, it is important to study other effective carbon sinks that may help achieve carbon neutrality. The current study revealed the high carbon burial rates of the benthic community in the GPSC, which not only extends our knowledge of ecosystem functioning in this area but also improves the understanding of natural carbon storage in a part of the “S2S” system.

Moreover, investigating the particle fluxes helps us better understand the transfer and fate of materials to the deep-sea ecosystem, which may help develop better research strategies for predicting the potential impacts of climate change.

5 Conclusion



In this study, I present the first quantitative analysis of carbon flows within the food webs of GPSC and adjacent slope. The LIM model results provided a rare opportunity to study how the canyon affects food web structure compared to the slope habitat. Moreover, this study also offers an insight into the ecosystem functioning of the submarine canyon from the aspect of energy flows and food web characteristics such as total system throughput, energy recycling, and food web maturity.

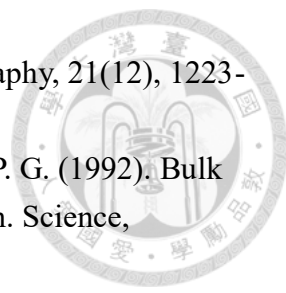
Moreover, it is the first study applying the LIM technique in Taiwan. There was no significant difference in the OC stocks between different sampling seasons. However, the standing stocks of each compartment significantly differed between the habitats. The relatively lower biodiversity and faunal carbon stocks in the canyon show that this is a fragile ecosystem under severe physical perturbation. The model results revealed that bacteria-related processes dominated the canyon head of the GPSC. By contrast, the higher contribution of fauna in carbon processing on the adjacent slope presents a relatively mature ecosystem. In addition, our models revealed a higher carbon burial rate in GC1, indicating that the GPSC not only transports sediment to the deep SCS but functions as an important role in carbon sequestration. Our simplified models may ignore the influence of larger-size faunas. Still, they effectively quantified the matter

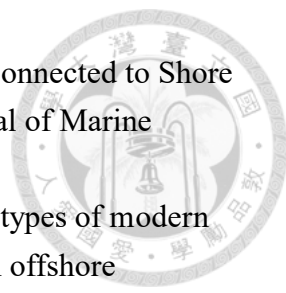
and energy transfer across the deep-sea systems, which are notoriously difficult to study.

Owing to the ongoing climate change, the geohazards in the submarine canyons might become more frequent due to new weather systems and a potentially higher flooding intensity in SMRs. Studying matter and energy transfer on the continental margin will help us understand how deep ecosystems are fueled, and determine their capacity to capture and store carbon. By better understanding carbon cycling in submarine canyons like GPSC, we may be able to predict the impact of climate change or human influence on deep-sea ecosystems.


6 Reference

- Aller, R. C. (1982). The effects of macrobenthos on chemical properties of marine sediment and overlying water. In *Animal-sediment relations* (pp. 53-102). Springer, Boston, MA.
- Aller, R. C. (1994). Bioturbation and remineralization of sedimentary organic matter: effects of redox oscillation. *Chemical Geology*, 114(3-4), 331-345.
- Allesina, S., & Ulanowicz, R. E. (2004). Cycling in ecological networks: Finn's index revisited. *Computational biology and chemistry*, 28(3), 227-233.
- Alongi, D. M. (1988). Bacterial productivity and microbial biomass in tropical mangrove sediments. *Microbial ecology*, 15(1), 59-79.
- Alongi, D. M., Sasekumar, A., Chong, V. C., Pfitzner, J., Trott, L. A., Tirendi, F., Dixon, P. & Brunskill, G. J. (2004). Sediment accumulation and organic material flux in a managed mangrove ecosystem: estimates of land-ocean-atmosphere exchange in peninsular Malaysia. *Marine geology*, 208(2-4), 383-402.
- Amaro, T., Witte, H., Herndl, G. J., Cunha, M. R., & Billett, D. S. (2009). Deep-sea bacterial communities in sediments and guts of deposit-feeding holothurians in Portuguese canyons (NE Atlantic). *Deep Sea Research Part I: Oceanographic Research Papers*, 56(10), 1834-1843.
- Anh, P. V., Everaert, G., Goethals, P., Vinh, C. T., & De Laender, F. (2015). Production and food web efficiency decrease as fishing activity increases in a coastal ecosystem. *Estuarine, Coastal and Shelf Science*, 165, 226-236.
- Archer, D., & Devol, A. (1992). Benthic oxygen fluxes on the Washington shelf and slope: A comparison of in situ microelectrode and chamber flux measurements. *Limnology and Oceanography*, 37(3), 614-629.
- Baguley, J. G., Hyde, L. J., & Montagna, P. A. (2004). A semi-automated digital microphotographic approach to measure meiofaunal biomass. *Limnology and Oceanography: Methods*, 2(6), 181-190.
- Baker, C. A., Estapa, M. L., Iversen, M., Lampitt, R., & Buesseler, K. (2020). Are all sediment traps created equal? An intercomparison study of carbon export methodologies at the PAP-SO site. *Progress in Oceanography*, 184, 102317.
- Banse, K., & Mosher, S. (1980). Adult body mass and annual production/biomass relationships of field populations. *Ecological monographs*, 50(3), 355-379.
- Baselga, A. (2010). Partitioning the turnover and nestedness components of beta diversity. *Global ecology and biogeography*, 19(1), 134-143.
- Baselga, A. (2012). The relationship between species replacement, dissimilarity derived

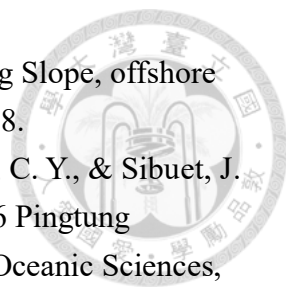
- 
- from nestedness, and nestedness. *Global Ecology and Biogeography*, 21(12), 1223-1232.
- Benner, R., Pakulski, J. D., McCarthy, M., Hedges, J. I., & Hatcher, P. G. (1992). Bulk chemical characteristics of dissolved organic matter in the ocean. *Science*, 255(5051), 1561-1564.
- Berg, P., Risgaard-Petersen, N., & Rysgaard, S. (1998). Interpretation of measured concentration profiles in sediment pore water. *Limnology and Oceanography*, 43(7), 1500-1510.
- Bernhardt, A., & Schwanghart, W. (2021). Where and why do submarine canyons remain connected to the shore during sea-level rise? Insights from global topographic analysis and Bayesian regression. *Geophysical Research Letters*, 48(10), e2020GL092234.
- Bianchelli, S., Gambi, C., Zeppilli, D., & Danovaro, R. (2010). Metazoan meiofauna in deep-sea canyons and adjacent open slopes: a large-scale comparison with focus on the rare taxa. *Deep Sea Research Part I: Oceanographic Research Papers*, 57(3), 420-433.
- Blair, N. E., Levin, L. A., DeMaster, D. J., & Plaia, G. (1996). The short-term fate of fresh algal carbon in continental slope sediments. *Limnology and Oceanography*, 41(6), 1208-1219.
- Bodini, A. (2012). Building a systemic environmental monitoring and indicators for sustainability: What has the ecological network approach to offer?. *Ecological Indicators*, 15(1), 140-148.
- Bouillon, S., Borges, A. V., Castañeda-Moya, E., Diele, K., Dittmar, T., Duke, N. C., Kristensen, E., Lee, S. Y., Marchand, C., Middelburg, J. J., Rivera-Monroy, V. H., Smith III, T. J., & Twilley, R. R. (2008). Mangrove production and carbon sinks: a revision of global budget estimates. *Global biogeochemical cycles*, 22(2).
- Burnett, B. R. (1979). Quantitative sampling of microbiota of the deep-sea benthos. II. Evaluation of technique and introduction to the biota of the San Diego Trough. *Transactions of the American Microscopical Society*, 233-242.
- Calow, P. (1977). Conversion efficiencies in heterotrophic organisms. *Biological reviews*, 52(3), 385-409.
- Canals, M., Puig, P., de Madron, X. D., Heussner, S., Palanques, A., & Fabres, J. (2006). Flushing submarine canyons. *Nature*, 444(7117), 354-357.
- Carter, L., Gavey, R., Talling, P. J., & Liu, J. T. (2014). Insights into submarine geohazards from breaks in subsea telecommunication cables. *Oceanography*, 27(2), 58-67.


- 
- Chiang, C. S., & Yu, H. S. (2022). Controls of Submarine Canyons Connected to Shore during the LGM Sea-Level Rise: Examples from Taiwan. *Journal of Marine Science and Engineering*, 10(4), 494.
- Chiang, C. S., Hsiung, K. H., Yu, H. S., & Chen, S. C. (2020). Three types of modern submarine canyons on the tectonically active continental margin offshore southwestern Taiwan. *Marine Geophysical Research*, 41(1), 1-17.
- Chiou, M. D., Jan, S., Wang, J., Lien, R. C., & Chien, H. (2011). Sources of baroclinic tidal energy in the Gaoping Submarine Canyon off southwestern Taiwan. *Journal of Geophysical Research: Oceans*, 116(C12).
- Clausen, I. B., & Riisgård, H. U. (1996). Growth, filtration and respiration in the mussel *Mytilus edulis*: no evidence for physiological regulation of the filter-pump to nutritional needs. *Marine Ecology Progress Series*, 141, 37-45.
- Conover, R. J. (1966). Assimilation of organic matter by zooplankton 1. *Limnology and oceanography*, 11(3), 338-345.
- Covault, J. A., & Graham, S. A. (2010). Submarine fans at all sea-level stands: Tectono-morphologic and climatic controls on terrigenous sediment delivery to the deep sea. *Geology*, 38(10), 939-942.
- Covault, J. A., Normark, W. R., Romans, B. W., & Graham, S. A. (2007). Highstand fans in the California borderland: The overlooked deep-water depositional systems. *Geology*, 35(9), 783-786.
- Crisp, D. J. (1971). Energy flow measurements. *Methods for the study of marine benthos*.
- Danovaro, R. (2009). *Methods for the study of deep-sea sediments, their functioning and biodiversity*. CRC press.
- Danovaro, R. (2012). Extending the approaches of biodiversity and ecosystem functioning to the deep ocean. *Marine Biodiversity and Ecosystem Functioning: Frameworks, methodologies, and integration*, edited by: Solan, M., Aspden, R.J., and Paterson, D.M., Oxford University Press, Oxford, 115-126.
- Danovaro, R., Dell'Anno, A., Corinaldesi, C., Magagnoli, M., Noble, R., Tamburini, C., & Weinbauer, M. (2008). Major viral impact on the functioning of benthic deep-sea ecosystems. *Nature*, 454(7208), 1084-1087.
- Danovaro, R., Marralle, D., Dell'Anno, A., Della Croce, N., Tselepidis, A., & Fabiano, M. (2000). Bacterial response to seasonal changes in labile organic matter composition on the continental shelf and bathyal sediments of the Cretan Sea. *Progress in oceanography*, 46(2-4), 345-366.
- De Leo, F. C., Smith, C. R., Rowden, A. A., Bowden, D. A., & Clark, M. R. (2010).

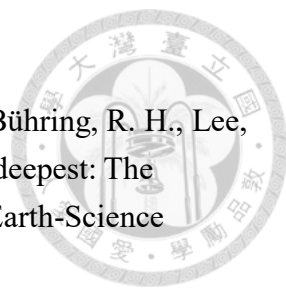
- Submarine canyons: hotspots of benthic biomass and productivity in the deep sea. *Proceedings of the Royal Society B: Biological Sciences*, 277(1695), 2783-2792.
- De Leo, F. C., Vetter, E. W., Smith, C. R., Rowden, A. A., & McGranaghan, M. (2014). Spatial scale-dependent habitat heterogeneity influences submarine canyon macrofaunal abundance and diversity off the Main and Northwest Hawaiian Islands. *Deep Sea Research Part II: Topical Studies in Oceanography*, 104, 267-290.
- De Smet, B., van Oevelen, D., Vincx, M., Vanaverbeke, J., & Soetaert, K. (2016). *Lanice conchilega* structures carbon flows in soft-bottom intertidal areas. *Marine Ecology Progress Series*, 552, 47-60.
- de Stigter, H. C., Boer, W., de Jesus Mendes, P. A., Jesus, C. C., Thomsen, L., van den Bergh, G. D., & van Weering, T. C. (2007). Recent sediment transport and deposition in the Nazaré Canyon, Portuguese continental margin. *Marine Geology*, 246(2-4), 144-164.
- Del Giorgio, P. A., & Cole, J. J. (1998). Bacterial growth efficiency in natural aquatic systems. *Annual Review of Ecology and Systematics*, 29(1), 503-541.
- Deming, J. W., & Carpenter, S. D. (2008). Factors influencing benthic bacterial abundance, biomass, and activity on the northern continental margin and deep basin of the Gulf of Mexico. *Deep Sea Research Part II: Topical Studies in Oceanography*, 55(24-26), 2597-2606.
- Donato, D. C., Kauffman, J. B., Murdiyarso, D., Kurnianto, S., Stidham, M., & Kanninen, M. (2011). Mangroves among the most carbon-rich forests in the tropics. *Nature geoscience*, 4(5), 293-297.
- Drazen, J. C., Reisenbichler, K. R., & Robison, B. H. (2007). A comparison of absorption and assimilation efficiencies between four species of shallow-and deep-living fishes. *Marine biology*, 151(4), 1551-1558.
- Duke, N. C., Meynecke, J. O., Dittmann, S., Ellison, A. M., Anger, K., Berger, U., Cannicik, S., Diele, K., Ewel, C. D., Field, C. D., Koedam, N., Lee, S. Y., Marchand, C., Nordhaus, I., & Dahdouh-Guebas, F. (2007). A world without mangroves?. *Science*, 317(5834), 41-42.
- Eleftheriou, A. (Ed.). (2013). *Methods for the study of marine benthos*. John Wiley & Sons.
- Epping, E., van der Zee, C., Soetaert, K., & Helder, W. (2002). On the oxidation and burial of organic carbon in sediments of the Iberian margin and Nazaré Canyon (NE Atlantic). *Progress in Oceanography*, 52(2-4), 399-431.
- Fath, B. D., & Patten, B. C. (1999). Review of the foundations of network environ


- 
- analysis. *Ecosystems*, 2(2), 167-179.
- Fenchel, T. (1982). Ecology of heterotrophic microflagellates. 11. Bioenergetics and growth. *Marine ecology progress series*, 8(22523), 1.
- Finn, J. T. (1976). Measures of ecosystem structure and function derived from analysis of flows. *Journal of theoretical Biology*, 56(2), 363-380.
- Fleeger, J. W., & Palmer, M. A. (1982). Secondary Production of the Estuarine, Meiobenthic Copepod *Microarthridion littorale*. *Marine ecology progress series*. Oldendorf, 7(2), 157-162.
- Fodrie, F. J., Levin, L. A., & Rathburn, A. E. (2009). High densities and depth-associated changes of epibenthic megafauna along the Aleutian margin from 2000–4200 m. *Journal of the Marine Biological Association of the United Kingdom*, 89(8), 1517-1527.
- Forster, S., & Graf, G. (1995). Impact of irrigation on oxygen flux into the sediment: intermittent pumping by *Callianassa subterranea* and “piston-pumping” by *Janice conchilega*. *Marine Biology*, 123(2), 335-346.
- Gage, J. D., & Tyler, P. A. (1991). Deep-sea biology: a natural history of organisms at the deep-sea floor. Cambridge University Press.
- Galy, V., France-Lanord, C., Beyssac, O., Faure, P., Kudrass, H., & Palhol, F. (2007). Efficient organic carbon burial in the Bengal fan sustained by the Himalayan erosional system. *Nature*, 450(7168), 407-410.
- Garcia, R., Koho, K. A., De Stigter, H. C., Epping, E., Koning, E., & Thomsen, L. (2007). Distribution of meiobenthos in the Nazare canyon and adjacent slope (western Iberian Margin) in relation to sedimentary composition. *Marine Ecology Progress Series*, 340, 207-220.
- Gaudin, M., Berné, S., Jouanneau, J. M., Palanques, A., Puig, P., Mulder, T., Círac, P., Rabineau, M., & Imbert, P. (2006). Massive sand beds attributed to deposition by dense water cascades in the Bourcart canyon head, Gulf of Lions (northwestern Mediterranean Sea). *Marine Geology*, 234(1-4), 111-128.
- Gavey, R., Carter, L., Liu, J. T., Talling, P. J., Hsu, R., Pope, E., & Evans, G. (2017). Frequent sediment density flows during 2006 to 2015, triggered by competing seismic and weather events: Observations from subsea cable breaks off southern Taiwan. *Marine Geology*, 384, 147-158.
- Giering, S. L., Sanders, R., Martin, A. P., Henson, S. A., Riley, J. S., Marsay, C. M., & Johns, D. G. (2017). Particle flux in the oceans: Challenging the steady state assumption. *Global Biogeochemical Cycles*, 31(1), 159-171.
- Glud, R. N. (2008). Oxygen dynamics of marine sediments. *Marine Biology Research*,

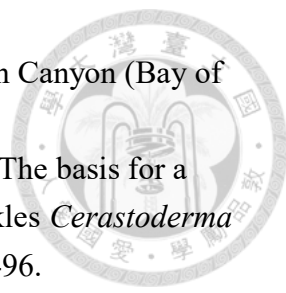
- 4(4), 243-289.
- Glud, R. N., Gundersen, J. K., Røy, H., & Jørgensen, B. B. (2003). Seasonal dynamics of benthic O₂ uptake in a semienclosed bay: Importance of diffusion and faunal activity. *Limnology and Oceanography*, 48(3), 1265-1276.
- Graf, G., & Rosenberg, R. (1997). Bioresuspension and biodeposition: a review. *Journal of Marine Systems*, 11(3-4), 269-278.
- Greene, C. H., Wiebe, P. H., Burczynski, J., & Youngbluth, M. J. (1988). Acoustical detection of high-density krill demersal layers in the submarine canyons off Georges Bank. *Science*, 241(4863), 359-361.
- Hall, R. A., & Carter, G. S. (2011). Internal tides in Monterey submarine canyon. *Journal of Physical Oceanography*, 41(1), 186-204.
- Hammond, D. E., & Fuller, C. (1979). The use of radon-222 to estimate benthic exchange and atmospheric exchange rates in San Francisco Bay.
- Hansell, D. A., & Carlson, C. A. (2001). Marine dissolved organic matter and the carbon cycle. *Oceanography*, 14(4), 41-49.
- Harris, P. T., & Whiteway, T. (2011). Global distribution of large submarine canyons: Geomorphic differences between active and passive continental margins. *Marine Geology*, 285(1-4), 69-86.
- Hecker, B. (1994). Unusual megafaunal assemblages on the continental slope off Cape Hatteras. *Deep Sea Research Part II: Topical Studies in Oceanography*, 41(4-6), 809-834.
- Herman, P. M. J., Heip, C., & Vranken, G. (1983). The production of *Cyprideis torosa* Jones 1850 (Crustacea, Ostracoda). *Oecologia*, 58(3), 326-331.
- Herman, P. M., & Heip, C. (1985). Secondary production of the harpacticoid copepod *Paronychocamptus nanus* in a brackish-water habitat. *Limnology and oceanography*, 30(5), 1060-1066.
- Hessler, R. R., & JuMARS, P. A. (1974, March). Abyssal community analysis from replicate box cores in the central North Pacific. In *Deep Sea Research and Oceanographic Abstracts* (Vol. 21, No. 3, pp. 185-209). Elsevier.
- Holling, C. S. (1966). The functional response of invertebrate predators to prey density. *The Memoirs of the Entomological Society of Canada*, 98(S48), 5-86.
- Hsu, F. H., Su, C. C., Wang, C. H., Lin, S., Liu, J., & Huh, C. A. (2014). Accumulation of terrestrial organic carbon on an active continental margin offshore southwestern Taiwan: Source-to-sink pathways of river-borne organic particles. *Journal of Asian Earth Sciences*, 91, 163-173.
- Hsu, H. H., Liu, C. S., Yu, H. S., Chang, J. H., & Chen, S. C. (2013). Sediment dispersal


- 
- and accumulation in tectonic accommodation across the Gaoping Slope, offshore Southwestern Taiwan. *Journal of Asian Earth Sciences*, 69, 26-38.
- Hsu, S. K., Kuo, J., Chung-Liang, L., Ching-Hui, T., Doo, W. B., Ku, C. Y., & Sibuet, J. C. (2008). Turbidity currents, submarine landslides and the 2006 Pingtung earthquake off SW Taiwan. *TAO: Terrestrial, Atmospheric and Oceanic Sciences*, 19(6), 7.
- Huang, T. H., Fu, Y. H., Pan, P. Y., & Chen, C. T. A. (2012). Fluvial carbon fluxes in tropical rivers. *Current Opinion in Environmental Sustainability*, 4(2), 162-169.
- Huffard, C. L., Durkin, C. A., Wilson, S. E., McGill, P. R., Henthorn, R., & Smith Jr, K. L. (2020). Temporally-resolved mechanisms of deep-ocean particle flux and impact on the seafloor carbon cycle in the northeast Pacific. *Deep Sea Research Part II: Topical Studies in Oceanography*, 173, 104763.
- Huh, C. A., Lin, H. L., Lin, S., & Huang, Y. W. (2009). Modern accumulation rates and a budget of sediment off the Gaoping (Kaoping) River, SW Taiwan: a tidal and flood dominated depositional environment around a submarine canyon. *Journal of Marine Systems*, 76(4), 405-416.
- Ikehara, K., Usami, K., & Kanamatsu, T. (2020). Repeated occurrence of surface-sediment remobilization along the landward slope of the Japan Trench by great earthquakes. *Earth, Planets and Space*, 72(1), 1-9.
- Ingels, J., Kiriakoulakis, K., Wolff, G. A., & Vanreusel, A. (2009). Nematode diversity and its relation to the quantity and quality of sedimentary organic matter in the deep Nazaré Canyon, Western Iberian Margin. *Deep Sea Research Part I: Oceanographic Research Papers*, 56(9), 1521-1539.
- Jahnke, R. A. (1996). The global ocean flux of particulate organic carbon: Areal distribution and magnitude. *Global Biogeochemical Cycles*, 10(1), 71-88.
- Jan, S., Lien, R. C., & Ting, C. H. (2008). Numerical study of baroclinic tides in Luzon Strait. *Journal of Oceanography*, 64(5), 789-802.
- Jørgensen, B. B., Glud, R. N., & Holby, O. (2005). Oxygen distribution and bioirrigation in Arctic fjord sediments (Svalbard, Barents Sea). *Marine Ecology Progress Series*, 292, 85-95.
- Kallmeyer, J., Smith, D. C., Spivack, A. J., & D'Hondt, S. (2008). New cell extraction procedure applied to deep subsurface sediments. *Limnology and Oceanography: Methods*, 6(6), 236-245.
- Kao, S. J., Hilton, R. G., Selvaraj, K., Dai, M., Zehetner, F., Huang, J. C., Hsu, S.C., Sparkes, R., Liu, J.T., Lee, T.Y., Yang, J.Y.T., Galy, A., Xu, X., & Hovius, N. (2014). Preservation of terrestrial organic carbon in marine sediments offshore

- 
- Taiwan: mountain building and atmospheric carbon dioxide sequestration. *Earth Surface Dynamics*, 2(1), 127-139.
- Keller, G. H., Lambert, D., Rowe, G., & Staresinic, N. (1973). Bottom currents in the Hudson Canyon. *Science*, 180(4082), 181-183.
- Kones, J. K., Soetaert, K., van Oevelen, D., & Owino, J. O. (2009). Are network indices robust indicators of food web functioning? A Monte Carlo approach. *Ecological Modelling*, 220(3), 370-382.
- Kones, J. K., Soetaert, K., van Oevelen, D., Owino, J. O., & Mavuti, K. (2006). Gaining insight into food webs reconstructed by the inverse method. *Journal of Marine Systems*, 60(1-2), 153-166.
- Koopmans, M., Martens, D., & Wijffels, R. H. (2010). Growth efficiency and carbon balance for the sponge *Haliclona oculata*. *Marine biotechnology*, 12(3), 340-349.
- Krause-Jensen, D., & Duarte, C. M. (2016). Substantial role of macroalgae in marine carbon sequestration. *Nature Geoscience*, 9(10), 737-742.
- Latham II, L. G., & Scully, E. P. (2002). Quantifying constraint to assess development in ecological networks. *Ecological Modelling*, 154(1-2), 25-44.
- Lee, I. H., Lien, R. C., Liu, J. T., & Chuang, W. S. (2009). Turbulent mixing and internal tides in Gaoping (Kaoping) submarine canyon, Taiwan. *Journal of Marine Systems*, 76(4), 383-396.
- Li, M., Peng, C., Wang, M., Xue, W., Zhang, K., Wang, K., Shi, G. & Zhu, Q. (2017). The carbon flux of global rivers: a re-evaluation of amount and spatial patterns. *Ecological Indicators*, 80, 40-51.
- Li, S. B., Chen, P. H., Huang, J. S., Hsueh, M. L., Hsieh, L. Y., Lee, C. L., & Lin, H. J. (2018). Factors regulating carbon sinks in mangrove ecosystems. *Global change biology*, 24(9), 4195-4210.
- Liao, J. X., Chen, G. M., Chiou, M. D., Jan, S., & Wei, C. L. (2017). Internal tides affect benthic community structure in an energetic submarine canyon off SW Taiwan. *Deep Sea Research Part I: Oceanographic Research Papers*, 125, 147-160.
- Liao, J. X., Wei, C. L., & Yasuhara, M. (2020). Species and Functional Diversity of Deep-Sea Nematodes in a High Energy Submarine Canyon. *Frontiers in Marine Science*, 591.
- Lichtschlag, A., Donis, D., Janssen, F., Jessen, G. L., Holtappels, M., Wenzhöfer, F., F., Mazlumyan, S., Sergeeva, N., Waldmann, C., & Boetius, A. (2015). Effects of fluctuating hypoxia on benthic oxygen consumption in the Black Sea (Crimean shelf). *Biogeosciences*, 12(16), 5075-5092.
- Liu, J. T., & Lin, H. L. (2004). Sediment dynamics in a submarine canyon: a case of

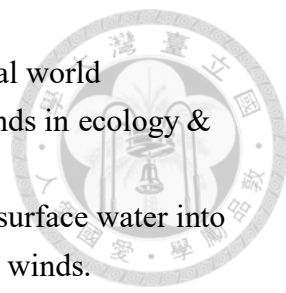
- 
- river-sea interaction. *Marine Geology*, 207(1-4), 55-81.
- Liu, J. T., Hsu, R. T., Hung, J. J., Chang, Y. P., Wang, Y. H., Rendle-Bühning, R. H., Lee, C. L., Huh, C. A. & Yang, R. J. (2016). From the highest to the deepest: The Gaoping River–Gaoping Submarine Canyon dispersal system. *Earth-Science Reviews*, 153, 274-300.
- Liu, J. T., Kao, S. J., Huh, C. A., & Hung, C. C. (2013). Gravity flows associated with flood events and carbon burial: Taiwan as instructional source area. *Annual Review of Marine Science*, 5, 47-68.
- Liu, J. T., Lin, H. L., & Hung, J. J. (2006). A submarine canyon conduit under typhoon conditions off Southern Taiwan. *Deep Sea Research Part I: Oceanographic Research Papers*, 53(2), 223-240.
- Liu, J. T., Liu, K. J., & Huang, J. C. (2002). The influence of a submarine canyon on river sediment dispersal and inner shelf sediment movements: a perspective from grain-size distributions. *Marine Geology*, 181(4), 357-386.
- Lochte, K., & Turley, C. M. (1988). Bacteria and cyanobacteria associated with phytodetritus in the deep sea. *Nature*, 333(6168), 67-69.
- Lohrer, A. M., Thrush, S. F., & Gibbs, M. M. (2004). Bioturbators enhance ecosystem function through complex biogeochemical interactions. *Nature*, 431(7012), 1092-1095.
- Loo, L. O., & Rosenberg, R. (1996). Production and energy budget in marine suspension feeding populations: *Mytilus edulis*, *Cerastoderma edule*, *Mya arenaria* and *Amphiura filiformis*. *Journal of Sea Research*, 35(1-3), 199-207.
- Loreau, M. (2008). Biodiversity and ecosystem functioning: the mystery of the deep sea. *Current Biology*, 18(3), R126-R128.
- Mahaut, M. L., Sibuet, M., & Shirayama, Y. (1995). Weight-dependent respiration rates in deep-sea organisms. *Deep Sea Research Part I: Oceanographic Research Papers*, 42(9), 1575-1582.
- Marchio Jr, D. A., Savarese, M., Bovard, B., & Mitsch, W. J. (2016). Carbon sequestration and sedimentation in mangrove swamps influenced by hydrogeomorphic conditions and urbanization in Southwest Florida. *Forests*, 7(6), 116.
- Mare, M. F. (1942). A study of a marine benthic community with special reference to the micro-organisms. *Journal of the Marine Biological Association of the United Kingdom*, 25(3), 517-554.
- Masson, D. G., Huvenne, V. A. I., De Stigter, H. C., Wolff, G. A., Kiriakoulakis, K., Arzola, R. G., & Blackbird, S. (2010). Efficient burial of carbon in a submarine

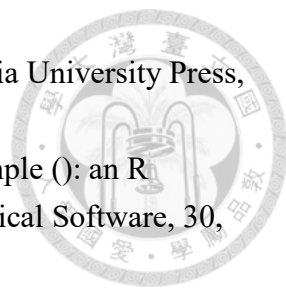
- 
- canyon. *Geology*, 38(9), 831-834.
- Maycas, E. R., Bourdillon, A., Macquart-Moulin, C., Passelaigue, F., & Patrity, G. (1999). Diel variations of the bathymetric distribution of zooplankton groups and biomass in Cap-Ferret Canyon, France. *Deep Sea Research Part II: topical studies in oceanography*, 46(10), 2081-2099.
- McClain, C. R., & Rex, M. A. (2015). Toward a conceptual understanding of β -diversity in the deep-sea benthos. *Annual review of ecology, evolution, and systematics*, 46, 623-642.
- McClain, C. R., Allen, A. P., Tittensor, D. P., & Rex, M. A. (2012). Energetics of life on the deep seafloor. *Proceedings of the National Academy of Sciences*, 109(38), 15366-15371.
- McClain, C. R., and Barry, J. P. (2010). Habitat heterogeneity, disturbance, and productivity work in concert to regulate biodiversity in deep submarine canyons. *Ecology*, 91(4), 964-976.
- Meade, R. H., & Moody, J. A. (2010). Causes for the decline of suspended-sediment discharge in the Mississippi River system, 1940–2007. *Hydrological Processes: An International Journal*, 24(1), 35-49.
- Meile, C., Koretsky, C. M., & Cappellen, P. V. (2001). Quantifying bioirrigation in aquatic sediments: an inverse modeling approach. *Limnology and oceanography*, 46(1), 164-177.
- Meyer-Reil, L. A. (1983). Benthic response to sedimentation events during autumn to spring at a shallow water station in the Western Kiel Bight. *Marine Biology*, 77(3), 247-256.
- Meyers, P. A. (1994). Preservation of elemental and isotopic source identification of sedimentary organic matter. *Chemical geology*, 114(3-4), 289-302.
- Montagna, P. A., Baguley, J. G., Hsiang, C. Y., & Reuscher, M. G. (2017). Comparison of sampling methods for deep-sea infauna. *Limnology and Oceanography: Methods*, 15(2), 166-183.
- Moodley, L., Heip, C. H., & Middelburg, J. J. (1998). Benthic activity in sediments of the northwestern Adriatic Sea: sediment oxygen consumption, macro-and meiofauna dynamics. *Journal of Sea Research*, 40(3-4), 263-280.
- Mukherjee, J., Karan, S., Chakrabarty, M., Banerjee, A., Rakshit, N., & Ray, S. (2019). An approach towards quantification of ecosystem trophic status and health through ecological network analysis applied in Hooghly-Matla estuarine system, India. *Ecological Indicators*, 100, 55-68.
- Mulder, T., Weber, O., Anschutz, P., Jorissen, F., & Jouanneau, J. M. (2001). A few

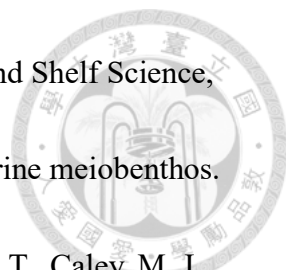
- 
- months-old storm-generated turbidite deposited in the Capbreton Canyon (Bay of Biscay, SW France). *Geo-Marine Letters*, 21(3), 149-156.
- Navarro, E., Iglesias, J. I. P., Ortega, M. M., & Larretxea, X. (1994). The basis for a functional response to variable food quantity and quality in cockles *Cerastoderma edule* (Bivalvia, Cardiidae). *Physiological zoology*, 67(2), 468-496.
- Nielsen, A. M., Eriksen, N. T., Iversen, J. L., & Riisgård, H. U. (1995). Feeding, growth and respiration in the polychaetes *Nereis diversicolor* (facultative filter-feeder) and *N. virens* (omnivorous)-a comparative study. *Marine Ecology Progress Series*, 125, 149-158.
- Nittrouer, C. A., & Wright, L. D. (1994). Transport of particles across continental shelves. *Reviews of Geophysics*, 32(1), 85-113.
- Odum, E. P. (1969). The Strategy of Ecosystem Development: An understanding of ecological succession provides a basis for resolving man's conflict with nature. *science*, 164(3877), 262-270.
- Ogura, N. (1972). Rate and extent of decomposition of dissolved organic matter in surface seawater. *Marine Biology*, 13(2), 89-93.
- Oliveira, A., Santos, A. I., Rodrigues, A., & Vitorino, J. (2007). Sedimentary particle distribution and dynamics on the Nazaré canyon system and adjacent shelf (Portugal). *Marine Geology*, 246(2), 105-122.
- Pape, E., van Oevelen, D., Moodley, L., Soetaert, K., & Vanreusel, A. (2013). Nematode feeding strategies and the fate of dissolved organic matter carbon in different deep-sea sedimentary environments. *Deep Sea Research Part I: Oceanographic Research Papers*, 80, 94-110.
- Polidoro, B. A., Carpenter, K. E., Collins, L., Duke, N. C., Ellison, A. M., Ellison, J. C., Farnsworth, E. J., Fernando, E. S., Kathiresan, K., Koedam, N. E., Livingstone, S. R., Miyagi, T., Moore, G. E., Nam, V. N., Ong, J. E., Primavera, J. H., Salmo III, S. G., Sanciangco, J. C., Sukardjo, S., Wang Y. & Yong, J. W. H. (2010). The loss of species: mangrove extinction risk and geographic areas of global concern. *PloS one*, 5(4), e10095.
- Puig, P., Palanques, A., Orange, D. L., Lastras, G., & Canals, M. (2008). Dense shelf water cascades and sedimentary furrow formation in the Cap de Creus Canyon, northwestern Mediterranean Sea. *Continental Shelf Research*, 28(15), 2017-2030.
- Pusceddu, A., Bianchelli, S., Canals, M., Sanchez-Vidal, A., De Madron, X. D., Heussner, S., Lykousis, V., de Stigter, H., Trincardi, F., & Danovaro, R. (2010). Organic matter in sediments of canyons and open slopes of the Portuguese, Catalan, Southern Adriatic and Cretan Sea margins. *Deep Sea Research Part I:*

- 
- Oceanographic Research Papers, 57(3), 441-457.
- R Core Team (2020). R: A language and environment for statistical computing. R Foundation for Statistical Computing, Vienna, Austria. URL <https://www.R-project.org/>.
- Rabouille, C., Caprais, J. C., Lansard, B., Crassous, P., Dedieu, K., Reyss, J. L., & Khripounoff, A. (2009). Organic matter budget in the Southeast Atlantic continental margin close to the Congo Canyon: In situ measurements of sediment oxygen consumption. *Deep Sea Research Part II: Topical Studies in Oceanography*, 56(23), 2223-2238.
- Rabouille, C., Gaillard, J. F., Relexans, J. C., Tréguer, P., & Vincendeau, M. A. (1998). Recycling of organic matter in Antarctic sediments: A transect through the polar front in the Southern Ocean (Indian Sector). *Limnology and Oceanography*, 43(3), 420-432.
- Ramalho, S. P., Adão, H., Kiriakoulakis, K., Wolff, G. A., Vanreusel, A., & Ingels, J. (2014). Temporal and spatial variation in the Nazaré Canyon (Western Iberian margin): Inter-annual and canyon heterogeneity effects on meiofauna biomass and diversity. *Deep Sea Research Part I: Oceanographic Research Papers*, 83, 102-114.
- Ramirez-Llodra, E., Company, J. B., Sarda, F., & Rotllant, G. (2010). Megabenthic diversity patterns and community structure of the Blanes submarine canyon and adjacent slope in the Northwestern Mediterranean: a human overprint?. *Marine Ecology*, 31(1), 167-182.
- Rex, M. A., Etter, R. J., Morris, J. S., Crouse, J., McClain, C. R., Johnson, N. A., Stuart, C.T., Deming, J.W., Thies, R., & Avery, R. (2006). Global bathymetric patterns of standing stock and body size in the deep-sea benthos. *Marine Ecology Progress Series*, 317, 1-8.
- Rowe, G. T. (1971). Observations on bottom currents and epibenthic populations in Hatteras Submarine Canyon. In *Deep Sea Research and Oceanographic Abstracts* (Vol. 18, No. 6, pp. 569-581). Elsevier.
- Rowe, G. T. (1983). Biomass and production of the deep-sea macrobenthos. *The sea*, 8, 97-121.
- Rowe, G. T., Sibuet, M., Deming, J., Tietjen, J., & Khripounoff, A. (1990). Organic carbon turnover time in deep-sea benthos. *Progress in oceanography*, 24(1-4), 141-160.
- Rowe, G. T., Wei, C., Nunnally, C., Haedrich, R., Montagna, P., Baguley, J. G., Bernhard, J. M., Wicksten, M., Ammons, A., Briones, E. E., Soliman, Y., & Deming, J. W. (2008). Comparative biomass structure and estimated carbon flow in

- food webs in the deep Gulf of Mexico. *Deep Sea Research Part II: Topical Studies in Oceanography*, 55(24-26), 2699-2711.
- Rowe, G., Sibuet, M., Deming, J., Khripounoff, A., Tietjen, J., Macko, S., & Theroux, R. (1991). 'Total' sediment biomass and preliminary estimates of organic carbon residence time in deep-sea benthos. *Marine Ecology Progress Series*, 99-114.
- Schlacher, T. A., Schlacher-Hoenlinger, M. A., Williams, A., Althaus, F., Hooper, J. N., & Kloser, R. (2007). Richness and distribution of sponge megabenthos in continental margin canyons off southeastern Australia. *Marine Ecology Progress Series*, 340, 73-88.
- Schroeder, L. A. (1981). Consumer growth efficiencies: their limits and relationships to ecological energetics. *Journal of Theoretical Biology*, 93(4), 805-828.
- Shepard, F. P. (1973). Submarine geology (No. 551.4 SHE).
- Shepard, F. P. (1981). Submarine canyons: multiple causes and long-time persistence. *AAPG bulletin*, 65(6), 1062-1077.
- Shepard, F. P., Dill, R. F., & Dill, R. F. (1966). Submarine canyons and other sea valleys. Rand McNally.
- Sibuet, M. (1977). Répartition et diversité des Echinodermes (Holothurides-Astérides) en zone profonde dans le Golfe de Gascogne. *Deep Sea Research*, 24(6), 549-563.
- Smallwood, B. J., Wolff, G. A., Bett, B. J., Smith, C. R., Hoover, D., Gage, J. D., & Patience, A. (1999). Megafauna can control the quality of organic matter in marine sediments. *Naturwissenschaften*, 86(7), 320-324.
- Smith Jr, K. L. (1987). Food energy supply and demand: A discrepancy between particulate organic carbon flux and sediment community oxygen consumption in the deep ocean 1. *Limnology and Oceanography*, 32(1), 201-220.
- Smith Jr, K. L., & Kaufmann, R. S. (1999). Long-term discrepancy between food supply and demand in the deep eastern North Pacific. *Science*, 284(5417), 1174-1177.
- Smith, C. R., De Leo, F. C., Bernardino, A. F., Sweetman, A. K., & Arbizu, P. M. (2008). Abyssal food limitation, ecosystem structure and climate change. *Trends in Ecology & Evolution*, 23(9), 518-528.
- Smith, K. L., Huffard, C. L., Sherman, A. D., & Ruhl, H. A. (2016). Decadal change in sediment community oxygen consumption in the abyssal northeast Pacific. *Aquatic geochemistry*, 22(5), 401-417.
- Snelgrove, P. V., Soetaert, K., Solan, M., Thrush, S., Wei, C. L., Danovaro, R., Fulweiler, R.W., Kitazato, H., Ingole, B., Norkko, A., Parkes, R.J., & Volkenborn, N. (2018). Global carbon cycling on a heterogeneous seafloor. *Trends in Ecology & Evolution*, 33(2), 96-105.

- 
- Snelgrove, P. V., Thrush, S. F., Wall, D. H., & Norkko, A. (2014). Real world biodiversity–ecosystem functioning: a seafloor perspective. *Trends in ecology & evolution*, 29(7), 398-405.
- Sobarzo, M., Figueroa, M., & Djurfeldt, L. (2001). Upwelling of subsurface water into the rim of the Biobio submarine canyon as a response to surface winds. *Continental Shelf Research*, 21(3), 279-299.
- Soetaert, K., & Herman, P. M. (2009). A practical guide to ecological modelling: using R as a simulation platform (Vol. 7, No. 7). New York: Springer.
- Soetaert, K., & van Oevelen, D. (2009). Modeling food web interactions in benthic deep-sea ecosystems: a practical guide. *Oceanography*, 22(1), 128-143.
- Steinberg, D. K., Van Mooy, B. A., Buesseler, K. O., Boyd, P. W., Kobari, T., & Karl, D. M. (2008). Bacterial vs. zooplankton control of sinking particle flux in the ocean's twilight zone. *Limnology and Oceanography*, 53(4), 1327-1338.
- Stratmann, T., Lins, L., Purser, A., Marcon, Y., Rodrigues, C. F., Ravara, A., Cunha, M. R., Simon-Lledó, E., Jones, D. O. B., Sweetman, A. K., Köser, K., & Van Oevelen, D. (2018). Abyssal plain faunal carbon flows remain depressed 26 years after a simulated deep-sea mining disturbance. *Biogeosciences*, 15(13), 4131-4145.
- Stratmann, T., Soetaert, K., Wei, C.-L., and van Oevelen, D.: The role of benthos in the global marine carbon cycle, *Global Biogeochem. Cy.*, unpublished.
- Su, C. C., Tseng, J. Y., Hsu, H. H., Chiang, C. S., Yu, H. S., Lin, S., & Liu, J. T. (2012). Records of submarine natural hazards off SW Taiwan. Geological Society, London, Special Publications, 361(1), 41-60.
- Talling, P. J., Paull, C. K., & Piper, D. J. (2013). How are subaqueous sediment density flows triggered, what is their internal structure and how does it evolve? Direct observations from monitoring of active flows. *Earth-Science Reviews*, 125, 244-287.
- Tyler, P. A., Grant, A., Pain, S. L., & Gage, J. D. (1982). Is annual reproduction in deep-sea echinoderms a response to variability in their environment?. *Nature*, 300(5894), 747-750.
- Ulanowicz, R. E. (1980). An hypothesis on the development of natural communities. *Journal of theoretical Biology*, 85(2), 223-245.
- Ulanowicz, R. E. (1986). A phenomenological perspective of ecological development. ASTM International.
- Ulanowicz, R. E. (2004). Quantitative methods for ecological network analysis. *Computational biology and chemistry*, 28(5-6), 321-339.
- Ulanowicz, R.E., (1997). Ecology the ascendent perspective. In: Allen, T.F.H., Roberts,

- 
- D.W. (Eds.), Complexity in Ecological Systems Series. Columbia University Press, New York
- Van den Meersche, K., Soetaert, K., & Van Oevelen, D. (2009). `xsample()`: an R function for sampling linear inverse problems. *Journal of Statistical Software*, 30, 1-15.
- Van Duyl, F. C., & Kop, A. J. (1994). Bacterial production in North Sea sediments: clues to seasonal and spatial variations. *Marine Biology*, 120(2), 323-337.
- Van Oevelen, D., Soetaert, K., Garcia, R., De Stigter, H. C., Cunha, M. R., Pusceddu, A., & Danovaro, R. (2011). Canyon conditions impact carbon flows in food webs of three sections of the Nazaré canyon. *Deep Sea Research Part II: Topical Studies in Oceanography*, 58(23-24), 2461-2476.
- Van Oevelen, D., Soetaert, K., Middelburg, J. J., Herman, P. M., Moodley, L., Hamels, I., ... & Heip, C. H. (2006). Carbon flows through a benthic food web: Integrating biomass, isotope and tracer data. *Journal of Marine Research*, 64(3), 453-482.
- Van Oevelen, D., Van den Meersche, K., Meysman, F. J., Soetaert, K., Middelburg, J. J., & Vézina, A. F. (2010). Quantifying food web flows using linear inverse models. *Ecosystems*, 13(1), 32-45.
- Van Santen, P., Augustinus, P. G. E. F., Janssen-Stelder, B. M., Quartel, S., & Tri, N. H. (2007). Sedimentation in an estuarine mangrove system. *Journal of Asian Earth Sciences*, 29(4), 566-575.
- Verdugo, P., Alldredge, A. L., Azam, F., Kirchman, D. L., Passow, U., & Santschi, P. H. (2004). The oceanic gel phase: a bridge in the DOM-POM continuum. *Marine Chemistry*, 92(1-4), 67-85.
- Vetter, E. W., & Dayton, P. K. (1998). Macrofaunal communities within and adjacent to a detritus-rich submarine canyon system. *Deep Sea Research Part II: Topical Studies in Oceanography*, 45(1-3), 25-54.
- Vetter, E. W., & Dayton, P. K. (1999). Organic enrichment by macrophyte detritus, and abundance patterns of megafaunal populations in submarine canyons. *Marine Ecology Progress Series*, 186, 137-148.
- Vézina, A. F., & Platt, T. (1988). Food web dynamics in the ocean. 1. Best-estimates of flow networks using inverse methods. *Marine ecology progress series*. Oldendorf, 42(3), 269-287.
- Walsh, J. P., Alexander, C. R., Gerber, T., Orpin, A. R., & Sumners, B. W. (2007). Demise of a submarine canyon? Evidence for highstand infilling on the Waipaoa River continental margin, New Zealand. *Geophysical Research Letters*, 34(20).
- Wang, Y. H., Lee, I. H., & Liu, J. T. (2008). Observation of internal tidal currents in the

- 
- Kaoping Canyon off southwestern Taiwan. *Estuarine, Coastal and Shelf Science*, 80(1), 153-160.
- Warwick, R. M., & Gee, J. M. (1984). Community structure of estuarine meiobenthos. *Marine Ecology Progress Series*, 18, 97-111.
- Wei, C. L., Rowe, G. T., Escobar-Briones, E., Boetius, A., Soltwedel, T., Caley, M. J., Soliman, Y., Huettmann, F., Qu, F., Yu, Z., Pitcher, C.R., Haedrich, R.L., Wicksten, M.K., Rex, M.A., Baguley, J.G., Sharma, J., Danovaro, R., MacDonald, I.R., Nunnally, C.C., Deming, J.W., Montagna, P., Lévesque, M., Marcin Weslawski, Jan, Wlodarska-Kowalczyk, Maria, Ingole, B.S., Bett, B.J., Billett, D.S.M., Yool, A., Bluhm, B.A., Iken, K., & Narayanaswamy, B. E. (2010). Global patterns and predictions of seafloor biomass using random forests. *PloS one*, 5(12), e15323.
- Wei, C. L., Rowe, G. T., Escobar-Briones, E., Nunnally, C., Soliman, Y., & Ellis, N. (2012). Standing stocks and body size of deep-sea macrofauna: Predicting the baseline of 2010 Deepwater Horizon oil spill in the northern Gulf of Mexico. *Deep Sea Research Part I: Oceanographic Research Papers*, 69, 82-99.
- Wenzhöfer, F., & Glud, R. N. (2002). Benthic carbon mineralization in the Atlantic: a synthesis based on in situ data from the last decade. *Deep Sea Research Part I: Oceanographic Research Papers*, 49(7), 1255-1279.
- Wenzhöfer, F., & Glud, R. N. (2004). Small-scale spatial and temporal variability in coastal benthic O₂ dynamics: Effects of fauna activity. *Limnology and Oceanography*, 49(5), 1471-1481.
- Yamamoto, N., & Lopez, G. (1985). Bacterial abundance in relation to surface area and organic content of marine sediments. *Journal of Experimental Marine Biology and Ecology*, 90(3), 209-220.
- Yoklavich, M. M., Greene, H. G., Cailliet, G. M., Sullivan, D. E., Lea, R. N., & Love, M. S. (2000). Habitat associations of deep-water rockfishes in a submarine canyon: an example of a natural refuge. *Fishery Bulletin*, 98(3), 625-625.
- Yu, H. S., Chiang, C. S., & Shen, S. M. (2009). Tectonically active sediment dispersal system in SW Taiwan margin with emphasis on the Gaoping (Kaoping) Submarine Canyon. *Journal of Marine Systems*, 76(4), 369-382.
- Zhang, L. J., Wang, L., Cai, W. J., Liu, D. M., & Yu, Z. G. (2013). Impact of human activities on organic carbon transport in the Yellow River. *Biogeosciences*, 10(4), 2513-2524.

Table



Table 1. Sampling cruises including dates, coordinates, and water depths of two sites. Different gears were used to collect sediment and benthic fauna samples. Cruises

were assigned to the corresponding seasons to test the seasonal effect.

Date	Season	Cruise	Station	Long (°E)	Lat (°N)	Depth (m)	Measurement	Gear
2014/11	AU	OR1_1096	GC1	120.4170	22.4170	222	Sediment TOC, Macrofauna	CTD, Boxcorer
			GS1	120.4006	22.2349	270	Sediment TOC, Macrofauna	CTD, Boxcorer
2015/03	SP	OR1_1099	GC1	120.3768	22.4017	395	Sediment TOC, Macrofauna	CTD, Multicorer
			GS1	120.4002	22.2328	277	Sediment TOC, Macrofauna	CTD, Multicorer
2015/04	SP	OR1_1102	GC1	120.4114	22.4173	323	Sediment TOC, Macrofauna	CTD, Boxcorer
			GS1	120.4006	22.2329	279	Sediment TOC, Macrofauna	CTD, Boxcorer
2015/08	SU	OR1_1114	GC1	120.4114	22.4172	320	Sediment TOC, Meiofauna, Macrofauna	CTD, Multicorer
			GS1	120.3998	22.2322	279	Sediment TOC, Meiofauna, Macrofauna	CTD, Multicorer
2015/11	AU	OR1_1126	GC1	120.4112	22.4175	318	Sediment TOC, Meiofauna, Macrofauna, DOU	CTD, Multicorer
			GS1	120.3995	22.2329	277	Sediment TOC, Meiofauna, Macrofauna, DOU	CTD, Multicorer
2016/02	SP	OR1_1128	GC1	120.4108	22.4171	319	Sediment TOC, Meiofauna, Macrofauna, TOU, DOU	CTD, Multicorer
2016/03	SP	OR1_1132	GS1	120.4008	22.2296	281	Meiofauna, Macrofauna	CTD, Multicorer
2016/10	AU	OR1_1151	GC1	120.4110	22.4176	317	Sediment TOC, Macrofauna, TOU, DOU	CTD, Multicorer
			GS1	120.4004	22.2315	272	Sediment TOC, Macrofauna, DOU	CTD, Multicorer
2018/03-04	SP	OR1_1190	GC1	120.4104	22.4172	321	Sediment TOC, Bacteria, Macrofauna, TOU, DOU	CTD, Multicorer
			GS1	120.3977	22.2309	279	Sediment TOC, Bacteria, Macrofauna, TOU, DOU	CTD, Multicorer
2019/03-04	SP	OR1_1219	GC1	120.4092	22.4179	318	Sediment TOC, TOU, DOU	CTD, Multicorer
			GS1	120.3772	22.2538	246	Sediment TOC, TOU, DOU	CTD, Multicorer
2019/10	AU	OR1_1242	GC1	120.4082	22.4168	271	Sediment TOC, TOU, DOU	CTD, Multicorer
			GS1	120.3776	22.2531	261	Sediment TOC, TOU, DOU	CTD, Multicorer
2020/11	AU	NOR1_T004	GC1	120.4121	22.4140	309	Sediment TOC, TOU, DOU	CTD, Multicorer



Table 2. Definition of each flow in Fig. 2. The flows are with direction, for example, “SED->BAC”

represents carbon flow from the detritus stock to bacteria stock.

Flow	Meaning
POC->SED	Organic carbon derived from the water column
SED->EXP_S	Sediment export(e.g. downslope, burial...)
SED->BAC	Bacteria feed on detritus OC
BAC->SED	Bacteria feces deposit on sediment
SED->MEI	Meiofauna feed on detritus OC
MEI->SED	Meiofauna feces deposit on sediment
SED->MAC	Macrofauna feed on detritus OC
MAC->SED	Macrofauna feces deposit on sediment
BAC->MEI	Meiofauna feed on bacteria
BAC->MAC	Macrofauna feed on bacteria
MEI->MAC	Macrofauna feed on meiofauna
MEI->EXP_B	Meiofauna predated by other benthopelagic/pelagic predators
MAC->EXP_B	Macrofauna predated by other benthopelagic/pelagic predators
BAC->DIC	Bacteria respiration
MEI->DIC	Meiofauna respiration
MAC->DIC	Macrofauna respiration



Table 3. The conceptual model of the food web structure formed the basis of our linear inverse model (LIM). See section “Structure” for description.

Inequality description	Calculation	GC1	GS1	Unit	Reference
Temperature limitation (Tlim)	$Q_{10} * \exp((T-20)/10)$, with $Q_{10} = 2$	1.05	1.09	-	
Bacteria growth efficiency		[0.02, 0.61]	[0.02, 0.61]	-	del Giorgio and Cole (1998)
DOU (Bacteria → DIC)	Maximum DOU= 30% TOU	[0.0, 21.77]	[0.0, 16.01]	mg C/m ² /d	Mahaut et al. (1995)
Maintenance respiration of meiofauna		Tlim * 0.01 * Stock	Tlim * 0.01 * Stock	mg C/m ² /d	van Oevelen et al. (2011)
Maintenance respiration of macrofauna		Tlim * 0.01 * Stock	Tlim * 0.01 * Stock	mg C/m ² /d	van Oevelen et al. (2011)
Assimilation efficiency of meiofauna		[0.456, 0.699]	[0.456, 0.699]	-	Conover (1966)
Assimilation efficiency of macrofauna		[0.6, 0.7]	[0.6, 0.7]	-	Loo and Rosenberg (1996)
P/B ratio of meiofauna		[0.0090, 0.0493]	[0.0090, 0.0493]	-	Fenchel (1982); Fleeger and Palmer (1982)
P/B ratio of macrofauna		[0.0008, 0.0048]	[0.0008, 0.0048]	-	Stratmann et al. (2018)
Net growth efficiency of meiofauna		[0.3, 0.5]	[0.3, 0.5]	-	Herman and Heip (1985); Banse and Mosher (1980); Herman et al. (1983; 1984)
Net growth efficiency of macrofauna		[0.6, 0.72]	[0.6, 0.72]	-	Navarro et al., 1994; Nielsen et al., 1995
Sedimentation rate		[75.93, 137.92]	[57.18, 66.80]	mg C/m ² /d	Huh et al. (2009)
Sediment burial efficiency		[0.24, 1]	[0.24, 1]	-	Hsu et al. (2014)

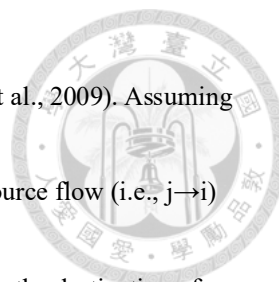


Table 4. Nomenclature of symbols used in calculation of network indices (Kones et al., 2009). Assuming

that a system has n compartments, and the flow value T_{ij} is defined as a sink-to-source flow (i.e., $j \rightarrow i$)

(Latham, 2006). The compartment imports to the internal network is labeled with 0, the destination of

usable exports (secondary production) is labeled $n + 1$, and the destination of unusable exports

(respiration/dissipation) is labeled $n + 2$ (Hirata & Ulanowicz, 1984).

Term	Description
n	Number of internal compartments in the network, excluding 0 (zero), $n + 1$ and $n + 2$
$j = 0$	External source
$j = n + 1$	Useable export from the food web (export)
$j = n + 2$	Unusable export from the food web (dissipation)
T_{ij}	Flow from compartment j to i where j represents the columns of the flow matrix and i the rows
T_{ij}^*	Flow matrix, excluding flows to and from the externals
T_i	Total inflows to compartment i
T_j	Total outflows from compartment j
T_i^c	Total inflows to compartment i excluding inflow from external sources
T_j^c	Total outflows from compartment j excluding outflow to external sources
$(x_i)_-$	A negative state derivative, considered as a gain to the system pool of mobile energy
$(x_i)_+$	A positive state derivative, considered as a loss from the system pool of mobile energy
Z_{i0}	Flow into compartment i from outside the network
Y_{n+j}	Flow out of the network for compartment j to compartments $n + 1$ and $n + 2$ respectively
C_{ij}	The number of species with which both i j interact divided by the number of species with which either i or j interact
I	Identity matrix



Table 5. Formula of the network indices; see Table 4. for the symbols.

Index type	Index name	Symbol	Formula	Reference
General indices	Total system throughput	T..	$\sum_{i=1}^{n+2} \sum_{j=0}^n T_{ij}$	Hirata & Ulanowicz (1984)
General indices	Total system throughflow	TST	$\sum_{i=1}^n \sum_{j=1}^n [T_{ij} + z_{i0} - (x_i)_-] = \sum_{i=1}^n \sum_{j=1}^n [T_{ij} + y_{n+j} - (x_i)_+]$	Latham (2006)
General indices	Total system cycled throughflow	TST _C	$\sum_{j=0}^n \left(1 - \frac{1}{q_{ij}}\right) T_j, \text{ where } Q = (I - G')^{-1}, \text{ where } G' = [T_{ij}^* / \max(T_i, T_j)]$	Finn (1976; 1978;1980), Patten & Higashi (1984); Patten et al. (1976)
Pathway analysis	Finn's cycling index	FCI	$\frac{TST_C}{TST}$	
Network uncertainty	Average mutual infromation	AMI	$k \sum_{i=1}^{n+2} \sum_{j=0}^n \frac{T_{ij}}{T_{..}} \log_2 \frac{T_{ij} T_{..}}{T_{i.} T_{.j}}$	Ulanowicz (2004)



Table 6. Standing stocks (in mg C/ m²) as mean± standard deviation of the food web compartments for

GC1 and GS1.

Compartment	GC1	GS1
Detritus	350270 ± 104003.4	524425.7 ± 34800.15
Bacteria	65.31 ± 12.74	42.80 ± 6.75
Meiofauna	1.49 ± 1.53	33.39 ± 26.48
Macrofauna	3.65 ± 7.70	80.20 ± 66.10

Table 7. Average bottom water temperature and the calculated "Tlim" of GC1 and GS1.

Station	Averaged bottom water temperature(°C)	<i>Tlim</i>
GC1	13.54	1.05
GS1	13.90	1.09

Table 8. PERMDISP and PERMANOVA on sediment carbon stock GC1 and GS1.

PERMDISP					
	Df	Sum of squares	Mean squares	F-value	Pr (>F)
Habitat	1	4.2034e+09	4203409008	3.0159	0.1051
Residuals	16	2.2300e+10	1393745915		
Season	1	6.2729e+09	6272856607	1.6005	0.2263
Residuals	16	6.2709e+10	3919334785		
PERMANOVA					
	Df	Sum of squares	R2	F-value	Pr (>F)
Habitat	1	1.3517e+11	0.61649	25.9645	0.0003***
Season	1	1.1106e+08	0.00051	0.0213	0.8816
Habitat:Season	1	1.1092e+10	0.05059	2.1306	0.1673
Residual	14	7.2883e+10	0.33241		
Total	17	2.1926e+11	1.00000		



Table 9. T-test on bacteria carbon stock of GC1 and GS1.

Welch Two Sample t-test				
Df	GC1 Mean	GS1 Mean	t	p-value
13.677	65.30876	42.80281	4.9356	0.0002347***

Table 10. PERMDISP and PERMANOVA on meiofaunal carbon stock of GC1 and GS1.

PERMDISP					
	Df	Sum of squares	Mean squares	F-value	Pr (>F)
Habitat	1	0.00083406	0.00083406	30.284	0.0001 ***
Residuals	16	0.00044066	0.00002754		
Season	2	0.00116895	0.00058448	25.979	0.0001 ***
Residuals	15	0.00033748	0.00002250		
PERMANOVA					
	Df	Sum of squares	R2	F-value	Pr (>F)
Habitat	1	0.0022880	0.49908	15.941	0.0002 ***
Residual	16	0.0022965	0.50092		
Total	17	0.0045845	1.00000		

Table 11. PERMDISP and PERMANOVA on macrofaunal carbon stock of GC1 and GS1.

PERMDISP					
	Df	Sum of squares	Mean squares	F-value	Pr (>F)
Habitat	1	2.4262	2.42623	37.932	0.0001 ***
Residuals	40	2.5585	0.06396		
Season	1	0.3203	0.32031	1.1371	0.298
Residuals	40	11.2673	0.28168		
PERMANOVA					
	Df	Sum of squares	R2	F-value	Pr (>F)
Habitat	1	4.6696224	0.35871952	22.9487	0.0001 ***
Season	1	0.3649373	0.02803441	1.793473	0.1906
Habitat:Season	1	0.2506460	0.01925458	1.2318	0.2816
Residual	38	7.7322695	0.59399149		
Total	41	13.0174751	1.00000		

Table 12. Average oxygen utilization rates (mg C/ m²/d) of all cruises in GC1 and GS1, represented as mean± standard deviation.

Station	TOU	DOU	BMU
GC1	72.58901 ± 16.603905	19.80919±22.72966	62.34343±45.86694
GS1	53.37575 ± 4.061608	11.67663±8.148866	62.01101±40.56152



Table 13. PERMDISP and PERMANOVA on TOU of GC1 and GS1.

PERMDISP					
	Df	Sum of squares	Mean squares	F-value	Pr (>F)
Habitat	1	1818.9	1818.92	3.3882	0.0763
Residuals	25	13420.9	536.84		
Season	1	196.5	196.50	0.3012	0.5893
Residuals	25	16310.9	652.43		
PERMANOVA					
	Df	Sum of squares	R2	F-value	Pr (>F)
Habitat	1	1675	0.04973	1.2060	0.2867
Season	1	20	0.00059	0.0143	0.9095
Habitat:Season	1	41	0.00122	0.0295	0.8687
Residual	23	31946	0.94846		
Total	26	33682	1.00000		

Table 14. PERMDISP and PERMANOVA on DOU of GC1 and GS1.

PERMDISP					
	Df	Sum of squares	Mean squares	F-value	Pr (>F)
Habitat	1	63.7	63.71	0.4053	0.5425
Residuals	65	10216.8	157.18		
Season	1	23	22.984	0.1453	0.7412
Residuals	65	10282	158.186		
PERMANOVA					
	Df	Sum of squares	R2	F-value	Pr (>F)
Habitat	1	375.8	0.02769	1.8035	0.1925
Season	1	69.9	0.00515	0.3355	0.5836
Habitat:Season	1	0.0	0.00000	0.0001	0.9935
Residual	63	13128.0	0.96716		
Total	66	13573.7	1.00000		



Table 15. PERMDISP and PERMANOVA on BMU of GC1 and GS1. Note that the Number of

permutations was only 999.

PERMDISP					
	Df	Sum of squares	Mean squares	F-value	Pr (>F)
Habitat	1	3.2609	3.2609	0.5498	0.554
Residuals	5	29.6562	5.9312		
Season	1	2.4125	2.4125	0.4027	0.596
Residuals	5	29.9550	5.9910		
PERMANOVA					
	Df	Sum of squares	R2	F-value	Pr (>F)
Habitat	1	0.001	0.00001	0.0000	0.999
Season	1	0.005	0.00006	0.0002	0.974
Habitat:Season	1	9.440	0.10341	0.3461	0.614
Residual	3	81.839	0.89652		
Total	6	91.286	1.00000		

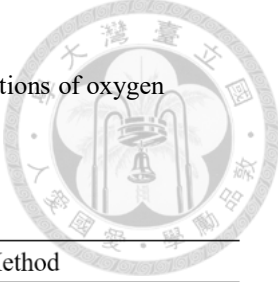
Table 16. Mean and standard deviation of the food web flows (mg C/ m²/ d) of the GC1 processed with the MCMC algorithm.

Flow	Mean	SD (±2%)
POC->SED	131.0813	15.718839894
SED->EXP_S	115.7699	12.745327433
SED->BAC	24.65287	7.984219083
BAC->SED	9.333087	6.129441886
SED->MEI	0.1351685	0.094398395
MEI->SED	0.1427569	0.052851363
SED->MAC	0.01158626	0.008464554
MAC->SED	0.01237802	0.002703155
BAC->MEI	0.1743825	0.113613234
BAC->MAC	0.01161126	0.008529056
MEI->MAC	0.01152755	0.008494257
MEI->EXP_B	0.04797334	0.014436516
MAC->EXP_B	0.01450261	0.002452046
BAC->DIC	15.13379e	4.724027779
MEI->DIC	0.1072931	0.031537262
MAC->DIC	0.007844448	0.001781753

Table 17. Mean and standard deviation of the food web flows (mg C/ m²/ d) of the GS1 processed with the MCMC algorithm.

Flow	Mean	SD ($\pm 2\%$)
POC->SED	78.9461651	3.37455051
SED->EXP_S	63.2342462	2.02409975
SED->BAC	24.5079327	4.21209840
BAC->SED	9.4396541	3.47065352
SED->MEI	3.8648229	2.01270266
MEI->SED	3.3291330	1.15358193
SED->MAC	0.4016262	0.25919974
MAC->SED	0.2936759	0.07290954
BAC->MEI	3.3326240	2.10875051
BAC->MAC	0.2084190	0.17275121
MEI->MAC	0.1984801	0.16944190
MEI->EXP_B	1.1590011	0.29228201
MAC->EXP_B	0.3252832	0.05975403
BAC->DIC	11.5272356	2.03033542
MEI->DIC	2.5108326	0.66658793
MAC->DIC	0.1895663	0.04661137

Table 18. Stock turnover (unit: year or day) calculated with the two different estimations of oxygen utilization rates.



Station	OC _{total} /TOU (yr)	OC _{bacteria} /DOU (d)	OC _(meiofauna+macrofauna) /BOU (d)	Method
GC1	13.22	3.2970	0.0824	Direct measurement
	62.94	4.3155	44.6422	Model results
GS1	19.80	3.6654	1.8318	Direct measurement
	101.02	3.7129	42.0642	Model results

Table 19. Comparison of network indices calculated for GC1 and GS1. The numbers indicate the fraction of network values that are higher in GC1.

Network indices	Fraction	Significance
T..	0.9987	*** (GC1>GS1)
TST	0.9623	*** (GC1>GS1)
TSTC	0.2926	
FCI	0.1034	Marginally GC1<GS1
AMI	0.2963	

Figure

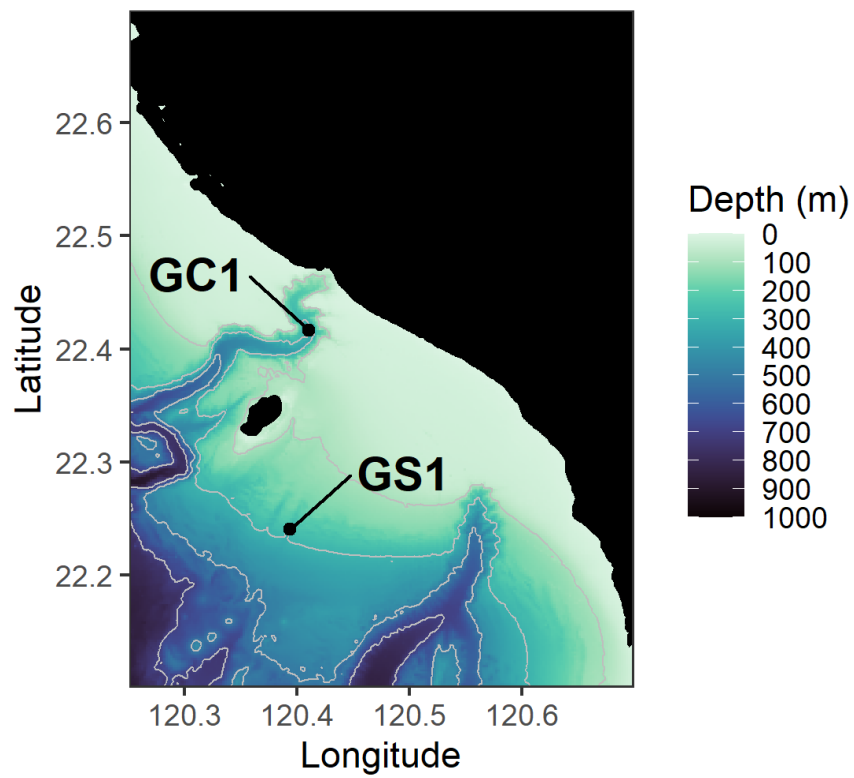


Figure 1. The map of sampling stations of the upper Gaoping Submarine Canyon (GC1) and Gaoping Slope (GS1).

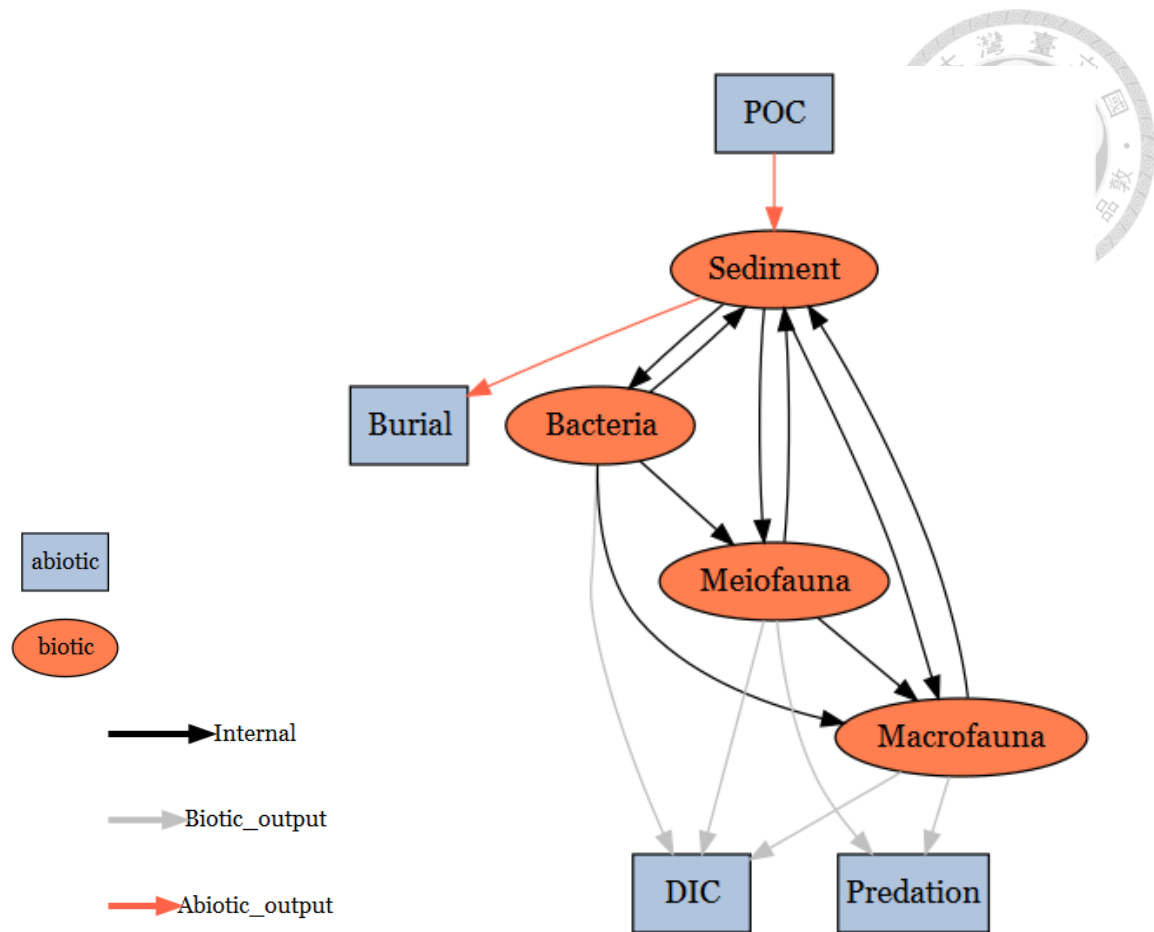


Figure 2. The conceptual model of the food web structure formed the basis of our linear inverse model

(LIM). See section “Structure” for description.

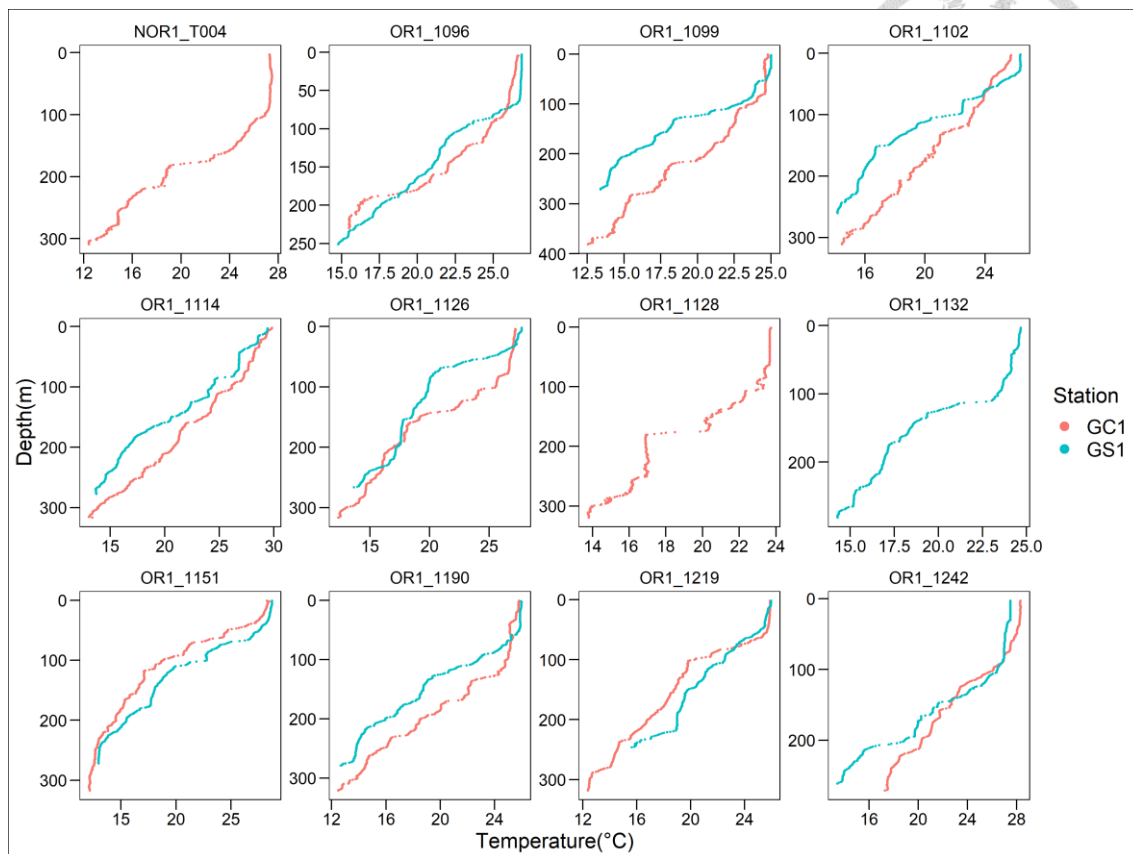


Figure 3 Water temperature profile for each cruise of the two sites.

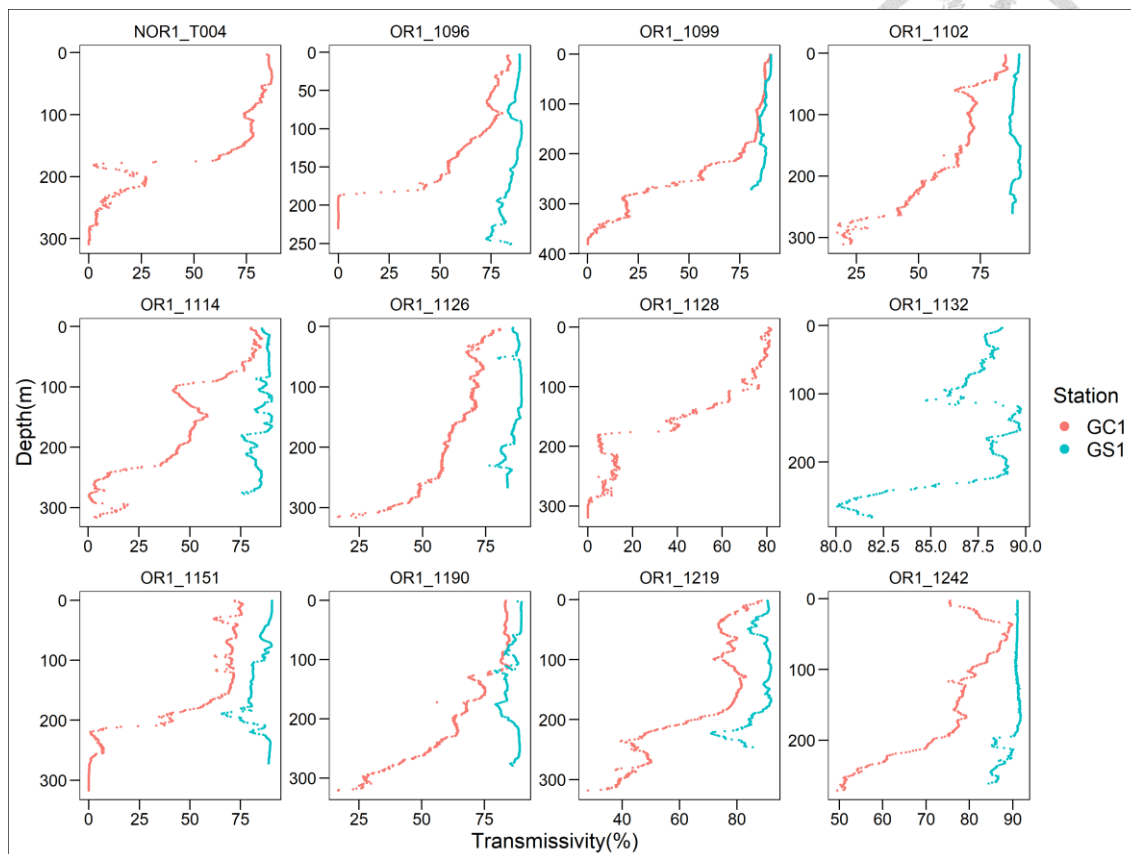


Figure 4. Light transmission profile for each cruise of the two sites. Note that GC1 has a very low light transmission below 200-meter depth in almost all the sampling cruises.

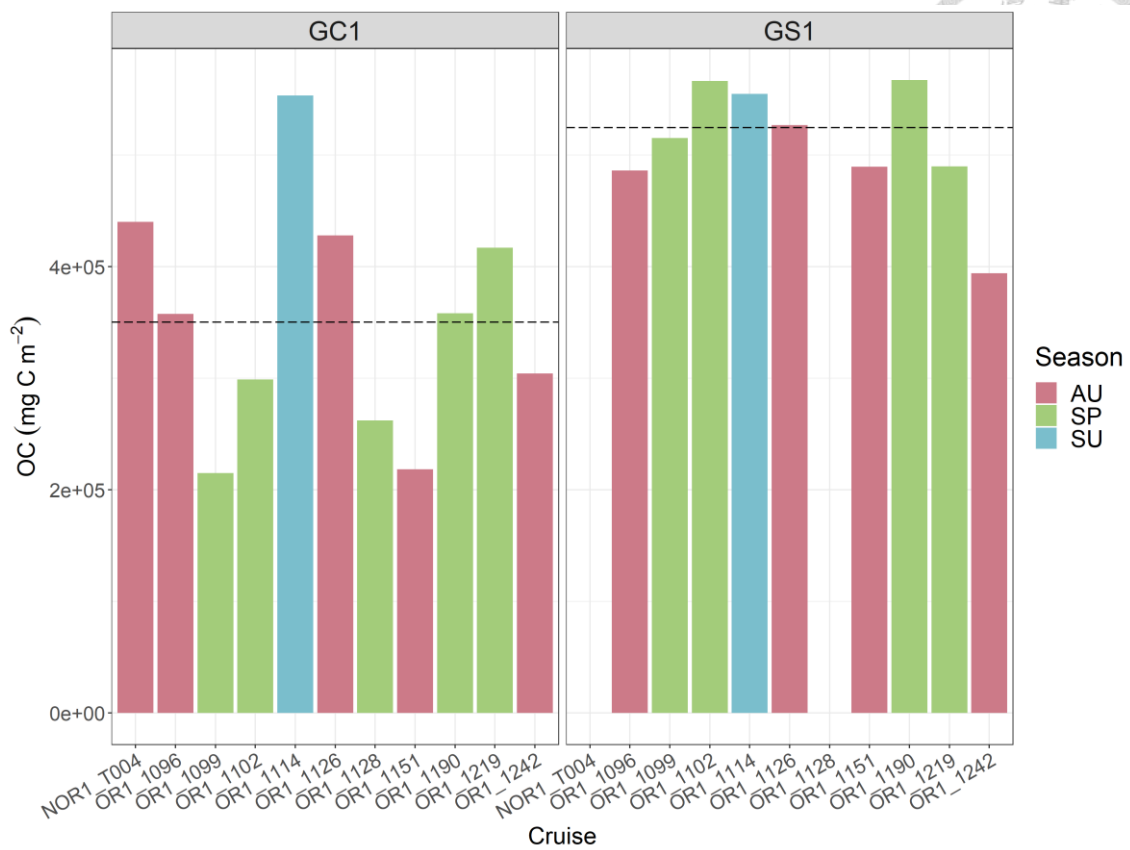


Figure 5. Carbon stocks of sediment of GC1 and GS1. The Cruises were labeled in different colors with different seasons. Note that there was no sampling in NOR1-T004 and OR1-1128 for GS1. The dotted lines represent the mean values of the stocks.

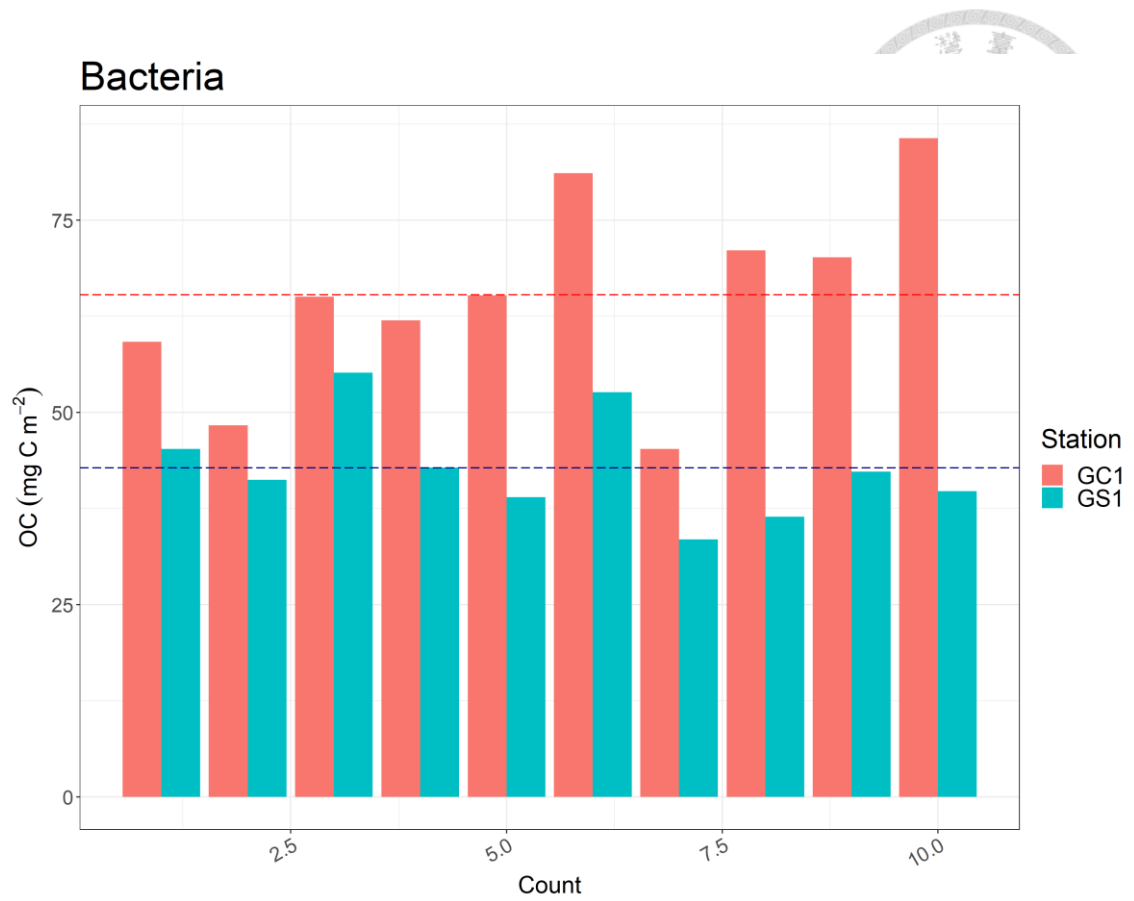


Figure 6. Carbon stocks of bacteria of GC1 and GS1. Note that bacteria were only collected in cruise

OR1-1190. The dotted line represents the mean value of each count.

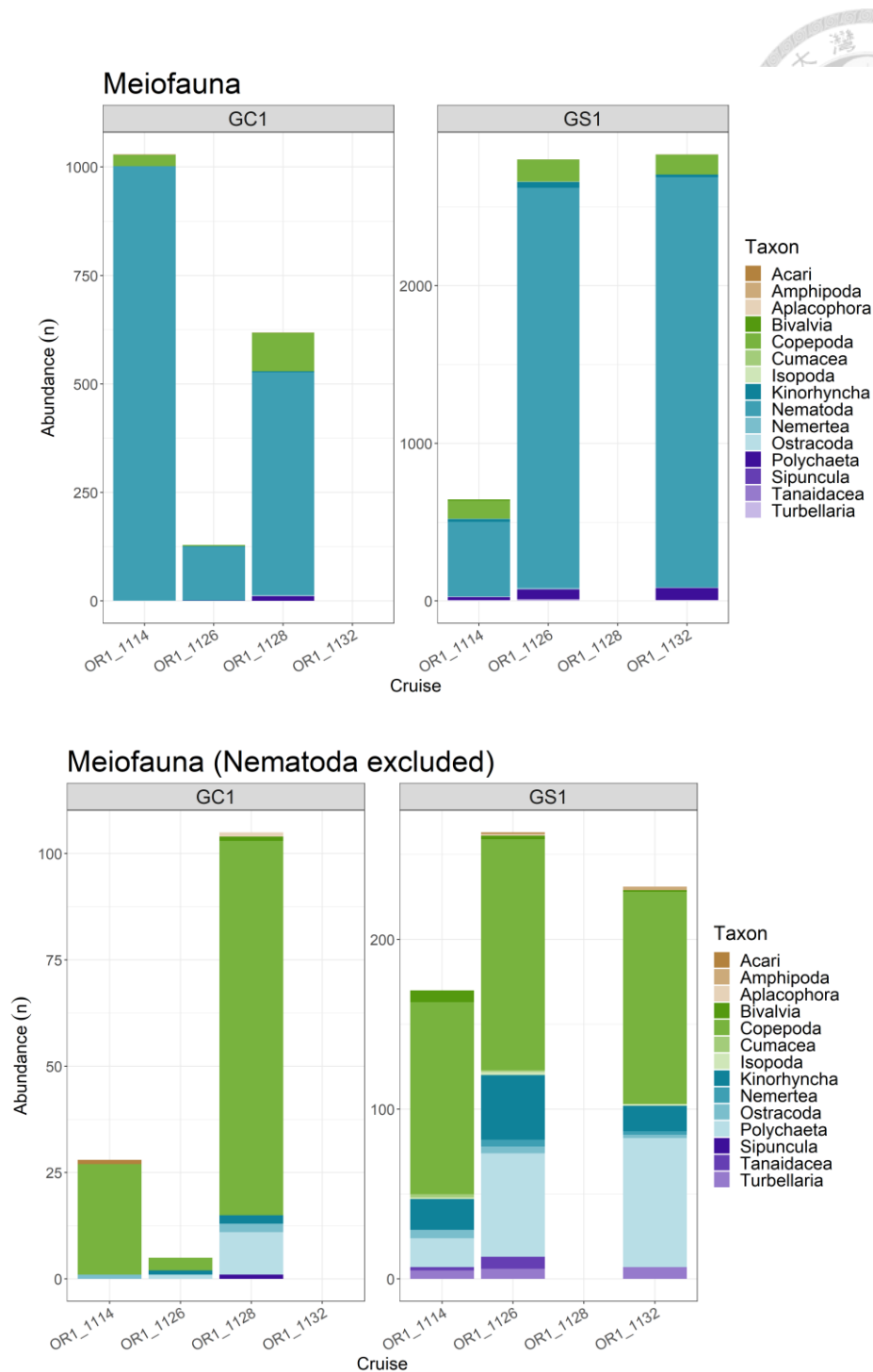


Figure 7. The abundance of meiofauna in each cruise of GC1 and GS1. Note that there was no sampling

in OR1-1132 for GC1 and OR1-1128 for GS1. The top figure included all the taxa, which were dominated

by Nematodes. The bottom one showed the composition without Nematodes.



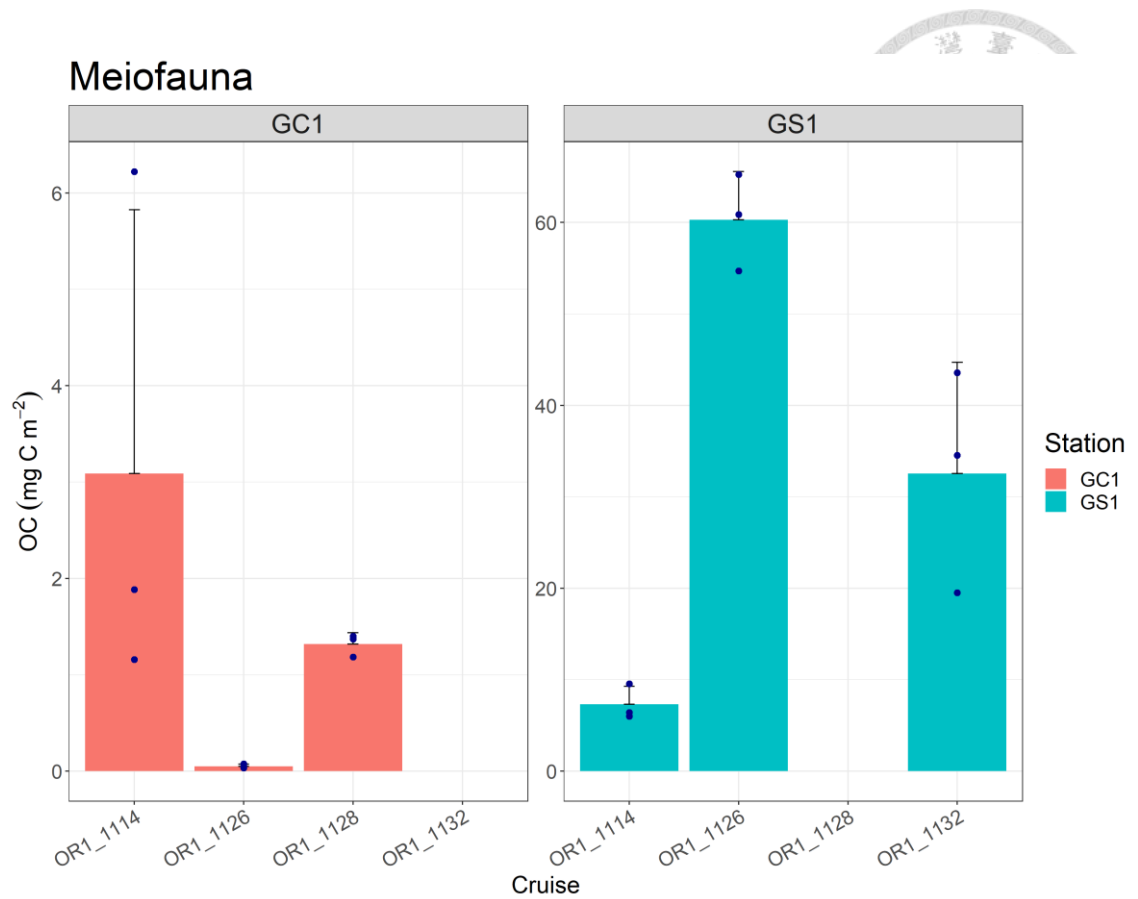


Figure 8. Carbon stocks of the meiofauna of GC1 and GS1. Note that meiofauna was only collected on three cruises for each site. The dot represents the sum of fauna biomass for each replicate. The bar represents the mean value of three replicates.

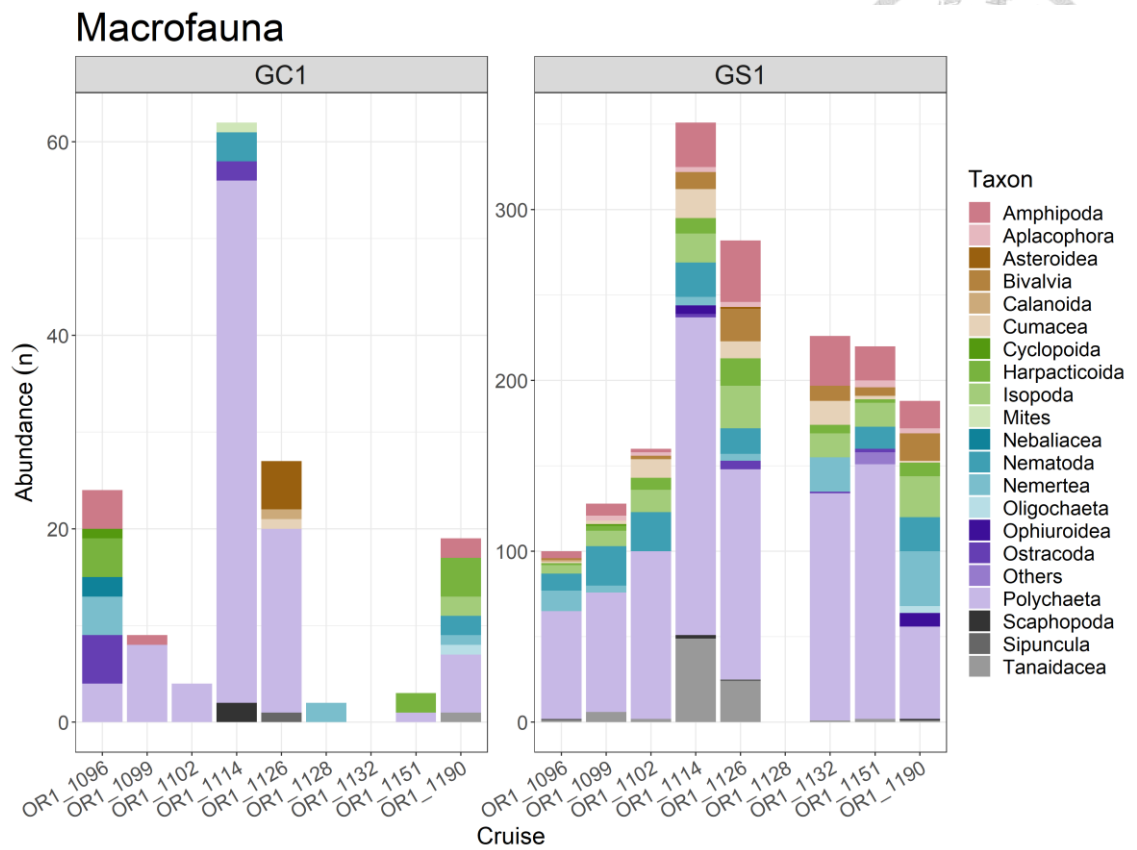


Figure 9. The abundance of macrofauna in each cruise of GC1 and GS1. Note that there was no sampling in OR1-1132 for GC1 and OR1-1128 for GS1.

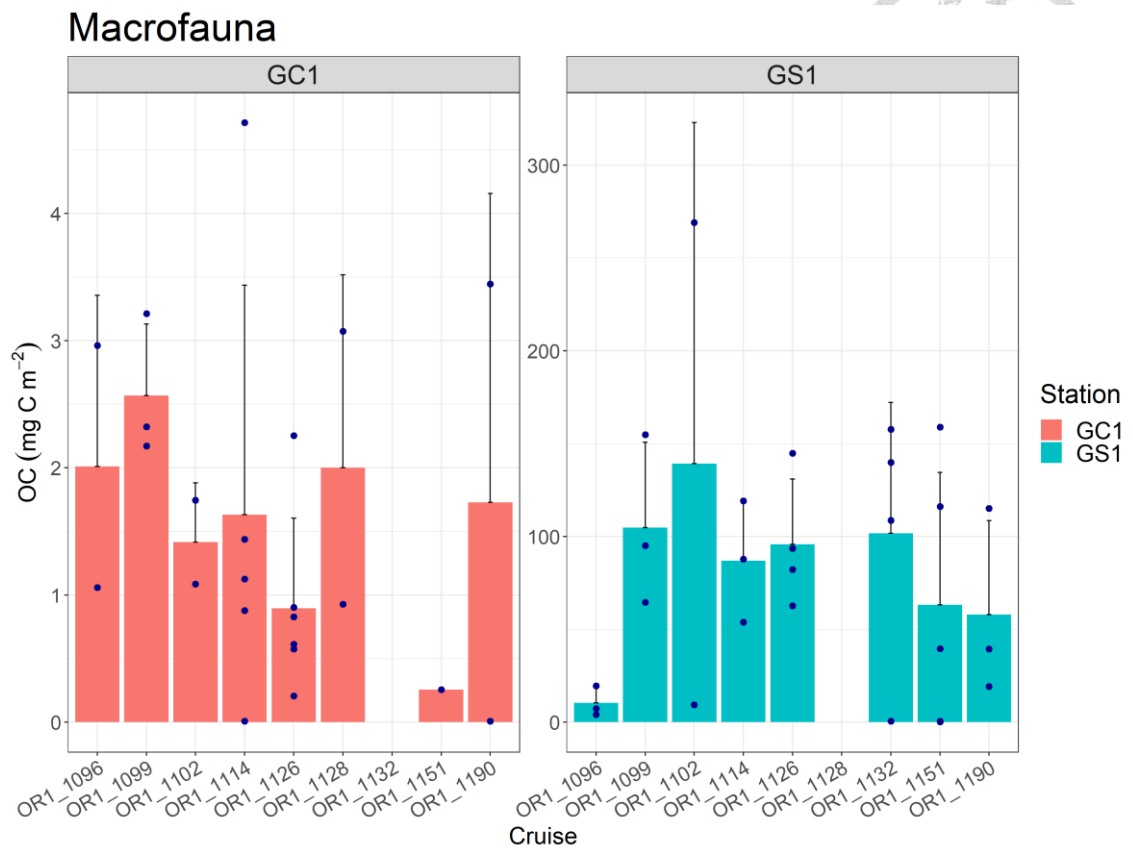


Figure 10. Carbon stocks of macrofauna of GC1 and GS1. Note that there was no sampling in OR1-1132

for GC1 and OR1-1128 for GS1. The dot represents the sum of fauna biomass for each replicate. The bar represents the mean value of three replicates.

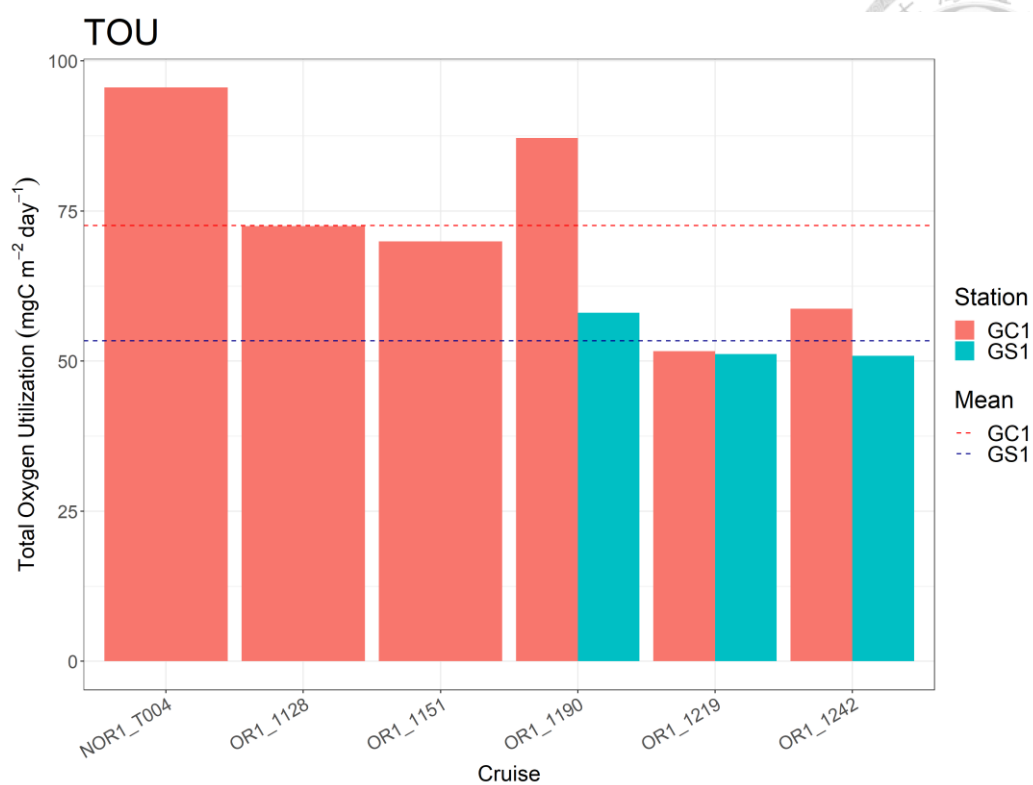


Figure 11. Average total oxygen utilization (TOU) for each cruise of GC1 and GS1. TOU was further divided into DOU and BOU. Note that there was no measurement in NOR1-T004 and OR1-1128 for GS1.

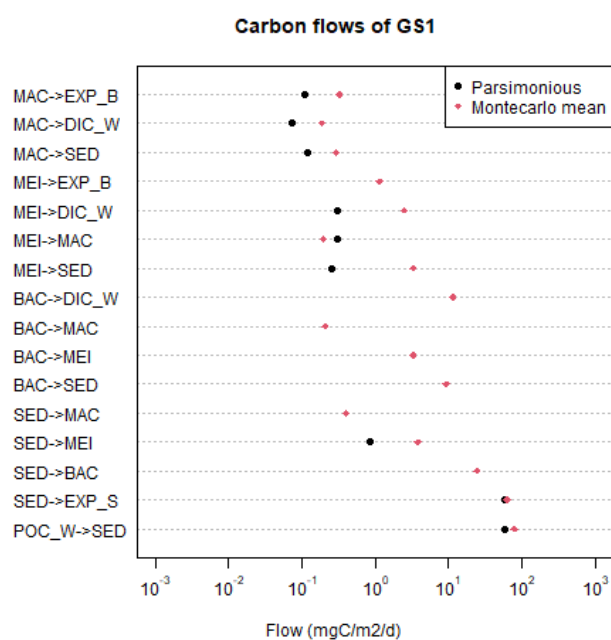
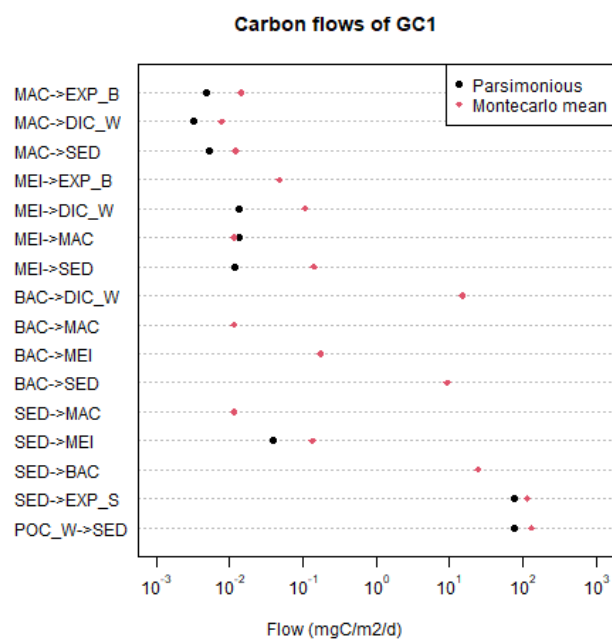


Figure 12. LIM results for each flow in the food web by the two different methods. Note that the value of some flows calculated with the parsimonious method was zero, which cannot be log-transformed. Thus these flows remain no black dot on the figure.

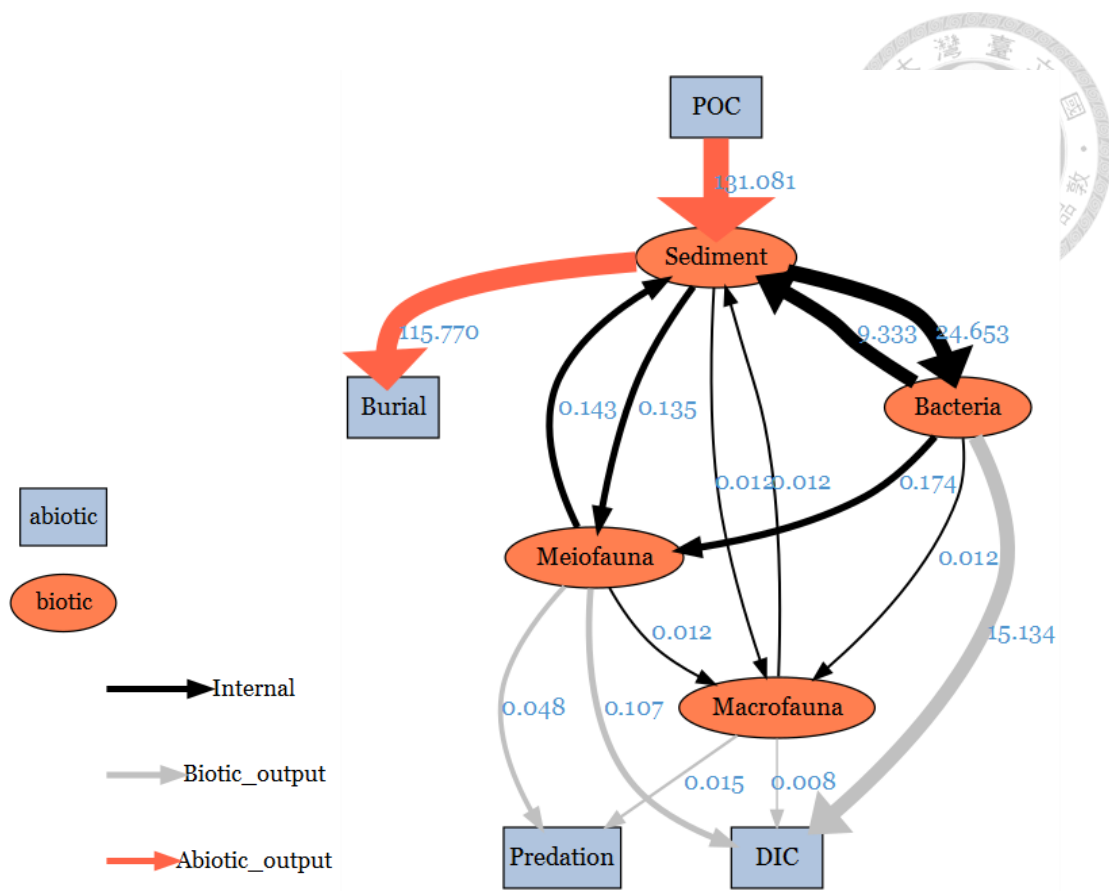


Figure 13. The conceptual model plotted with LIM results of GC1 processed with the MCMC algorithm.

The flows were drawn to scale.(Unit: mg C/ m²/ d)

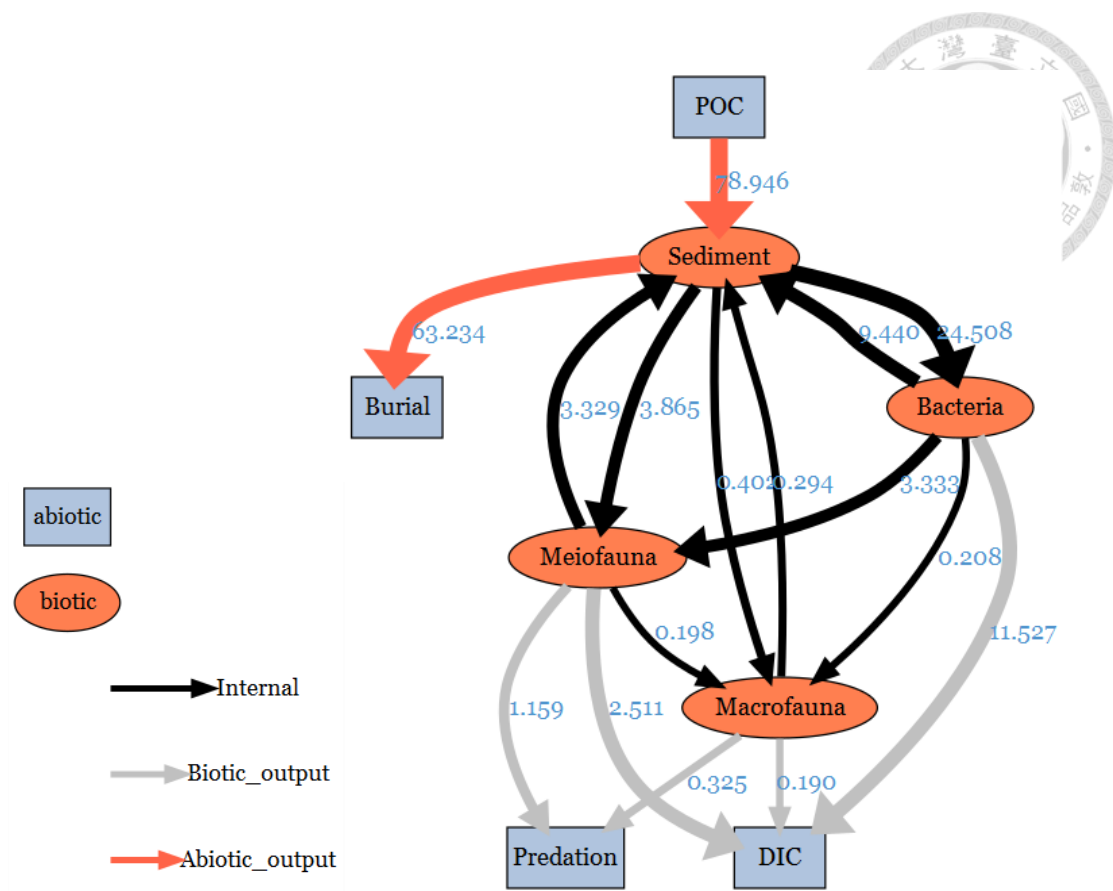


Figure 14. The conceptual model plotted with LIM results of GS1 processed with the MCMC algorithm.

The flows were drawn to scale. (Unit: mg C/ m²/ d)

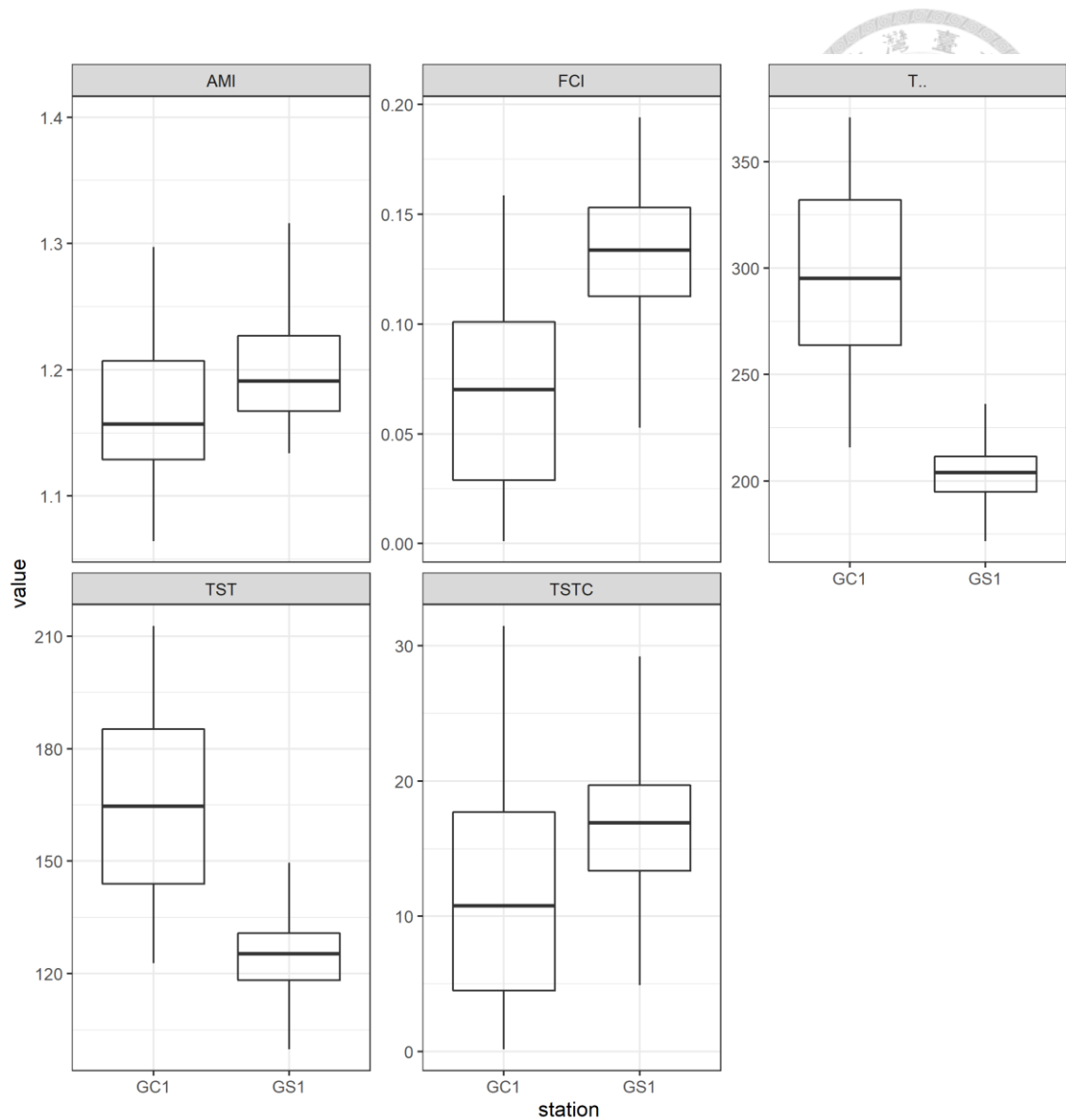


Figure 15. The selected network indices of GC1 and GS1. The indices were calculated from 10,000 solutions of the LIM. As a result, there were also 10,000 values for each index. Therefore, they were presented as box plots.